A Fundamental Approach to Predicting Mass Transfer Coefficients in Bubble Column Reactors

Persis Yefon Manjo (MNJPER001)

Thesis submitted
In fulfilment of the requirements for the degree of

Master of Science
In
Chemical Engineering

Under the Supervision of:
Associate Professor Randhir Rawatlal

Department of Chemical Engineering
University of Cape Town, South Africa

30 April 2014
Cape Town, South Africa

Keywords: bubble column reactor, mass transfer coefficient,
Bubble Cell Model, Film theory

Plagiarism declaration

I certify that this submission is my own, unaided work, except for information obtained from literature sources. All sources of information have been adequately acknowledged and referenced using the Harvard convention.

Persis Yefon Manjo
MNJPER001

A Fundamental Approach to Predicting Mass Transfer Coefficients in Bubble Column Reactors

Persis Yefon Manjo

Abstract

A bubble column reactor is a vertical cylindrical vessel used for gas-liquid reactions. Bubble Columns have several applications in industry due to certain obvious advantages such as high gas-liquid interfacial area, high heat and mass transfer rates, low maintenance requirements and operating costs. On the other hand, attempts at modelling and simulation are complicated by lack of understanding of hydrodynamics and mass transfer characteristics. This complicates design scale-up and industrial usage.

Many studies and models have attempted to evolve understanding of the hydrodynamic complexity in Bubble Columns reactors. A closer look at these studies and models reveals a variety of solution methods for different systems (Frössling, 1938; Clift *et al*., 1978; Hughmark, 1967; Dutta, 2007; Ranz and Marshall, 1952; Benitez, 2009; Buwa *et al.,* 2006; Suzzia *et al.,* 2009; Wylock *et al.,* 2011). Numerous correlations (Frössling, 1938; Clift *et al*., 1978; Hughmark, 1967; Dutta, 2007; Ranz and Marshall, 1952; Benitez, 2009; Buwa *et al.,* 2006) exist but to date in literature, there is no general approach to determining accurate estimates of average mass transfer coefficient values. Good estimates of the average mass transfer coefficient will improve the predictive capacity of the associated models.

Recent attempts at modelling micro-scale bubble-fluid interaction resulted in the Bubble Cell Model, BCM, (Coetzee *et al*., 2009) which simulates the velocity vector field around a single gas bubble in a flowing fluid stream using a Semi-Analytical model.

The aim of the present study is to extend the BCM applications by integrating the mass balance into the framework to predict the average mass transfer coefficient in bubble columns. A nitrogen-water steady state system was simulated in an axisymmetric grid where mass transfer occurs between the gas and liquid.

A concentration gradient may develop around the bubble which may be represented as concentration contours, where the mass boundary layer thickness as defined in the film theory is identified as one of these contours. The width of the irregularly shaped mass boundary layer thickness may be averaged and together with the nitrogen mass diffusivity used to calculate the average mass transfer coefficient.

The local fluid velocity affects the thickness of the film and together with the nitrogen mass diffusivity influences the rate of mass transfer across the concentration boundary layer. Increasing the inlet velocity decreases the mass boundary layer thickness and thereby increases the average mass transfer coefficient.

The CFD results from the simulation were integrated into the BCM by developing an algebraic function using the curve fitting approach. Three different ways of estimating mass transfer coefficient were developed, namely, the Sherwood number, concentration boundary layer (film theory) and boundary layer models. The best and fastest model with R^2 value of 0.9956 was the film theory now called the BCM Extension, which estimates the mass transfer coefficient as a function of Re and Sc numbers.

The BCM extension results were compared to different correlations such as those of Frössling (1938), Clift *et al*. (1978), Ranz and Marshall (1952); the estimated results showed not only the expected trend but also similar values to the mass transfer coefficient. The close estimates show there is a relation between the simulation model and correlations from experiments.

Therefore, a two dimensional semi-analytical fundamental model, the BCM, can be used to generate the steady-state velocity vector and pressure fields and when given the Reynolds and Schmidt numbers, predict the gas-liquid mass transfer rate from spherical bubbles in bubble columns in a homogeneous regime.

Acknowledgements

I thankfully acknowledge the DST-NRF Centre of Excellence in Catalysis (c*change) and the University of Cape Town for funding this research.

I will like to express my sincere gratitude to **Associate Professor Randhir Rawatlal** for his exceptional guidance, patience and genuine criticism which gave me more confidence, led to great improvements in my career and the completion of this work.

I am very thankful to **Waldo Coetzee** for guiding and mentoring me from day one of postgraduate studies. I want to also thank **Mopeli Kharma** for the continuous encouragement never to give up.

I cannot fully express my gratitude to my entire MANJO family for the constant support and encouragement through-out my entire education.

- Julius Berdu Manjo
- Matilda Fon Manjo
- Robert Fon Manjo
- Julius-Ikoli Mbimbi Manjo
- Larissa Jila Manjo

Contents

List of Figures

List of Tables

Nomenclature

a	Gas-liquid interfacial area per unit liquid volume, m^{-1}
C	Concentration, kg m^{-3}
C_A	Concentration of species A, kg m^{-3}
C_{Ab}	Bulk liquid Concentration of species A, kg m^{-3}
C_{Ai}	Concentration of species A at the interphase, kg m^{-3}
C_{As}	Concentration of species A at bubble surface, kg m^{-3}
$C_{A\infty}$	Bulk Concentration of species A, kg m^{-3}
D	Mass diffusivity, m^2 s^{-1}
D_{AB}	Mass diffusivity of species A into species B, m^2 s^{-1}
d	Spherical diameter of bubble, m
d_s	Sauter mean bubble diameter, m
g	Acceleration due to gravity, m s^{-1}
k_l	Liquid mass transfer coefficient, m s^{-1}
k_{lav}	Average mass Coefficient over the length of the plate, m s^{-1}
L	Characteristic length, m
p	Fluid pressure

Re_x Plate Reynolds number based on plate length x,

r_w Mean renewal rate, s^{-1}

s Time -seconds

Sh_{av} Average Sherwood Number

t Time variable, s

u Fluid velocity, m s^{-1}

u_∞ Bulk Fluid Velocity, m s^{-1}

x Plate/vertical distance, m

x,y Horizontal and vertical coordinates

Symbols

δ Momentum Boundary layer thickness, m

δ_m Mass Boundary layer thickness, m

σ Surface tension coefficient, kg s^{-2}

r,θ Radial and angular coordinates

μ Dynamic viscosity of fluid, kg $m^{-1}s^{-1}$

ρ Density, kg m^{-3}

ε_g Gas holdup

Δ Differential

∇ Gradient

$f_1, \alpha,$ Overall stage one model, stage one parameter

f_2 and ς Stage two model and parameters

Chapter 1 Introduction

1. Background and Theory

Multiphase reactors have been routinely applied in several industries such as chemical, biochemical, food and petroleum, metallurgical and pharmaceutical industries (Degaleesan *et al*., 2001; Deckwer *et al*., 1992). The degree of phase contact in these broad applications is used as selection criteria for particular processes. The commonly used reactors are: trickle bed reactors (fixed or packed bed), fluidized bed reactors and bubble column reactors (Kantarci *et al*., 2005; Levenspiel, 1999; Kayode Coker, 2001; Trambouze *et al.*, 1988; Krishna, 1994).

A gas-liquid bubble column reactor is a cylindrical vessel with a gas distributor (sparger) at the bottom as in Figure 1. The gas is sparged continuously at the inlet forming bubbles in the liquid hence the name “gas-liquid bubble column”. The bubbles, regarded as the dispersed phase, travel upwards through the column in the liquid (continuous phase).

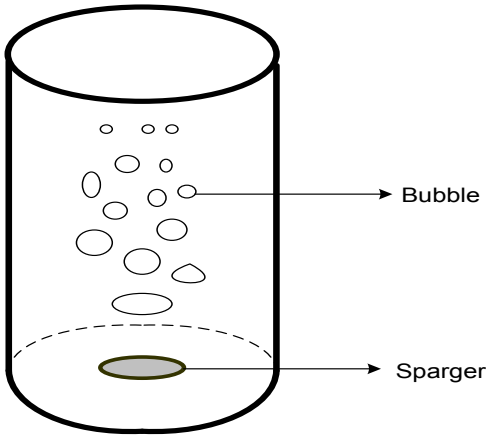

Figure 1 : Schematic diagram of a Gas-Liquid Bubble Column Reactor

Bubble columns have attracted significant interest in recent years due to their numerous applications in the Fischer–Tropsch synthesis (Krishna and Sie, 2000; Bukur and Daly, 1987), manufacture of fine chemicals, oxidation reactions,

chlorination, alkylation, polymerization, hydrogenation, coal liquefaction and fermentation reactions (Ekambara, 2005; Chang, 1989; Chrysikopoulos, 2003; Clarke, 2008; Fleischer *et al*., 1996; Gomez-Diaz and Navaza, 2005; Carra and Morbidelli, 1987; Deckwer, 1974; Troshko, 2009).

Bubble column reactors exhibit a number of advantages (Kantarci *et al*., 2005; Shaikh and Al-Dahhan, 2007) such as:

- Effective mixing
- High interfacial area
- High heat and mass transfer rates
- Low maintenance requirements
- Low operating costs due to lack of moving parts

On the other hand, bubble columns have the following disadvantages (Lemione *et al.*, 2008):

- Significant back mixing (increased blending of reactants and products)
- Bubble-bubble interactions in the heterogeneous regime
- Complexity of scale-up due to the lack of knowledge on hydrodynamics and mass transfer characteristics under typical industrial conditions.

The major design parameters associated with the performance of bubble columns are the fluid hydrodynamics (inlet gas velocity), gas hold-up, gas-liquid interfacial area, the gas-liquid mass and heat transfer coefficients (Madhavi, 2007; Kantarci *et al*., 2005). Gas hold-up and superficial gas velocity affect the surface area of the bubbles and the amount of time the gas bubble is present in the reactor. The surface area of the bubbles in turn affects the rate of mass transfer which influences the overall bubble column performance.

It is therefore necessary to understand the effect of hydrodynamics on mass transfer when attempting to optimise design and performance of bubble column reactors. It should be noted that significant research efforts have been applied in the past years to improve the performance, design and scale-up of bubble column reactors (Joshi 2001, 2003).

1.1. Gas-Liquid Flow Regimes

Gas-liquid bubble columns are reactors where gas enters at the bottom and rises through a liquid due to the inlet velocity and buoyancy. When the gas is sparged into the liquid, the bed of liquid begins to expand homogeneously (moves uniformly), while the bed height and the gas hold-up increase almost linearly with the superficial gas velocity. This regime is referred to as the homogeneous or bubbly flow regime which occurs at very low to moderate superficial gas velocities (0 to 0.4 $m.s^{-1}$) and is characterized by small spherical bubbles with diameters ranging between 0.003 and 0.008 m (Ranade, 2002; Van Baten and Krishna, 2004; Krishna, 2003; Shaikh and Al-Dahhan, 2007).

As the gas velocity is increased (< 0.08 $m.s^{-1}$), the gas hold-up increases and the regime transitions from the homogenous to the heterogeneous regime or churn turbulent regime. The regime transition causes the formation of bubbles with different shapes and sizes. The large bubbles travel in the center of the column while the small bubbles travel along the sides of the walls or are trapped in the wake of larger bubbles (Ranade, 2002; Van Baten and Krishna, 2004; Krishna, 2003; Shaikh and Al-Dahhan, 2007).

Increasing the gas velocity even further, a point is reached where the gas velocity becomes insufficient and bubbles coalesce forming larger bubbles which span the entire cross section of the column. This undesired flow regime is called slug flow and frequently occurs in pipelines transporting gas-oil mixtures (Zhang *et al*., 2007; Shaikh and Al-Dahhan, 2007).

The type of flow regime in a reactor is strongly dependent on the inlet gas velocity and significantly influences the hydrodynamics of a system. To illustrate this dependency, the different flow regimes frequently observed in bubble columns are presented in Figure 2.

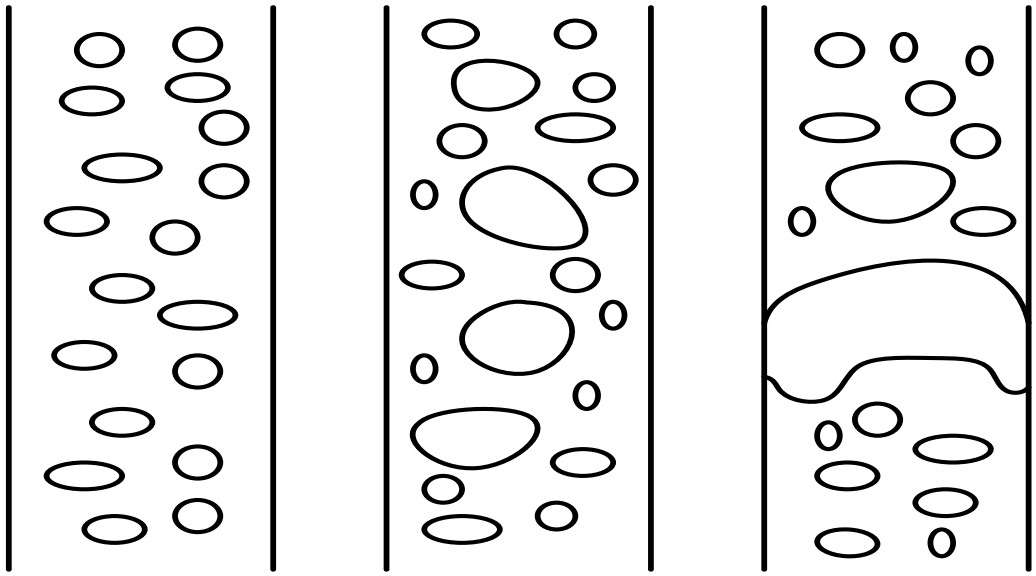

Figure 2: Flow Regimes observed in gas-liquid reactors: homogeneous flow (left), heterogeneous flow (middle) and slug flow (right)

Buwa and Vivek (2004) showed that in turbulent flow, there is a complex relationship between the gas hold-up distribution, column operating and design variables. As such, the initial scope of the present study is restricted to the homogeneous regime and will extend application to the heterogeneous regime only once the core model principles are established.

1.1.1. Bubble Physics

In Figure 2 above, different bubble shapes are observed in the different flow regimes. Clift *et al*. (1978) describes the different bubble shapes extensively and most importantly demonstrates that the bubble shape depends on the Reynolds number (density, viscosity).

It is generally expected that the bubble will either reduce or increase in size due to coalescence or break-up as it rises through the column. There are many factors that can affect the shape of bubbles, such as, the fluid density, fluid viscosity, gravitation acceleration, surface tension, terminal gas velocity and characteristic length (diameter of the volume-equivalent sphere). This change in bubble size occurs when the bubble is subjected to these external factors until the forces balance at the gas-fluid interface.

The factors that affect bubble shape are summarised and grouped in the following dimensionless numbers: Reynolds (Re, Eq. 1), Eötvös (Eo, Eq. 2) and Morton Number (Mo, Eq. 3). The Weber number (We, Eq. 4) is another dimensionless number mostly used to analyse fluid flows where an interface exists between two different fluids as is the case in multiphase flows (Michealides, 2006).

$$\mathbf{Re} = \frac{\boldsymbol{\rho \mathrm{d} u}}{\boldsymbol{\mu}} \propto \frac{\textbf{Inertia Forces}}{\textbf{Viscous Forces}} \qquad (\mathbf{1})$$

$$\mathbf{Eo} = \frac{\boldsymbol{\Delta \rho g d^2}}{\boldsymbol{\sigma}} \propto \frac{\textbf{Buoyancy Forces}}{\textbf{Surface Tension Forces}} \qquad (\mathbf{2})$$

$$\mathbf{Mo} = \frac{\boldsymbol{g u^4}}{\boldsymbol{\rho * \sigma^3}} \propto \frac{\textbf{Viscous Forces}}{\textbf{Surface Tension Forces}} \qquad (\mathbf{3})$$

$$\mathbf{We} = \frac{\boldsymbol{\rho u^2 d}}{\boldsymbol{\sigma}} \propto \frac{\textbf{Inertia Forces}}{\textbf{Surface Tension Forces}} \qquad (\mathbf{4})$$

In fluid dynamics, the density and viscosity (Eötvös, Eq. 2 or Reynolds number, Eq. 1) are used to characterise the shape of bubbles or drops moving in a continuous phase (Clift *et al*., 1978). There are three main groups of bubble shapes namely: *spherical* which appear when the viscous forces are more significant than the inertia forces, *ellipsoidal* which have a convex interface around the entire surface and *spherical-cap* which are almost flat and look like cuts from spheres (see Figure 3) (Clift *et al*., 1978). The bubble shape is initially spherical and upon deformation, it is transformed to other shapes like wobbling, skirted and/or dimpled ellipsoidal cap (Smolianski *et al*., 2008).

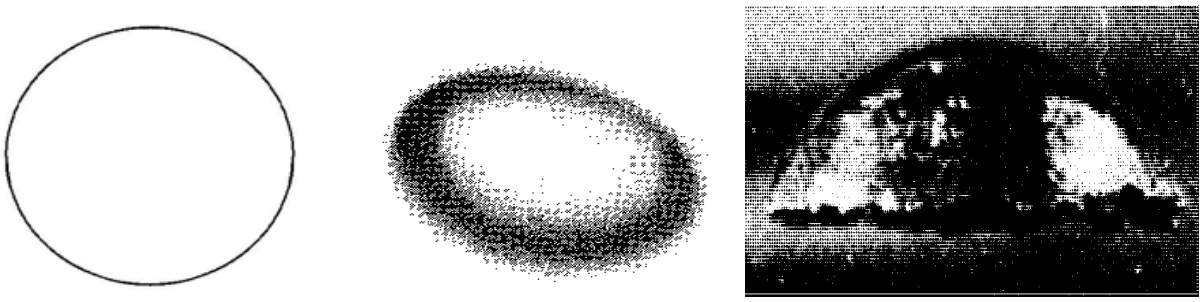

Figure 3: Different Bubble Shapes: Spherical (left), ellipsoidal (middle) and spherical-cap (right) (Clift et al., 1978)

It therefore follows that when modelling a bubble column system, the operating regime has to be clearly specified.

1.2. Measuring BCR Characteristics

Amongst the parameters affecting the bubble column performance, the overall volumetric mass transfer coefficient ($k_l a$) is key as mass transfer from the gas phase to liquid phase or *vice versa* significantly influences the rate of mass transfer (Cussler, 2003).

The mass transfer coefficient in bubble column reactors has been reported in literature in a variety of correlations and models (Frössling, 1938; Garner and Keey, 1958, 1959; Lochiel and Calderbank, 1964; Clift *et al*., 1978; Rowe *et al*, 1965; Ranz and Marshall, 1952; Brain and Hales, 1969; Bowman *et al*., 1961; Friedlander, 1957; Hughmark, 1967; Motarjemi and Jameson, 1978; Linton and Suterland, 1960). A more general, consistent means of estimating the average mass transfer coefficient is sought.

Mass transfer due to diffusive flux across a theoretical film is defined as the movement of a component in a mixture from a region of higher concentration to a region of a lower concentration across an interface (molecular diffusion). When different fluid phases are involved, convective mass transfer is included in the overall mass transfer process since diffusion follows the direction of the bulk fluid (Cussler, 2003). Therefore, Convective Mass Transfer involves the transport of a component between an interface and a moving fluid or between two relatively immiscible moving fluids. It is necessary to understand how the $k_l a$ parameter relates and varies with velocity, density and fluid viscosity.

Figure 4 illustrates the concentration boundary layer that develops when fluid flows around a bubble for any of the species diffusing from the gas to liquid phase (contour line with same concentration). In the film theory, the mass boundary layer thickness is defined as the distance from the bubble surface to where the concentration of the diffusing species is 99% of the bulk liquid concentration (Bird *et al*., 1960). More explanations regarding this definition are discussed in Section 2.1.

There are three types of boundary layers (contour lines) when fluid flows over any surface, namely, the velocity, concentration and thermal boundary layers. The corresponding layer thicknesses result from the gradient differences by momentum, mass and thermal diffusion, respectively (Dutta, 2007). For species mass transfer, only the concentration boundary layer is investigated in order to calculate $k_l a$ whereas the thermal boundary layer is used to calculate the heat transfer coefficient.

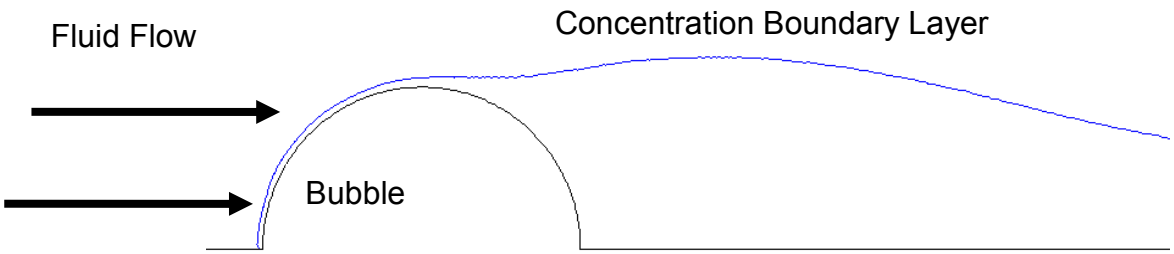

Figure 4: Concentration boundary layer formation around bubble

According to a review by Bouaifi *et al*. (2001), very few research studies have separated k_l from a and therefore, a better understanding of this parameter ($k_l a$) will help determine which of the two factors really controls the mass transfer. Akita and Yoshida (1974) also propose this separation.

1.2.1. Interfacial Area

For bubble columns, the variation in the overall volumetric mass transfer coefficient is primarily influenced by interfacial area (Kantarci *et al*., 2005). For spherical bubbles, the specific interfacial area can be expressed as the relative ratio of the gas hold-up ε_g and Sauter mean bubble diameter d_s (Eq. 5; Baehr and Karl, 2006). However, measuring and simulating the gas hold-up is difficult because it depends on the superficial gas velocity (Bouaifi *et al*., 2001; Hughmark, 1967; Akita and Yoshida, 1973, 1974).

$$a = \frac{6\varepsilon_g}{d_s} \qquad (5)$$

1.2.2. Mass Transfer Coefficient

Bubble column reactors are widely used due to observed high mass transfer rates. The overall volumetric mass transfer rate per unit volume of the dispersion in a bubble column is governed by the liquid side mass transfer coefficient k_l. The gas side resistance (that is, concentration gradients within the bubble) is assumed negligible (Deckwer, 1992; Kantarci *et al*., 2005). The liquid mass transfer coefficient k_l is defined as the ratio of diffusivity D_{AB} to the mass boundary layer thickness δ_m according to the film theory (Eq. 6; Cussler, 2003). Appendix A contains details on the derivation of the film theory.

$$k_l = \frac{D_{AB}}{\delta_m} \qquad (6)$$

The expected concentration boundary layer formation around a stagnant bubble is illustrated in Figure 5a where a uniform spherical mass boundary layer thickness,$\boldsymbol{\delta_m}$ is observed. This clearly defined boundary layer changes with angular position when fluid flows over the bubble as seen in Figure 5b. A large mass boundary layer thickness exists at low velocities and ultimately results in small k_l whereas high velocities yield smaller mass boundary layer thickness and high k_l values. At this point, the different angular spherical boundary layers for the moving bubble are averaged to get a uniform value.

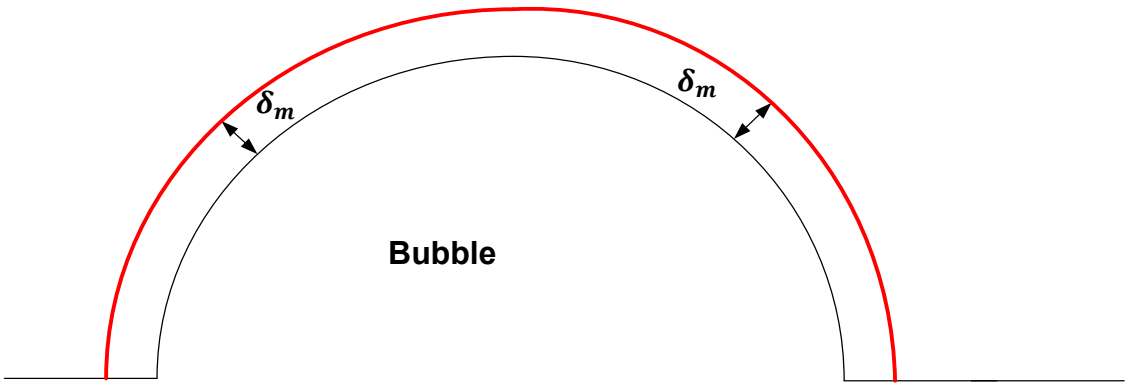

(a) Concentration Boundary Layer formation around stagnant bubble

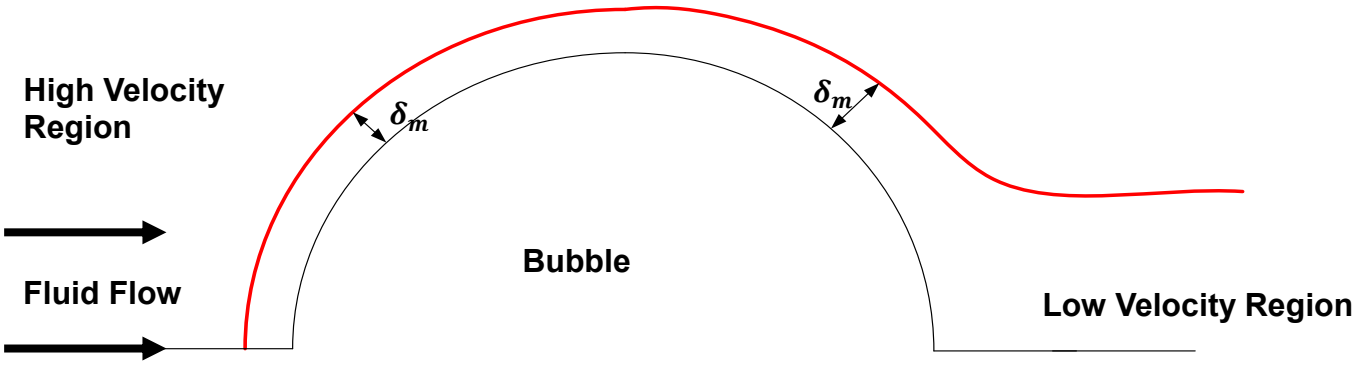

(*b) Concentration boundary layer formation when fluid flows over bubble*

Figure 5: Concentration Boundary Layer formation around (a) Stagnant bubble and (b) bubble with moving fluid

The mass diffusivity D_{AB} can easily be calculated *via* kinetic theory of gases or estimated from experiments (Thirumaleshwar, 2006; Cussler, 2003) whereas the mass boundary layer thickness $\boldsymbol{\delta_m}$ cannot be easily calculated because it depends on the hydrodynamics of the system.

As a result, with the estimated mass diffusivity and simulated mass boundary layer thickness, the mass transfer coefficient in a bubble column can be calculated. Various methods and theories are used to calculate the mass transfer coefficient. It should be specified that aim of the present research is to predict the average mass transfer coefficient over a bubble and not the local mass transfer coefficient. Amongst these methods, dimensionless numbers are often used to correlate mass transfer data.

1.2.2.1. Dimensionless Groups

The mass transfer coefficient in a non-reacting system can also be described systematically using dimensionless numbers such as Reynolds number, viscosity ratio, Peclet number, ratio of diffusion coefficients and distribution coefficients (Kantarci *et al*., 2005).

The Peclet number (Eq. 7) is the ratio of advection rate to diffusion rate, which is the product of the Reynolds number and Schmidt number, and is important in describing

mass transfer. Equation 1 shows that when the inertia forces dominate, the Re is high and leads to large k_l values. However, the reverse occurs when the viscous forces dominate. The Schmidt number, Sc, on the other hand is a ratio of the viscous diffusivity to mass diffusivity (Eq. 8; Ranade, 2001).

$$\boldsymbol{Pe = Re \times Sc = \frac{du}{D_{AB}}} \qquad (7)$$

$$\boldsymbol{Sc = \frac{\mu}{\rho D_{AB}}} \qquad (8)$$

The mass diffusivity is directly proportional to the k_l (Eq. 6) and this ultimately makes k_l a function of Re and Sc. The Sherwood number Sh (Eq. 9) is defined as the ratio of convective to diffusive transport (Sherwood *et al*., 1975; Basmadjian, 2004; Incropera *et al*., 2011). The Schmidt (Eq.8) and Sherwood (Eq. 9) numbers are particularly used when describing mass transfer.

$$\boldsymbol{Sh = \frac{k_l L}{D_{AB}}} \qquad (9)$$

1.3. Computer Fluid Dynamics – CFD

1.3.1. Empirical Correlations

Correlations are a useful way of collating experimental data and providing estimates of fluid properties. Many studies have been carried out on mass transfer coefficients and thus numerous empirical correlations for calculating k_la are established in the literature (Hughmark, 1967; Hikita *et al*., 1980, 1981).

However, these correlations are specific to the equipment type, the particular system, geometry and operating conditions (Dudley, 1995). The correlations have different methods used which are inconsistent and subject to many uncertainties (errors). Therefore, it would be advantageous if these experimental studies can be supported by mathematically developed models.

1.3.2. Numerical Calculations

For decades, Computational Fluid Dynamics (CFD) tools have been applied in modelling bubble columns to establish a rational basis for the interpretation of fluid dynamics variables. CFD Modelling of gas-liquid phase flows has shown remarkable progress and it can be used as a tool for predicting k_la. The most frequently applied approaches are the Euler-Euler, Euler-Lagrange (Zhang *et al*., 2007) and Direct

Numerical Simulation (Dani *et al*., 2006) methods.

With the Euler-Euler approach, both phases are modelled as two inter-penetrating continua whilst the Euler-Lagrange approach tracks each bubble, bubble-bubble and bubble-liquid interactions (Lain, 2002; Pfleger and Becker, 2001). These methods are, however, computationally expensive depending on the level of detail required such as the geometry, hydrodynamics of the system and scale. The Direct Numerical Simulation (DNS) is dependent on closure models and though frequently used, it is still computationally expensive.

Computing capability is one of the significantly observed challenges in the numerical modelling of bubble columns. However, progress has been registered in understanding the hydrodynamics properties and mass transfer characteristics of bubble columns. Bubble columns have advantages which explain its extensive use in industries but face difficulties in the optimization of their performance in different applications. Therefore, a less computationally expensive method is needed to model bubble columns and thereafter conduct optimization studies.

1.4. Summary

The efficiency of gas-liquid bubble columns relies on the inlet gas velocity, gas hold-up, gas-liquid interfacial area and gas-liquid heat and mass transfer coefficients. The inlet gas velocity determines the type of flow regime in the bubble column. The flow regime can be either be homogeneous, heterogeneous or slug flow and has an influence on how long the gas bubbles are present in the column. The gas velocity alongside fluid density and viscosity also determine the shape of the bubble as it enters the column which thereafter has an impact on the mass transfer rate.

The volumetric mass transfer coefficient is a key parameter when dealing with mass transfer and significantly improves bubble column performance. Mass transfer in a gas-liquid involves transport of a component from gas phase to liquid phase or *vice versa*. In doing so, the diffusing component develops a concentration profile with which the mass boundary layer thickness can be calculated. The mass boundary layer thickness along with the mass diffusivity of diffusing component is used to calculate the average mass transfer coefficient using the film theory.

Chapter 2 Literature Review

2. Literature Review

The mass transfer coefficient is a key parameter for optimising bubble columns performance and can be estimated from different experimental methods, theories and computational methods. This chapter focuses on understanding the basic principles and conditions used to define and develop methods of estimating mass transfer coefficients.

2.1. Modelling Mass Transfer

Predicting or modelling the mass transfer rate in a bubble column can be complicated. To design and optimize bubble columns, precise information regarding the mass transfer coefficient and interfacial area is required. Due to the complexity of the bubble hydrodynamics in gas-liquid systems and mass transfer characteristics involved, it is difficult to reliably predict the rate of mass transfer.

A number of simplified models exist that can be useful in describing mass transfer, namely: film theory, boundary layer theory, surface renewal theory and Higbie's penetration theory (Dutta, 2007). Table 1 show the different models used in calculating mass transfer coefficients.

Table 1: Mass transfer Coefficients Calculations from different theories

Theory	State	k_l Expression	Dependence on Diffusivity	Model Parameter (unit)
Film	Steady	$K_l = D/\delta_m$	$k_l \propto D$	δ_m (m)
Penetration	Unsteady	$k_l = 2[D/\pi t]^{1/2}$	$k_l \propto D^{1/2}$	$t\,(s)$
Surface Renewal	Unsteady	$k_l = [Dr_w]^{1/2}$	$k_l \propto D^{1/2}$	r_w (s^{-1})
Boundary Layer	Steady	$Sh = \frac{k_l L}{D}$	$k_l \propto D^{2/3}$	

As shown in Table 1, the surface renewal and Higbie penetration theories are mostly used to describe unsteady state systems and inappropriate for this study.

2.1.1. Film Theory

The film theory described by Whitman (1923, 1962) is based on the assumption that mass transfer only occurs by molecular diffusion at steady state through a thin gas film existing between the gas phase and the liquid phase (Seader and Henley, 1998, 2006). This film around the surface has a thickness of δ_m and outside this film, the fluid has the same concentration everywhere as that of the bulk fluid C_{Ab}. It is important to note that this thickness δ_m is defined by the boundary layer theory as the point where the concentration of the diffusing component in the bulk liquid is 99%.

Figure 6 illustrates mass transfer from a single bubble to a laminar flowing liquid. The concentration of the dissolved gas $\mathrm{C_{Ai}}$ decreases within the interphase film until it reaches the bulk liquid concentration $\mathrm{C_{Ab}}$. Molecular diffusion is responsible for mass transfer near the surface while convection mass transfer dominates away from it.

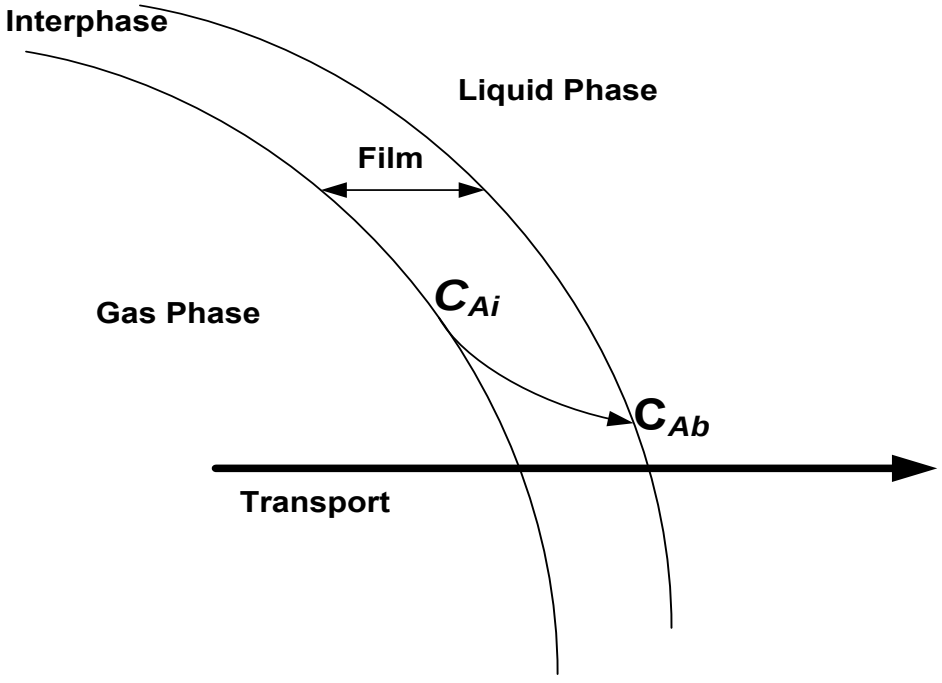

Figure 6 : Concentrations profile in gas and liquid films

In convective mass transfer, the molar flux N_A is expressed as the product of mass transfer coefficient k_l, mass transfer area *a* and concentration gradients ∇C_A , which acts as the driving force (Eq. 10).

$$N_A = k_l a \nabla C_A \qquad (10)$$

According to Fick's first law, steady state diffusion occurs where the flux goes from high to low concentrations yielding the molar flux in Equation 11 (Cussler, 2003).

$$N_A = -D_{AB}\left(\frac{dC_A}{dx}\right) \qquad (11)$$

The gas phase transfer coefficient is always relatively high in bubble column reactors due to the bubbles being relatively small and due to the concentration gradients being relatively low thus leading to negligible gas-phase resistance. This study therefore only focuses on the liquid mass transfer coefficient.

2.1.2. Boundary Layer Theory

The boundary layer theory is based on the formation of a velocity boundary layer around a surface when in contact with a flowing fluid in a laminar regime is illustrated over a flat plate in Figure 7. Initially, the velocity on the plate surface is considered to be zero but gradually increases along the plate reaching a momentum boundary layer thickness δ. The momentum boundary layer thickness δ is defined as the region where the fluid velocity changes from zero to the free stream velocity (u_∞) and is calculated using Equation 12 (Benitez, 2009).

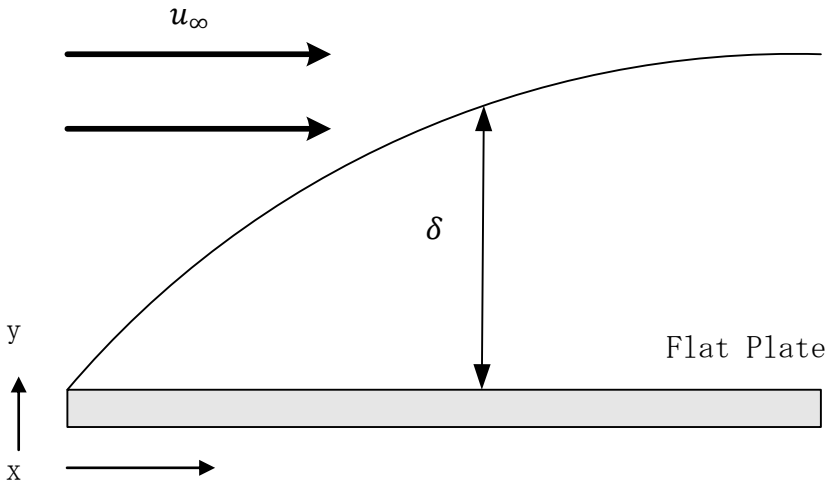

Figure 7 : Laminar Velocity boundary layer development on a flat plate

$$\boldsymbol{\delta = \frac{5x}{\sqrt{u_\infty x/v}} = \frac{5x}{\sqrt{Re_x}}} \qquad \mathbf{(12)}$$

If the plate in Figure 7 was to have a soluble component, a velocity boundary layer is formed on the plate as well as a concentration boundary layer. Heat transfer can be represented in a similar fashion whereby if the same plate was heated; thermal and velocity boundary layers are been formed.

The bubble is then perceived as a virtual flat plate. As mentioned previously, the mass boundary layer thickness δ_m is defined as the distance from the bubble surface to where the concentration of the diffusing species is 99% of the bulk concentration. In other words, it can be expressed in dimensionless form as seen below in Equation 13 (Incropera *et al*., 2010). Appendix B shows how to calculate the final concentration $\boldsymbol{C_A}$, in the stream when using Eq. 13.

$$\boldsymbol{\frac{C_{AS} - C_A}{C_{AS} - C_{A\infty}} = 0.99} \qquad \mathbf{(13)}$$

The momentum and mass boundary layers thickness are linked in Equation 14 and valid if $Sc \geq 0.6$. If the flow over the momentum boundary layer thickness δ is laminar (Re < 270), the average mass transfer coefficient in terms of the average Sherwood number yields Equation 15 (Dutta, 2007). Equation 15 has also been experimentally verified by Welty *et al*. (1984) and gives accurate results for $Re_x < 3 \times 10^5$ (Benitez, 2009). The boundary layer theory predicts the mass transfer coefficient with dependence on diffusivity. Many experimental results reasonably agree with the theory (Dutta, 2007)

$$\boldsymbol{\frac{\delta}{\delta_m} = Sc^{1/3}} \qquad \boldsymbol{Sc \geq 0.6} \qquad \mathbf{(14)}$$

$$\boldsymbol{Sh_{av} = \frac{k_{lav}\delta_m}{D_{AB}} = 0.664 Re_x^{1/2} Sc^{1/3}} \qquad \mathbf{(15)}$$

The theories used to describe mass transfer are reasonably accurate though only for specific cases and do not incorporate the hydrodynamics even though the flow greatly influences the mass transfer rate. However, the exception is the boundary layer theory which can be used for predictive purposes. Consequently, a model that

can be used to predict mass transfer coefficient and incorporate the hydrodynamic properties of a system is required.

2.2. Mass Transfer Studies

Bubble columns have numerous applications in the chemical industries especially as gas-liquid reactors and absorbers amongst others. The design and scale-up of bubble column reactors are challenging due to underlying factors in the hydrodynamics, phase mixing and fluid properties. A model developed to predict reactor performance and thereby optimize, would render bubble columns more economical.

Many studies have been undertaken to investigate the factors affecting mass transfer in bubble columns with the prediction of the mass transfer coefficient being the central focus (Akita and Yoshida, 1973, 1974; Van Baten and Krishna, 2004; Hughmark, 1967; Kojima *et al*., 1997; Hikita *et al*., 1980, 1981; Kantarci *et al*., 2005; Bouaifi *et al*., 2001; Lau *et al*., 2004; Mashelkar and Sharma, 1970; Alvarez-Cuenca and Nerenberg, 1981; Deindoerfer and Humphrey, 1961; Yoshida, 1965; Garcia-Ochoa and Gomez, 2004; Deckwer *et al*., 1974; Kawase *et al*., 1987,1992; Vermeer and Krishna, 1981; Martin *et al*., 2009a).

Kojima *et al*. (1997) found that gas hold-up and k_la increase with increasing pressure. Lu *et al*. (2003) investigated the influence of flow and viscosity (Re and Sc) on k_la and found out that k_la increases with increasing values of Pe indicating that either or both an increase in Re and Sc number increases the mass transfer coefficient.

Similarly, Paschedag *et al*. (2005) performed a sensitivity analysis for mass transfer at a single droplet mathematically. The results showed that the dimensionless numbers Re, Sc and Pe are affected by the material properties and operating conditions. Martin *et al*. (2009b) also found that bubble oscillations affect k_l since concentration profiles surrounding the bubbles are influenced by other bubbles in the surrounding.

The volumetric mass transfer coefficient can be predicted using experimentally determined correlations, empirical models and predictive models. As far back as

1967, Hughmark developed empirical correlations to predict the mass transfer coefficient. Many other correlations were developed for predicting the volumetric mass transfer coefficient, $k_l a$, in bubble column reactors over the years. There are certain similarities observed by the different correlations whereby there is good agreement with experimental values (Akita and Yoshida, 1973, 1974; Gestrich *et al*., 1976; Hikita *et al*., 1980, 1981; Hammer *et al*., 1984; Ozturk and Schumpe, 1987; Delnoij *et al*., 1997, 1999; Deen *et al*., 2001).

These correlations depend on the choice of the gas-liquid system investigated, as well as the velocity and fluid properties. For example, Table 2 shows a selection of correlations for mass transfer coefficients for forced and free convection flow.

Dudley (1995) reviewed different correlations for predicting $k_l a$ and found that these correlations are inconsistent since the methods are specific to the equipment type, the gas–liquid system and operating conditions. Hence, the selection criteria for a correlation for a specific system cannot be determined.

Table 2 : Mass Transfer Correlations for Convection flow

References	Mass Transfer Coefficient Correlation	Conditions/ Geometry
Frössling, 1938	$Sh = 2(1 + 0.273\mathrm{Re}^{0.5}\mathrm{Sc}^{0.33})$	Evaporation
Garner et Keey, 1958, 1959	$Sh = 0.94Re^{0.5}Sc^{0.33}$	Single solid spheres
Lochiel and Calderbank, 1964	$Sh = 0.6Re^{0.5}Sc^{0.33}$	Rigid bubble surface
Clift *et al*., 1978	$Sh = 1(1 + 0.564\mathrm{Pe}^{0.66})^{0.75}$	Creeping Regime
Rowe *et al*, 1965	$Sh = 2 + 0.68\mathrm{Re}^{0.5}\mathrm{Sc}^{0.33})$	Spherical particles in fluid
	$Sh = 2 + 0.79\mathrm{Re}^{0.5}\mathrm{Sc}^{0.33})$	
Ranz and Marshall, 1952	$Sh = 2(1 + 0.3\mathrm{Re}^{0.5}\mathrm{Sc}^{0.33})$	Drops
Brain and Hales, 1969	$Sh = \left[4 + 1.21(\mathrm{ReSc})^{0.67)}\right]^{0.5}$	Mass transfer into liquids
Bowman *et al*., 1961	$Sh = 0.978(ReSc)^{\frac{1}{3}}$	Single sphere in fluid
	$Sh = 2 + 0.57\mathrm{ReSc} + 0.14\mathrm{ReSc}^2$	
Friedlander, 1957	$Sh = 0.89(ReSc)^{0.33}$	Single sphere

Hughmark, 1967	$Sh = 2 + \left[Re^{0.484} Sc^{0.339} \frac{dg}{D_{AB}^{2/3}}^{1/3} \right]^{1.61}$	Single bubbles in liquid
Calderbank (Motarjemi and Jameson,1978)	$k_l Sc^{0.5} = 0.42 \left(\frac{\mu g}{\rho}\right)$	Small bubbles
Linton and Suterland, 1960	$Sh = 0.582 Re^{0.5} Sc^{0.33}$	Bubbles

Lemione et al. (2008) also performed a detailed survey on mass transfer studies in bubble column reactors and it showed that the hydrodynamics and mass transfer characteristics depend on fluid properties, operating variables, reactor size and gas distributor type. Lemione's survey showed that the correlations do not take into account the aforementioned factors, thus concluding that there is a need to precisely predict hydrodynamics and mass transfer parameters needed for modelling.

Clearly, there has been remarkable progress in understanding the hydrodynamics and mass transfer characteristics in bubble column. However, the results of these studies are conflicting and the empirical correlations are not consistent with system type and conditions. The different conditions and geometries show the difficulty in the reproducibility, resulting in under or over-estimated values. A more fundamental approach is required to aid in the understanding and design of bubble columns characteristics as well as allow for more consistent predictions.

2.3. Modelling Multiphase Flows

Experiments have been carried out to predict the mass transfer coefficient in bubble column reactors under various operating conditions (Frössling, 1938; Garner et Keey, 1958, 1959; Lochiel and Calderbank, 1964; Clift *et al*., 1978; Rowe *et al*, 1965; Ranz and Marshall, 1952; Brain and Hales, 1969; Bowman *et al*., 1961; Friedlander, 1957; Hughmark, 1967; Motarjemi and Jameson, 1978; Linton and Suterland, 1960). The overall results from these experiments have been consolidated in correlations. However, these correlations need to be supported by more fundamental modeling methods for simpler and more unified predictors to be developed.

2.3.1. Fluid Dynamic Approaches

It is noted from literature that the design and scale up of reactors are primarily based on empiricism. In order to reduce empiricism (Akita and Yoshida, 1973, 1974; Gestrich *et al*., 1976; Hikita *et al*., 1980, 1981; Hammer *et al*., 1984; Ozturk and Schumpe, 1987; Delnoij *et al*., 1997, 1999; Deen *et al*., 2001) several attempts to explore other alternatives to solve the problems in fluid dynamics and mass transfer have been made such as the Experimental Fluid Dynamics (EFD), Analytical Fluid Dynamics (AFD) and Computational Fluid Dynamics (CFD) as seen in Table 3. EFD is based on the development of new measurement techniques, AFD deals with the mathematics of physics and problem formulation (equations and flow models) and CFD develops simulations that give a good prediction of the behavior of bubble columns.

Table 3: Advantages and Disadvantages of the different Fluid Dynamic Approaches (Ekambara, 2005; Brennen, 2005)

Approach	Advantages	Disadvantages
Experimental	• More realistic • Applications are possible	• Equipment required • Scaling problems • Measurement difficulties • Operating costs
Analytical	• Clean, general information in formula form	• Limited to simple geometry and physics • Restricted to linear problems

Computational	• Complicated physics can be treated • Can obtain time evolution of flow	• Boundary conditions problems • Computer costs

Experimental approaches are used in different applications but are limited by equipment size and scale-up problems. Consequently, the predictive capability and understanding of complex fluid flow especially for industrial designs rely on the AFD and/or CFD approaches (Brennen, 2005).

Literature shows that over a long period of time, significant research has been conducted in the utilization of CFD in modeling multiphase reactors and in the application of CFD to gas-liquid flows in bubble column reactors (Kuzmin and Turek, 2000；Schlüter, 1995；Buwa *et al*.,2006；Wang and Wang,2007；Akhtar,2006；Suzzia *et al*., 2009；Coetzee *et al*., 2009；Coetzee *et al*., 2012 a,b,c；Wylock *et al*.,2011；Irani and Khodagholi, 2011；Kumar *et al*., 2011；Singh and Majumder, 2011). However, most studies ignore or overlook the mass transfer and chemical reaction aspects in a system due to excessive computational power and memory requirements (Darmana, 2007). However, a modern advance in computing power is a cause for re-examining these methods.

2.3.2. Computational Fluid Dynamics

CFD uses numerical methods to solve the ordinary or partial differential equations required to study fluid flow. There are numerous all-purpose CFD packages namely: FLUENT, CFX/AEA, STAR-CD, CFDRC, FLOWLAB, just to name a few and the majority use finite volume method that can easily solve fluid flow and mass transfer problems (Mohapatra and Rakh, 2007).

CFD Process

Computational Fluid Dynamics (CFD) involves solving the Navier-Stokes equations that describe fluid flow numerically and enables the macroscopic properties such as velocity, pressure, mass (species transport) and temperature to be studied. The CFD process can be represented by a road map which consists of three elements namely: the pre-processor, solver and post-processor as shown in Figure 8 and described in

detail below (Hung *et al*., 2007; Garcia et al., 2008).

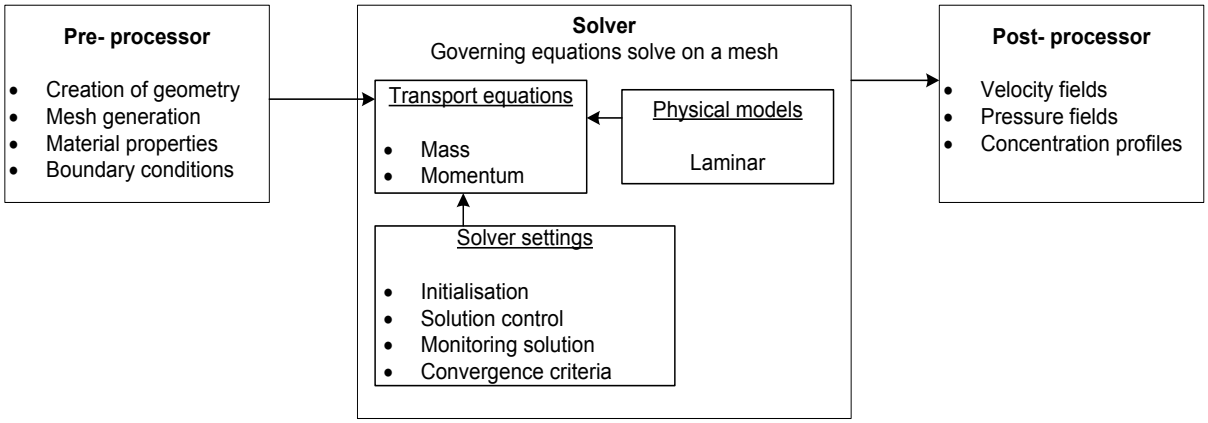

Figure 8 : The inter-connectivity functions of the three main elements within a CFD analysis

2.3.2.1. Pre-processor

The first step in any CFD analysis regardless of the type of fluid flow begins with creating the geometry, geometry parameters, domain shape and size (Garcia *et al*., 2008). The domain geometry created requires mesh generation which can either be structured or unstructured (Peraire *et al*., 1989; Baker, 2005; Thompson *et al*., 1998; Samareh, 2005). The mesh has nodes at each cell and the solution obtained can be improved by mesh refinements (number of cells). More cells mean improved accuracy but higher computational costs and hence long calculation turnover times. Hence, there always exists a trade-off between accuracy and turnover time (Tu *et al*., 2008).

Once the geometry and mesh are defined, the next step is to set up the material properties that are unique to a particular fluid flow system. The simulation is then classified according to the following (Garcia *et al*., 2008):

- Steady state/unsteady state flow
- Compressible/incompressible
- Laminar/turbulent flow regime

Together with the boundary conditions, there is in principle sufficient data to solve the partial differential equations. For fluid flow, inflow and outflow boundary conditions are required to explain the fluid behavior when entering or leaving the created flow geometry.

2.3.2.2. Solver

The solver is used to solve the discretized governing equations which consist of the mass, momentum, energy and other transport equations described below. The Navier-Stokes equations which have been used for decades describe fluid flow by assuming that fluid behaves as a continuum rather than as discrete particles (MacCormack and Baldwin, 1975; Lohner, 2001; Crumpton *et al*., 1997; Burnett, 1987; Tu *et al*., 2008).

Mass equations

The principle of conservation of mass states that mass can neither be destroyed nor created. This principle is combined with the Gauss's divergence theorem to an arbitrary fixed volume in space for a compressible fluid yielding Eq. 16. This equation describes the mass flux in and out of a fixed volume (can be fixed in space or move with the fluid) where the change of mass with time is equal to the convective flux ignoring any change in mass (Irani and Khodagholi, 2011).

$$\frac{\partial \rho}{\partial t} + \nabla . (\rho \mathbf{u}) = 0 \quad (16)$$

Equation 16 can rearranged to Equation 16b using the material derivative of the density field in Equation 16a.

$$\frac{\partial \rho}{\partial t} + \nabla \rho . \mathbf{u} = \frac{d\rho}{dt} \quad (16a)$$

$$\frac{1}{\rho}\frac{d\rho}{dt} + \nabla \mathbf{u} = 0 \quad (16b)$$

For an incompressible fluid where the density is assumed to be constant, Equation (16) reduces to Equation (17) below.

$$\frac{1}{\cancel{\rho}}\frac{\cancel{d\rho}}{dt} + \nabla \mathbf{u} = 0$$

$$\nabla . \mathbf{u} = 0 \ (17)$$

Momentum equations

The momentum equations can be derived from Newton's second law of motion which states that the rate of change of momentum equals the sum of forces acting on the fluid. There are two sources of force acting on the moving fluid which are body forces and surface forces. The body forces result from the location of the control volume in a force field whereas the surface forces are due to interactions between the control volume fluid and its surroundings. Therefore, the momentum balance for a control volume can be represented by Equation 18 below (Tu *et al*., 2008).

$$\sum \mathbf{F} = \iint \boldsymbol{\rho}\mathbf{v}\,(\mathbf{v}.\mathbf{n})\,\boldsymbol{dA} + \frac{\boldsymbol{\partial}}{\boldsymbol{\partial t}} \iiint \boldsymbol{\rho}\mathbf{v}\,\boldsymbol{dV} \quad (\mathbf{18})$$

Further evaluation of this equation with the assumptions of incompressible flow, and Newtonian fluid flow yields the Navier-Stokes equation shown in Equation 19 (Clift *et al*., 1978).

$$\frac{\boldsymbol{\partial u}}{\boldsymbol{\partial t}} + (\boldsymbol{u}.\boldsymbol{\nabla})\boldsymbol{u} = -\boldsymbol{\nabla p} + \mu\boldsymbol{\nabla}^{\mathbf{2}}\mathbf{u} \qquad \mathbf{(19)}$$

Analytical solutions to these equations can be obtained only under severely restrictive assumptions. For example, the creeping flow approximation is derived by neglecting the inertia terms of the Navier-Stokes equation and applies only to very low Reynolds's number Re < 0.1. However, most practical applications operate at moderate to high Re (150 < Re < 270) hence the need to engage with CFD. This then requires that accurate solutions are obtained by numerical solution of the full Navier-Stokes equation (Clift *et al*., 1978).

Three discretization methods can be used to solve the governing equations, namely: finite difference, finite volume/element and spectral methods. The advantages and disadvantages of the different methods are listed in Table 4 below.

Table 4: Advantages and Disadvantages of the different discretization methods (Kumar, 2009)

Method	Description	Advantages	Disadvantages
Finite Difference	• Finds discrete solutions on a grid/mesh	• Simple	• Complicated Domains • Discretized classical solutions
Finite Element/ Volume	• Based on a partition of the domain into small finite elements	• Better in irregular domains	• More complex to set up and analyze
Spectral Methods	• Solutions are approximated by a truncated expansion in the eigenfunction of some linear operator.	• Highly accurate for problems with smooth solutions	• Not so useful on irregular domains or for problems with discontinuities

The finite volume method is favourable to this research because of its applicability to arbitrary geometries, structured and unstructured meshes and its local conservation of numerical fluxes. This makes the finite volume technique very attractive when modelling problems where flux is important as is the case in the proposed work to predict average mass transfer coefficients (Eymard *et al.*, 2006).

2.3.2.3. Post-processing and Analysis

The last step in the CFD process is the post-processor which involves collecting the required output be it in the form of velocity, pressure or concentration profiles. The analysis of the data collected is done to explain results for the research study (Hung *et a*l., 2007; Garcia *et al.*, 2008).

2.4. Macro Modelling

The previous section discussed the mass transfer between the fluid and a single bubble (micro-modelling). The mass transfer mechanism in the entire Bubble Column can be simulated through the use of Multiphase CFD techniques. When modelling multiphase flows, there are two common approaches, namely, the Euler-Lagrange and Euler-Euler approaches. These models have shown that the CFD predictions for

the entire bubble column is at a reliable level since solutions from them have been in good agreement with experimental macroscopic flow properties in bubble columns (Becker *et al*., 1994).

2.4.1. The Euler-Lagrange Approach

In this approach, the fluid phase is treated as a continuum by solving the time-averaged Navier-Stokes equations, while the dispersed phase is solved by tracking a large number of particles, bubbles, or droplets through the calculated flow field (Delnoij *et al*., 1997). The dispersed phase can exchange momentum, mass and energy with the fluid phase. A fundamental assumption made in this model is that the dispersed second phase occupies a low volume fraction, even though a high mass loading (the mass of particle is greater than equal to the mass of the fluid) is acceptable (Kumar, 2009).

The particle or droplet trajectories are computed individually at specified intervals during the fluid phase calculation. This individual computation makes the model appropriate for the modeling of spray dryers, coal and liquid fuel combustion and some particle laden flows, but inappropriate for the modeling of liquid-liquid mixtures, fluidized beds or any application where the volume fraction of the second phase is not negligible (Mohapatra and Rakh, 2007). In summary, this approach solves the flow field by computing each individual bubble by considering the bubble-bubble and bubble-liquid interactions. (Zhang *et al*., 2007)

2.4.2. The Euler-Euler Approach

In the Euler-Euler approach, the different phases are treated mathematically as interpenetrating continua (Delnoij *et al*., 1997). The volume of a phase cannot be occupied by the other phase; Hence the introduction of the volume fraction concept. This means that the bubble size is represented by the volume fraction (Zhang *et al*., 2007).

These volume fractions are assumed to be continuous functions of space and time and their sum is equal to one. Conservation equations for each phase are derived to obtain a set of equations, which have similar structure for all phases. These equations are closed by providing constitutive relations that are obtained from empirical information or, in the case of granular flows, by application of kinetic theory (Kumar, 2009). This approach is limited because it must be coupled with the population balance to obtain more information on the bubble size distribution (Zhang *et al*., 2007).

Some other CFD Methods have been recently developed such as the Large Eddy Simulation (LES) and Direct Numerical Simulation (DNS) (Apte *et al*., 2004; Mahesh, 2006). For example, the DNS approach requires closure models and is only practically applicable to a finite number of bubbles and limits the simulation of other processes. Figure 9 shows a framework which can be used for bubble column simulation selection.

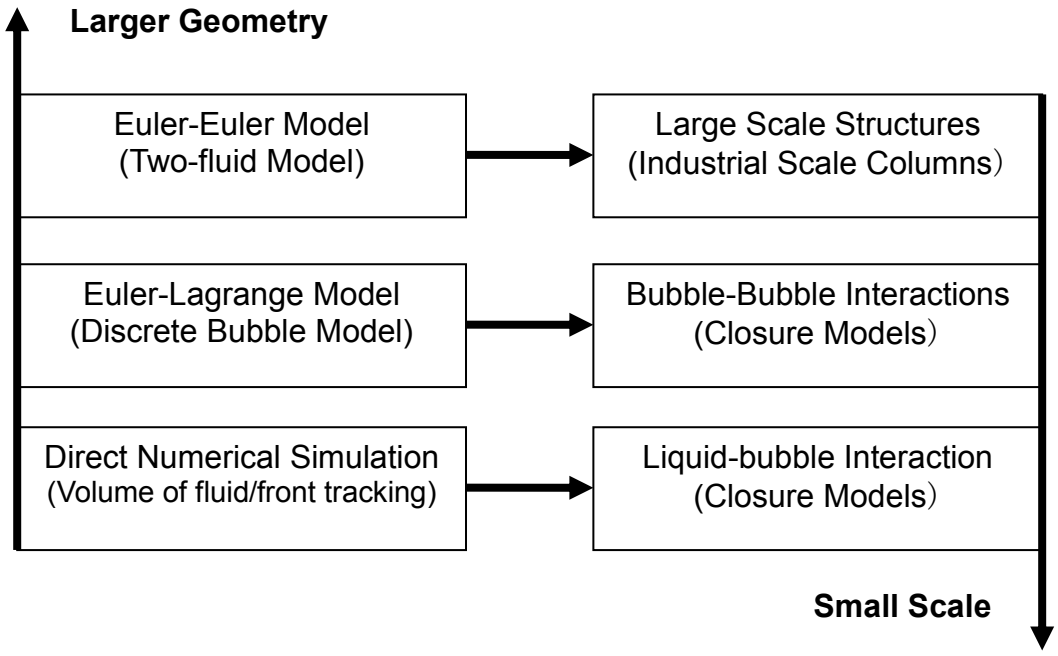

Figure 9 : Framework for selecting CFD bubble column simulation approaches (Van der hoef et al., 2006; Buwa et al., 2006)

During recent years, there has been an increase in the number of different models to simulate bubble columns in the analysis done by Kumar (2009) and Mahajan (2010). Kuzmin and Turek (2000) used the Euler-Euler model to study mass transfer and

chemical reaction for gas-liquid flows in Bubble Columns. The computational results showed the implications of reaction enhanced mass transfer in bubble columns and called for more grounds to continue research in this field.

Schlüter (1995) used the BCR computer code, a modular structured computer program to simulate steady state bubble columns. The code can be used for different options by determining the local pressure, temperature and concentration profiles over the column height. However, there is little information on the validation of the BCR model.

Buwa *et al*. (2006) experimentally validated the Eulerian-Langrangian models and gathered useful data for the simulation of mass transfer and reactions in bubble columns. Akhta (2006) validated the simulation of a bubble column against experimental results with different distributors using the Two-fluid Eulerian model. The influence of different distributors on the hydrodynamics of the system was investigated.

Wang and Wang (2007) used the Computation Fluid Dynamics-Population Balance Model (CFD-PBM) coupled model to simulate bubble columns. The simulation results showed that the CFD-PBM is an efficient method for predicting the hydrodynamics, bubble size distribution, interfacial area and gas-liquid mass transfer rate in a bubble column. This is a good method of simulation because it evaluates the bubble size in the column which is an important aspect in improving bubble column simulation.

Suzzia *et al*. (2009) validated the use of Euler-Euler and Euler-Lagrange approaches to simulate bubble columns. The Euler-Euler approach showed promising results for coarser mesh sizes and the Euler-Lagrange approach proved to be a more advance method for simulation. Zhang *et al*. (2008) continued to use the Euler-Euler model to simulate mass transfer and chemical reaction in a bubble column.

Coetzee *et al*., (2009) developed a rapid evaluating semi analytical model called the Bubble Cell Model (BCM). The BCM provides the steady state velocity and pressure

fields around individual bubbles as a function of Reynolds number (Figure 10). BCM is dependent on the Re number of the bubble and avoids the use of closure models while providing micro structure flow information (Coetzee *et al*., 2012).

The main BCM advantages over other models are as follows (Kumar, 2009; Mahajan 2010):

- The solving of complex PDEs in the regions around the bubble is avoided
- Small scale flow information is provided by the cell model
- Rapid evaluation compared to conventional techniques (Euler-Euler and Euler-Lagrange)

Figure 10 : Velocity vector fields around an individual generated in the BCM

Coetzee *et al*. (2012, a, b, c) adapted the BCM to a macro fluid model such that the entire bubble column could be simulated. It was constructed by extending the range of the creeping and potential flow analytical solutions by incorporating a stochastic model. This model accounts for deviations from the analytical solutions that is, flow separation and the non-linear wake feature.

Wylock *et al*. (2011) used the Direct Numerical Simulation approach to simulate bubble mass transfer with chemical reaction and showed that there is a clear difference between the 1D and 2D models. The results from the study by Irani and

Khodagholi (2011) showed that simple two dimensional models cannot be used in engineering calculations required in the design of bubble columns.

Kumar *et al*. (2011) validated the two and three phase up-flow in a bubble column with experimental values and obtained axial liquid velocity profiles. Singh and Majumder (2011) studied the co and counter-current mass transfer in bubble columns using a mechanistic model to predict mass transfer efficiency. It was suggested that the concentration variation may be useful for future understanding of the mass transfer phenomena in bubble column reactors.

2.5. Summary

The development of numerous CFD models used in the simulation of bubble columns has gradually increased in recent years. Considerable work has been accomplished in the understanding of bubble columns characteristics depending on the size and scale (Kumar, 2009; Mahajan 2010). In general, studies have shown that the different models are unique and limited to a practical system (Kuzmin and Turek, 2000；Schlüter, 1995；Buwa *et al*., 2006 ；Wang and Wang ,2007；Akhtar, 2006 ；Suzzia *et al*., 2009；Coetzee *et al*., 2009 ；Coetzee *et al*., 2012 a, b, c ；Wylock *et al*., 2011 ；Irani and Khodagholi, 2011 ；Kumar *et al*., 2011；Singh and Majumder, 2011). Models are validated to ensure that the modeled system is appropriately predicted. Some models however are purely theoretical while others have been experimentally validated (Schlüter, 1995; Wang and Wang, 2007; Coetzee *et al*., 2009; Coetzee *et al*., 2012 a, b, c).

It is worth noting that many studies are trying new approaches and drifting away from the common Euler-Euler and Euler-Lagrange models in favor of greater computational efficiency (Wang and Wang, 2007; Coetzee *et al*., 2009 ；Coetzee *et al*., 2012 a, b, c). Models like the Direct Numerical Simulation are now frequently used for bubble column simulation but still rely on closure models (Wylock *et al*., 2011). The CFD-PBM is appropriate for analyzing bubble size in detail (Wang and Wang, 2007).

Studies have shown that the mass transfer coefficients can be predicted using the CFD approach that requires closure models. However, there is still a gap in the fundamental understanding of the mass transfer and chemical reaction properties. It is not clear which is the most appropriate and less computationally expensive CFD approach to investigate mass transfer and chemical reaction.

Chapter 3 Motivation and Objectives

3. Motivation and Objectives

In this study, a fast-solving semi-analytical model called the Bubble Cell Model (BCM) proposed by Coetzee *et al*., (2009; 2012 a, b, c) is used to simulate gas-liquid flows around individual bubbles in a bubble column. This model provides an alternative multiphase modeling approach and substitutes the conventional closure models with a statistical model of the micro flow structure.

Many mass transfer experiments have been carried out in the literature but each of these sets of results are very specific to the chemical system, equipment type and operating conditions. Therefore, a more general method is needed to predict k_l from fundamental principles in a computationally inexpensive way.

The Bubble Cell Model (Coetzee *et al*., 2009; 2012 a, b, c) approach in its current state simulates the steady state velocity and pressure fields that develop in the immediate vicinity of individual bubbles. At present, the BCM incorporates only the local velocity vector field and does not predict the concentration field. As such, the model cannot be used in the present form to predict mass transfer rates or local reaction rates.

The concentration field can be predicted by coupling the mass balance to the momentum balance in the BCM. These concentration lines will show how the film thickness varies axisymmetrically around the bubble, hence, allowing for prediction of the mass transfer rates in the system.

The objective of the present study is therefore to extend the BCM to mass transfer applications. This model uses the film theory to calculate k_l for a homogeneous nitrogen-water system as a function of the Re and Sc numbers. As a significant outcome, such a model would be used to reliably predict the average mass transfer coefficients in a bubble column rather than through empirical correlations and experiments.

Hypothesis

The hypothesis of the present study is that *"the average mass transfer coefficient in a bubble column can be reliably predicted as a function of Reynolds number (Re) and Schmidt number (Sc) by coupling a material balance to a Bubble Cell Model."*

Key Questions

These questions will aid in either proving or disproving the hypothesis and are as follows:

1. How will the mass boundary layer thickness be averaged around bubble?
2. What is the impact of the Reynolds and Schmidt numbers on the average mass transfer coefficients?

Chapter 4 Model Development

4. Model Development

4.1. Model Geometry

In an industrial environment, bubble columns usually operate in turbulent regimes where Re > 1000 due to the high level of contact associated with strong mixing. The turbulent regime is complex due to the multiphase hydrodynamics (bubble-bubble interactions) that result in varying bubbles shapes. These varying shapes are an output of either increasing or decreasing the Reynolds, Morton and Eötvös numbers as described in section 1.1.1. Figure 11 illustrates the formation of the different shapes with respect to Re, Eo and Mo, the spherical bubble shape is observed before deformation to other oblate ellipsoidal and spherical cap shapes.

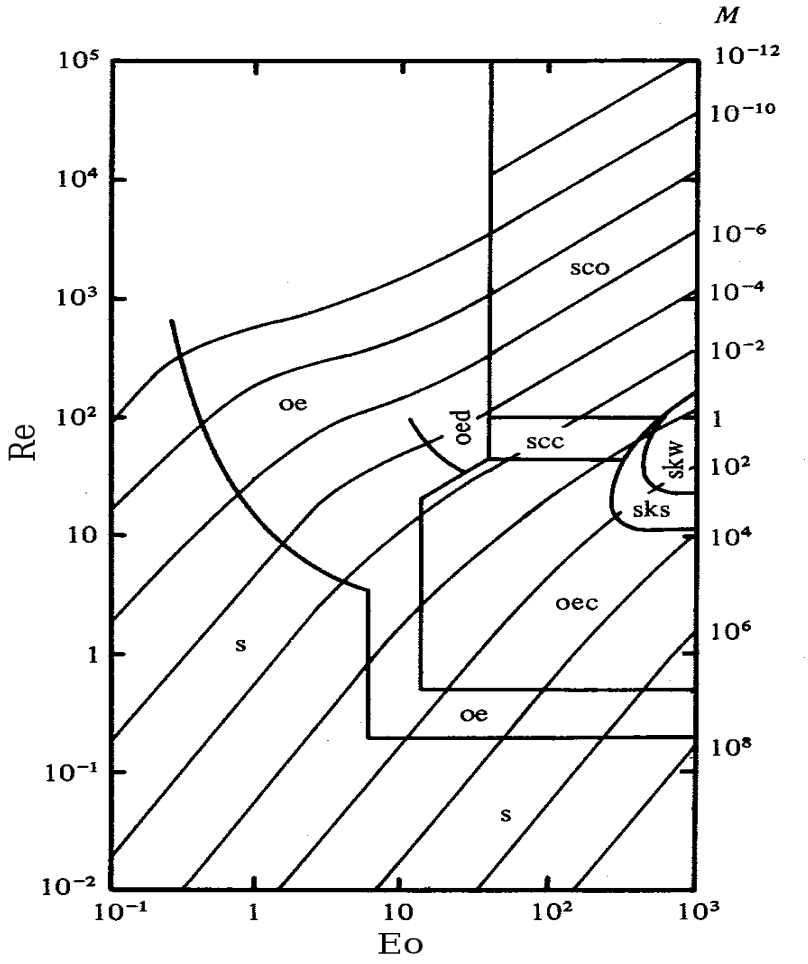

Figure 11: Typical bubbles shapes in aqueous sugar solutions (Bhaga & Weber, 1981)

S: Spherical, OE: oblate ellipsoidal, OED: oblate ellipsoidal disk, OEC: oblate ellipsoidal cap, SCC: spherical cap, closed wake, SCO: spherical cap, open wake, SKS: skirted, steady skirt, SWS: skirted, wavy skirt.

Experimental investigations have shown that flow changes dramatically with increasing Reynolds number. In order to obtain a steady axisymmetric and steady planar-symmetric flow regime, the Reynolds number lies in the different ranges respectively 20 < Re <210 and 210 < Re <270 (Taneda,1956,1978; Wu,1993; Natarajan,1993; Nakamura,1976; Margavey and Bishop, 1961). It is clear from Figure 11 that increasing the Re makes the flow more complex with varying bubble shapes. For simplicity, the present study was limited to a steady state flow regime with Re ≤ 270 and simulate only flow over a spherical bubble shape.

In a bubble column, fluid flowing around the moving bubbles in the entire column can be modelled most intuitively using a moving frame of reference. An alternative way of modelling is to fix a stationary bubble in the column and track the relative velocity between the fluid and the bubble. In this present study, the bubble is assumed to be stationary and the bubble size does not change as the fluid flows over the bubble surface. In practice, the velocity vector field is supposed to change since the bubble dissolves (Ponoth and McLaughlin, 2000); the velocity field was assumed to be steady as in the case of a bubble at its terminal velocity.

4.1.1. Mesh Generation

In order to simulate the fluid flow over a spherical bubble as assumed above, a good quality mesh is generated using the software called Gambit. Gambit software is used for meshing applications where it defines the domain geometry and generates the mesh grid.

A two dimensional axisymmetric grid is used under the assumption that there are no velocity gradients in the angular direction. For spherical coordinates, the points are referenced as (r, θ,φ) but with the axisymmetric condition, gradients with respect to φ are zero. Therefore the geometry axisymmetrically revolves around the x-axis of the domain alongside with the two dimension grid makes the Navier stokes equation easier to solve and requires less time to solve and is thus more computationally

efficient.

A two dimensional axisymmetric rectangular mesh grid of width 0.025m, height 0.015m and triangular structured mesh elements is used for the simulation with a bubble of diameter d= 0.005m. Using the general accepted rules of thumb in the field of CFD modelling (Thompson *et al*., 1998), the spherical bubble is located 10xd away from the inlet walls so that wall effects on the sphere are negligible.

The typical boundary conditions for the mesh grid; velocity inlet, outlet, wall, axis, and the bubble wall are implemented in the mesh generation to describe the required flow pattern. Additionally, the conditions of the simulation are provided as follows:

- **Velocity inlet -** The Dirichlet boundary condition involves specification of the inlet velocity as stated in Equation 19. The inlet velocity was varied from 0.02675 to 0.2408 m s^{-1} corresponding to the Reynolds number range of 30 to 270 for laminar flow at 298.15K.

- **Outflow -** In this case, there is no pressure or velocity specification since the solution at the outlet is extrapolated from the interior. The outflow boundary, which is intended for incompressible flow and is also where mass balance correction is applied.

- **Bubble -** A nitrogen mass fraction of $1.75\ \mathrm{e}^{-5}$ was specified for the species boundary condition. The calculation of the mass fraction is explained in section 6.1. It has been shown that the boundary condition on a bubble in a contaminant free system corresponds to a zero-shear-stress one, rather than a no-slip boundary condition, which would be applicable to rigid particles (Hadamard, 1911). Vasconcelos *et al*. (2002) also showed that surfactants affect the mass transfer rates and bubbles to behave like solid spheres. It is therefore assumed that there are no contaminants in the liquid and that the interfacial tension is constant

- **Wall -** The walls are also assumed to be stationary with no flux of species (zero diffusive flux). This is because, these walls do not represent the actual

walls of a bubble column, but are only used to create a computational domain where the fluid around the bubble is bound. Therefore, the effects of the confining wall are neglected and zero-shear-stress (free-slip) condition is applied.

Figure 12 illustrates the axisymmetric geometry which is finer closer to the bubble and coarser in the outer region. Meshes are made finer in the regions where there are large variations from node to node and enable the gradients of velocity and concentration near the sphere to be resolved numerically.

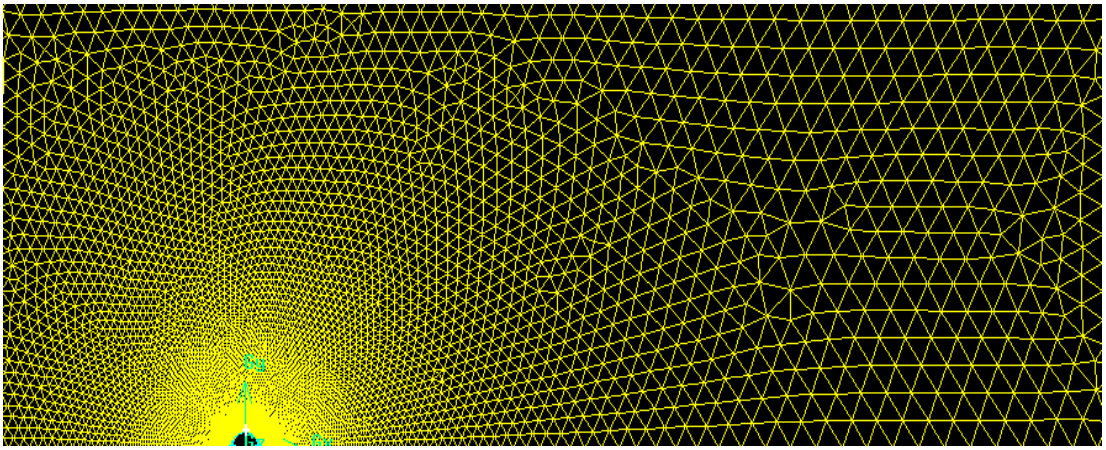

Figure 12: Axisymmetric grid and mesh generation around spherical bubble

4.1.2. Mesh Optimization

It is required of any CFD simulation that the solution be converged and independent of the resolution of the mesh. Mesh quality is usually measured by the grid skewness; Equisize Skew and EquiAngle Skew, smoothness and aspect ratio (Thompson *et al*., 1998; Lee *et al*., 1991; Silva *et al*., 2011; You *et al*., 2006).

Mesh quality simply means, the ability of the mesh to capture and improve resolution of all relevant features without increasing the computational effort. An acceptable mesh must have low skewness, smooth change in size and an aspect ratio of one in order to be accurate. The difference between an element with low and high skewness is shown below in Figure 13.

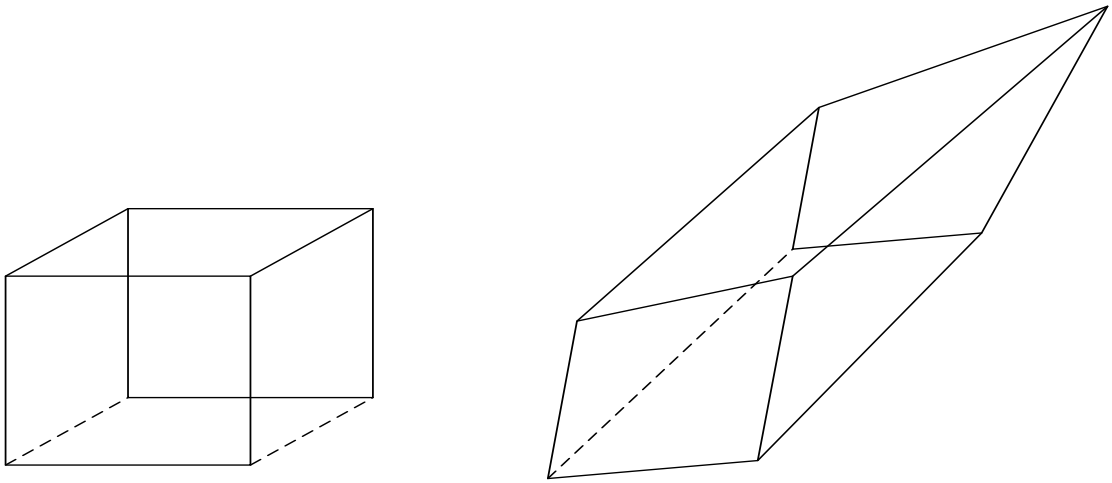

Figure 13: An Element with low skewness (left) and high skewness (right)

Depending on the cell geometry, the desired situation is obtained when majority of the cells are found with Equisize Skew and EquiAngle Skew values between 0 and 0.7 respectively. Most often, a tetrahedral mesh does not meet this criterion (Silva *et al*., 2011).

Different mesh grids with different mesh faces are generated and simulated in order to get the mesh grid which is independent of the solution. Finally, a mesh size with approximately $1.68\,\mathrm{e}^5$ mesh faces and 100% of the cells within the Equisize Skew range is chosen as the grid used for the entire simulation process.

4.2. Model System

The BCM developed in Coetzee *et al*., (2009), simulates the immediate flow regions around individual bubbles in a Bubble column from the Reynolds number using an algebraic flow model. In other words, the BCM is a hybrid between analytical and statistical methods which improves the simulation accuracy and reduces the number of parameters of the flow model by solving the Navier-stokes equation over a fixed spherical bubble.

The discretization schemes for solving the governing equations was the Second-order Upwind whereas the pressure-velocity coupling scheme was Phase Coupled SIMPLE in Fluent 13.0. The SIMPLE scheme is a standard pressure correction algorithm for finite volume calculations and is adequate for incompressible viscous flow. This scheme was chosen because it minimizes the false diffusion presented in

other interpolation techniques such as the first order upwind. (Tu *et al*., 2008; Pantankar, 1980)

The parameters for the BCM are estimated in two fitting stages as shown in Figure 14 below. Stage one involves fitting every steady state velocity vector field with respect to the radial and angular coordinates at a specified Reynolds number range. Stage two involves the cross correlation of stage one model with respect to Reynolds number.

In simpler terms, in stage one the BCM parameters are fitted for any given Reynolds number while in stage two, the BCM parameter is varied in Reynolds number and a model is proposed for each parameter as a function of Reynolds number. This enables the entire velocity vector field to be generated when given only the Reynolds number.

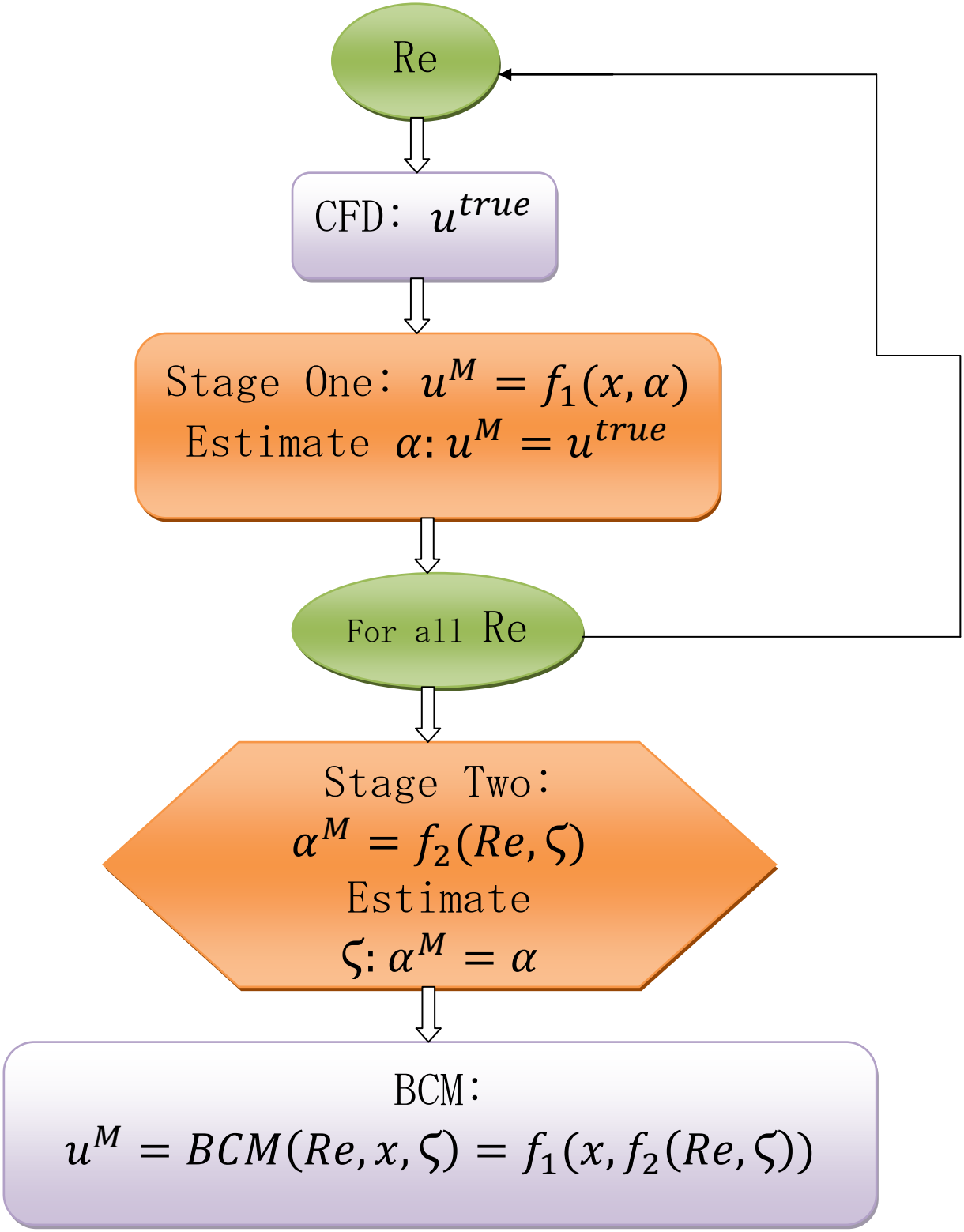

Figure 14: BCM fitting stage strategy where f_1, α, f_2 and ς are the overall stage one model, stage one parameter, stage two model and parameters respectively (Coetzee et al.,2009)

4.2.1. Stage One: Analytical and Statistical Modelling

4.2.1.1. Analytical Modelling

In modelling those regions of the fluid where the fluid flow rate is extremely low, the steady-state incompressible Navier−Stokes equations were solved using the creeping flow and axisymmetric flow assumption. Formulating the Navier−Stokes equations in terms of the Stokes stream function ($\boldsymbol{\varphi}$) in spherical coordinates simplify the problem considerably. The stream function is shown below in Equation 20.

$$\boldsymbol{\varphi} = -\frac{1}{2}\boldsymbol{r^2}[\boldsymbol{u_\infty}]\boldsymbol{sin^2\theta} \quad \textbf{(20)}$$

The Creeping Flow (CF) means the convective terms in Equation 17 become zero (Re << 0.1). Combining the Creeping Flow boundary conditions with Slattery (1999)'s solution where stream function is proposed to be a fourth order polynomial in equations 21-25 yielding equations 26-27. Figure 15 shows the simulated creeping flow velocity contours at Re=270 with the radial and angular components, r and θ, centered on the bubble and u_∞ is the actual bubble velocity (Coetzee *et al*., 2012b, c).

$$\boldsymbol{u_r} = \frac{\mathbf{1}}{\boldsymbol{r^2}\,\mathbf{sin}(\boldsymbol{\theta})}\frac{\boldsymbol{\partial\varphi}}{\boldsymbol{\partial\theta}} \quad \textbf{(21)}$$

$$\boldsymbol{u_\theta} = \frac{\mathbf{1}}{\boldsymbol{r}\,\mathbf{sin}(\boldsymbol{\theta})}\frac{\boldsymbol{\partial\varphi}}{\boldsymbol{\partial r}} \quad \textbf{(22)}$$

$$\boldsymbol{u_{r|\,r\to\infty}} = \boldsymbol{u_\infty}\,\mathbf{cos}\,\boldsymbol{\theta} \quad \textbf{(23)}$$

$$\boldsymbol{u_{r|\,r=R}} = \mathbf{0} \quad \textbf{(24)}$$

$$\frac{\boldsymbol{du_{\theta|\,r=R}}}{\boldsymbol{dr}} = \mathbf{0} \quad \textbf{(25)}$$

$$\boldsymbol{u_r CF(r,\theta)} = \boldsymbol{u_\infty}\left[\mathbf{1} - \frac{\mathbf{3}}{\mathbf{4}}\left(\frac{\boldsymbol{R}}{\boldsymbol{r}}\right) - \frac{\mathbf{1}}{\mathbf{4}}\left(\frac{\boldsymbol{R^3}}{\boldsymbol{r}}\right)\right]\mathbf{cos}\,\boldsymbol{\theta} \quad \textbf{(26)}$$

$$u_\theta CF(r,\theta) = u_\infty \left[1 - \frac{3}{8}\left(\frac{R}{r}\right) - \frac{1}{8}\left(\frac{R^3}{r}\right)\right] \sin\theta \quad (27)$$

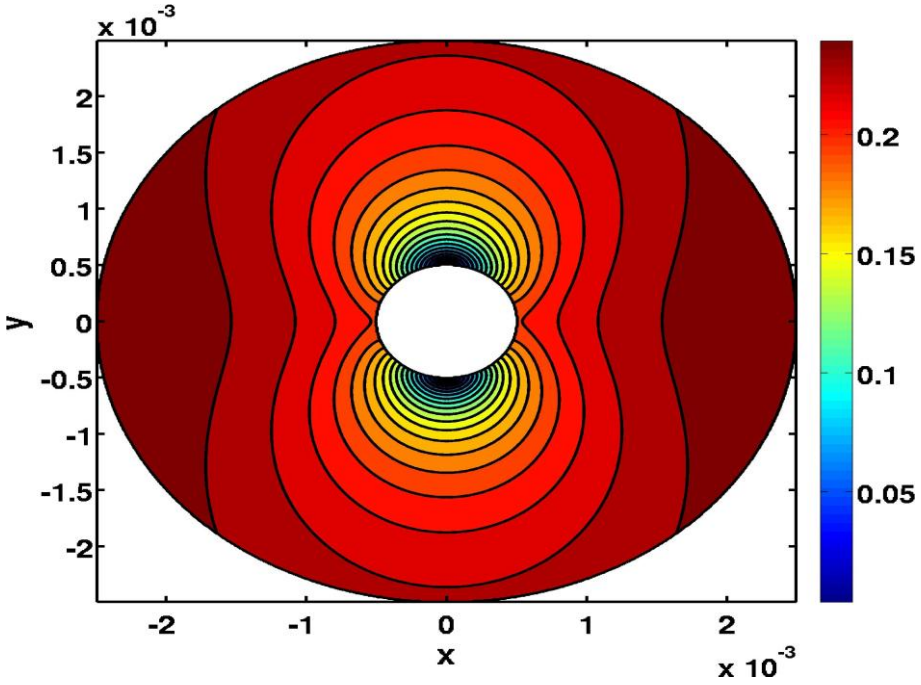

Figure 15: Velocity vector fields around bubble in Creeping Flow at Re=270 (*Coetzee et al., 2012b, c)*

The opposite extreme to creeping flow is inviscid flow meaning a fluid with no viscosity. Zero viscosity fluids do not exist; however, the assumption provides a good description of the velocity profile except near the body and beyond the line of flow separation. The velocity potential, Φ, is defined such that $u = -\nabla\ \Phi$, the free slip boundary condition, upon differentiation yields Potential Flow (PF) velocities in equation below 28-29. It should be noted that Potential Flow as follows from Equation 17 is when the viscous terms are zero and Reynolds numbers goes to Infinity (Coetzee *et al*., 2012b, c).

The simulation carried out with the Potential flow conditions yields the solution shown in Figure 16. A complete solution from the Navier stokes equations simulated in CFD illustrated in Figure 17 (Coetzee *et al*., 2012b, c).

$$u_r PF(r,\theta) = u_\infty \left[-1 + \left(\frac{R^3}{r}\right)\right] \cos\theta \quad (28)$$

$$u_\theta PF(r,\theta) = u_\infty \left[1 + \frac{1}{2}\left(\frac{R^3}{r}\right)\right] \sin\theta \quad (29)$$

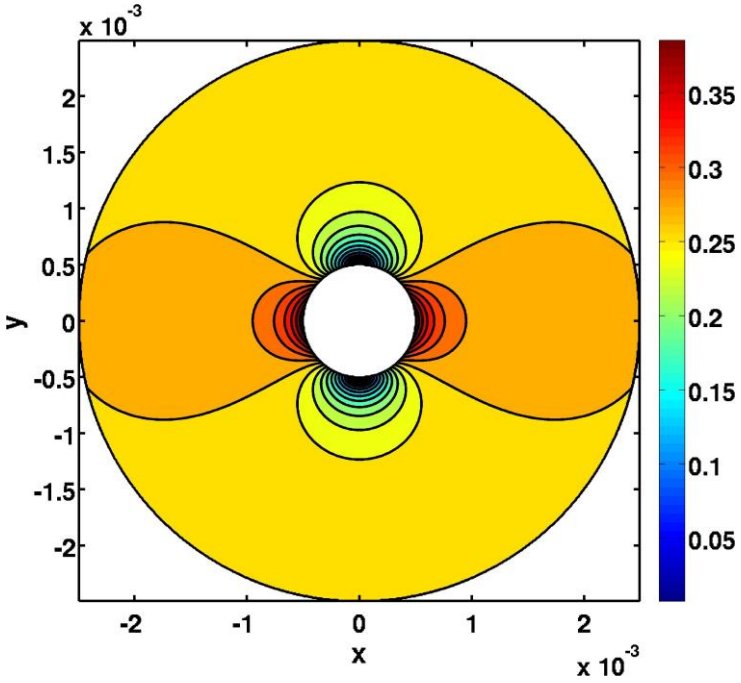

Figure 16: Velocity vector fields around bubble in Potential Flow at Re=270 (Coetzee et al., 2012b, c)

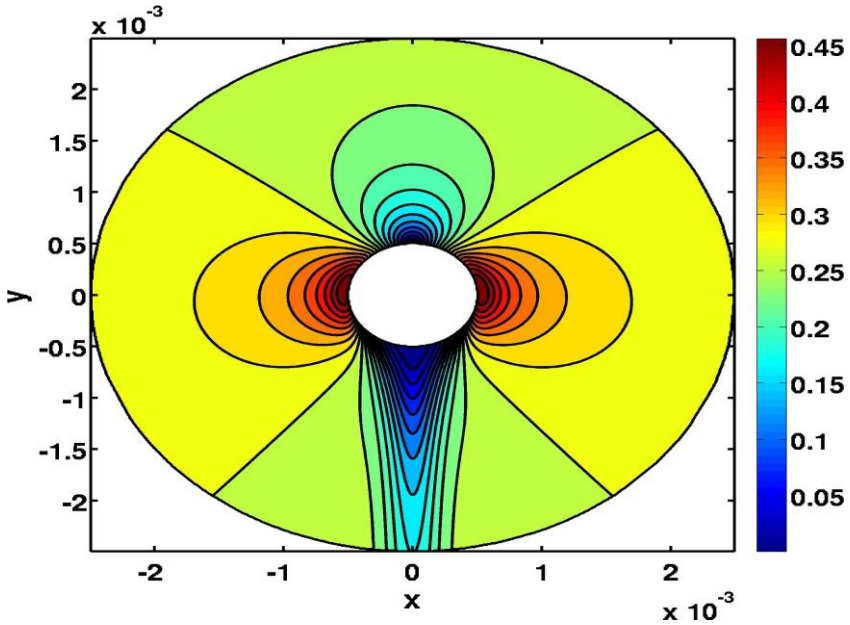

Figure 17: Velocity vector fields around bubble from complete simulation of Navier-Stokes Equations at Re=270 (Coetzee et al., 2012b, c)

Under these assumptions, simple analytical solutions in the form of algebraic expressions result; these forms can be rapidly evaluated and incur minor computational expense. Unfortunately, the analytical solution is not able to capture the flow separation and wake features at the rear of the bubble, which occur at very low Reynolds number. Therefore, the analytical model cannot predict flow at the rear of the bubble and limits its applicability for hydrodynamic calculations (Coetzee *et al.*, 2012b, c).

4.2.1.2. Statistical Modelling

The two extreme conditions in modeling fluid flow are creeping and potential (Inviscid) flow models where $Re = 0 \; and \; Re = \infty$; are combined to account for accurate flow structure in any flow regime. The stage one parameters, α_{ij}, are defined such that $_i$ is either the radial or angular coordinate and $_j$, the type of flow model. The linear combination of the two solutions is shown in Equation 30-31 where $\alpha_{1,1} \; to \; \alpha_{2,2}$ are the weighting coefficients obtained through linear least squares with respect to the true velocity, u^{true} (Coetzee *et al.*, 2012b, c).

$$\boldsymbol{u_{r,A}^{M} = \alpha_{1,1} \, u_r, CF + \alpha_{1,2} \, u_r, PF} \boldsymbol{(30)}$$

$$\boldsymbol{u_{\theta,A}^{M} = \alpha_{2,1} \, u_\theta, CF + \alpha_{2,2} \, u_\theta, PF} \boldsymbol{(31)}$$

The residuals for the nonlinear data in Equations 30 and 31 are evaluated using the regression with Empirical modelling strategy. An accurate CFD computational solution is characterized by convergence of the iterative process, the grid independence and the use of acceptable solution methods. The grid independence justifies the grid choice for simulation. The convergence of the iterative process is obtained by calculating the imbalances, called residuals, in the algebraic equations.

Residuals can be viewed as estimates of computational errors that indicate how accurate the results are. Accurate results further indicate that the system has reached quasi-steady state. Once this state is achieved, average quantities are calculated in terms of the time, axial and radial coordinates. It should be noted that Fluent 13.0 is a deterministic model and therefore does not have any experimental errors coupled with it.

4.2.1.2.1. Empirical Method

The residuals of the radial and angular velocity are treated by fitting the residual velocity surfaces across the Reynolds operating range and identifying where simple functions can form residuals to the solution. The symmetry at *x=0* helps to simplify the problem (Coetzee *et al*., 2012 b, c).

$$\boldsymbol{u_{r,res} = u_r^{true} + u_{r,A}^{M}} \ (\mathbf{32})$$

$$\boldsymbol{u_{\theta,res} = u_\theta^{true} + u_{\theta,A}^{M}} \ (\mathbf{33})$$

The residual of the radial velocity in Equation 32 was basically in the bubble wake region and by identifying the critical angle and the final model had 17 parameters (Figure 18; Coetzee *et al*., 2012b, c). The residual of the angular velocity in Equation 33 was at maximum at the bubble surface which decayed into the radial direction and had 11 parameters left to be solved (Figure 19; Coetzee *et al*., 2012b, c).

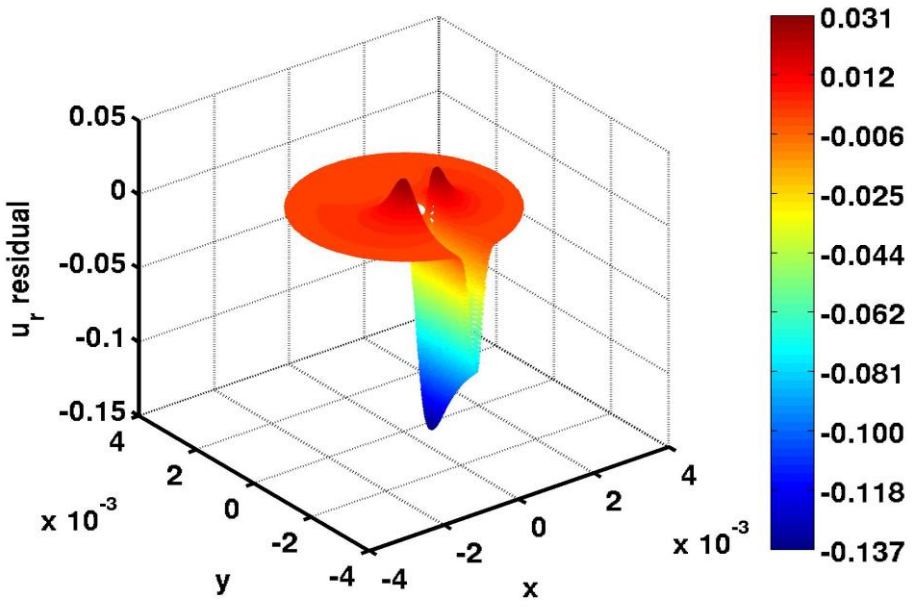

Figure 18: Radial residual around bubble (Coetzee et al., 2012b, c)

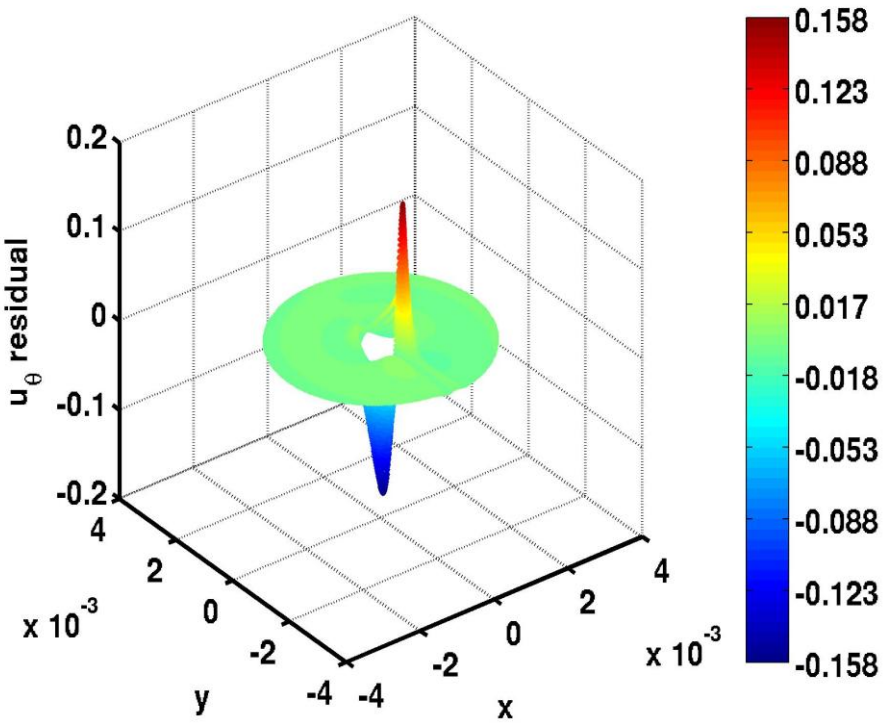

Figure 19: Radial residual around bubble (Coetzee et al., 2012b, c)

Coetzee *et al.,* (2012b, c) discuss these aspects in detail but the final solution results in reasonable approximations to the true model with lower error distributions and the accuracy of the approximation increases with Reynolds number. The close approximation is due to the deviations from the potential flow solution whereby, the wake becomes concentrated in the smaller region as Re increases leading to lower overall error distribution. At lower Re range, the wake spreads out and the approximations become better as creeping flow is reached, and this is expected.

4.2.2. Stage Two: Parameter Optimisation

Stage Two just ensures all first stage parameters, α_{ij}, are in phase and have a good response with respect to the Reynolds number. On exploring a subsequent Re value, the first stage fit was carried out using the parameters of the closest Re value as the initial guess. The α_{ij} with respect to the Re was found to be described by the first and second order polynomial and exponential models. The final parameters to the BCM were found by optimizing all the parameters ς with respect to the original CFD surfaces (Coetzee *et al*., 2012c). A typical example of the behavior of the weighting

coefficients is shown in Figure 20 (Coetzee *et al*., 2012b).

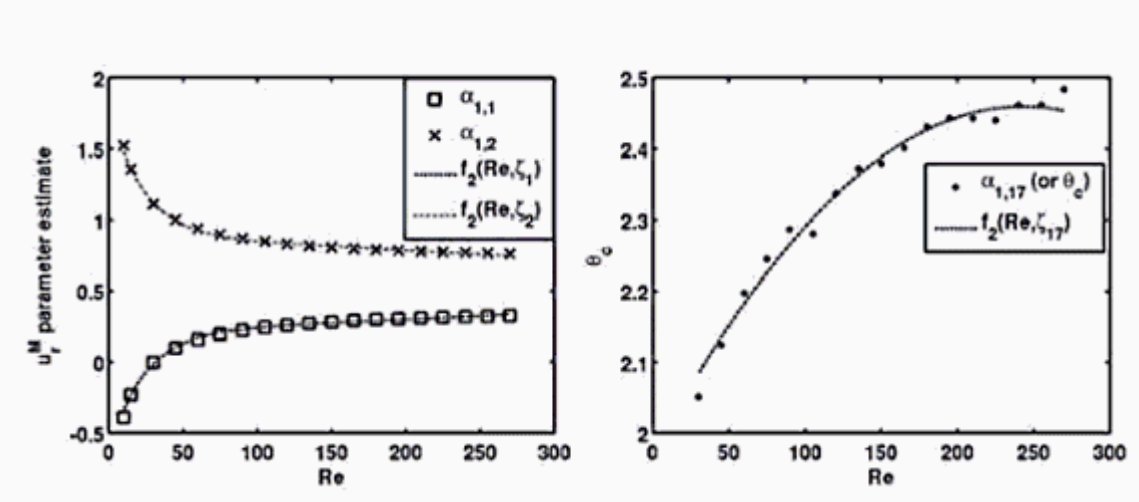

Figure 20: Second Stage Fit of parameters $\alpha_{1,1}$ $and\alpha_{1,2}$ (Coetzee et al., 2012b)

4.2.3. BCM Development

The creeping and potential flow analytical solutions discussed in the Section 4.2.1.1 provide good approximations and explain some significant areas of the velocity flow field around the bubble for Re ≤270. Unfortunately these analytical solutions do not describe clearly the flow at the rear of the bubble especially at Low Reynolds Numbers.

On the other hand, statistical/Empirical models also gave good fits. Any statistical model must accurately account for deviations from analytical solutions, flexible for any data or bubble shape and require a sensible amount of parameters.

A hybrid between analytical solutions and statistical models has been investigated and gives accurate approximations. Figure 21 and 22 illustrate individual models, the simulated results from combining both models for appreciation and comparison with CFD data are validated.

Therefore, a new approach was been developed by Coetzee et al. (2009) to simulate bubble columns derived by combining the analytical and statistical modeling solutions to obtain steady state velocity field vectors over a sphere（Coetzee *et al*., 2012b).

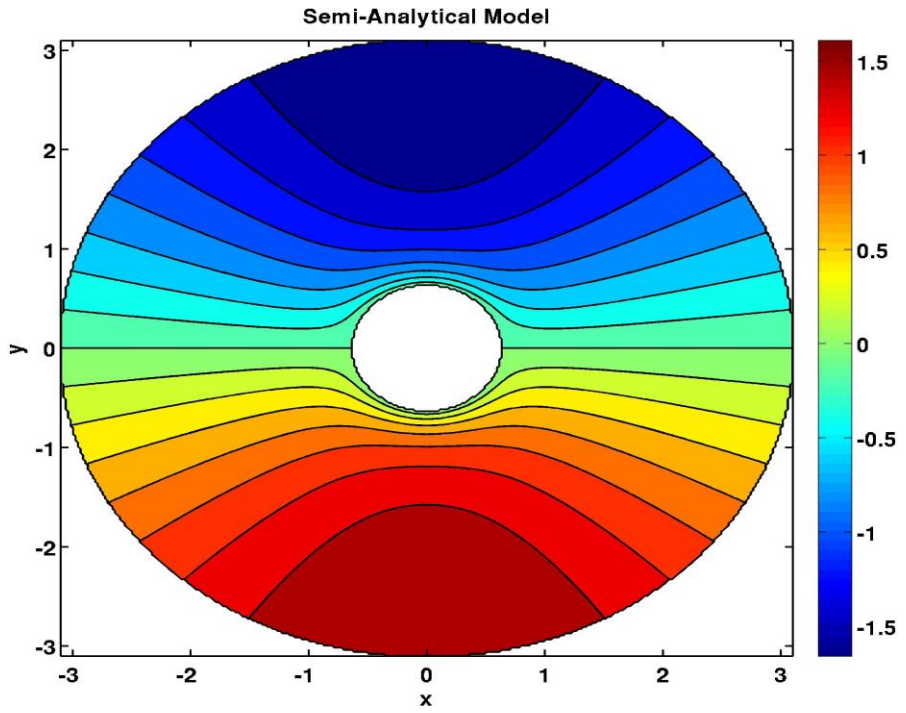

(a) Semi-Analytical Model for Radial Co-ordinates

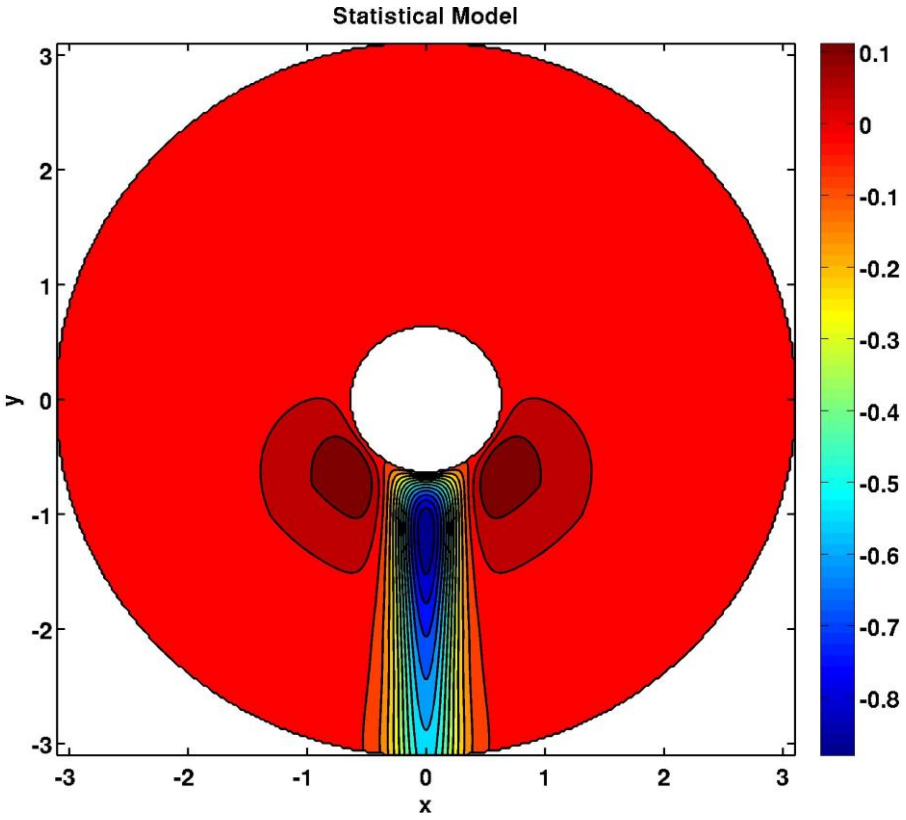

(b) Statistical Model for Radial Co-ordinates

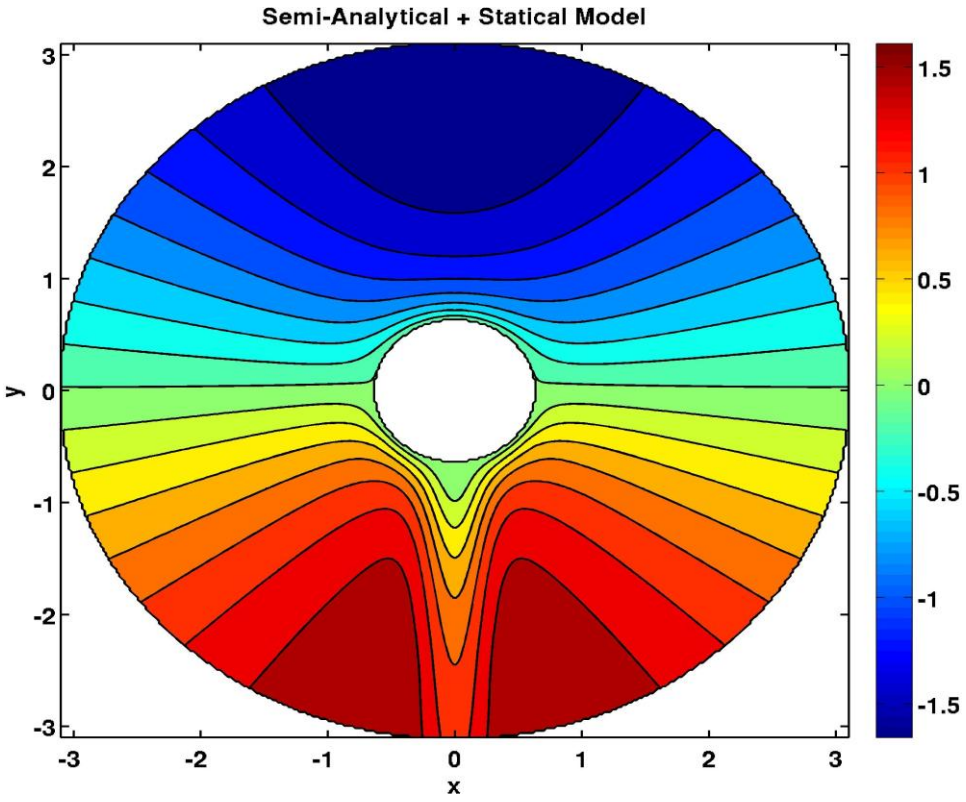

(c) Semi-Analytical and Statistical Model for Radial Co-ordinates

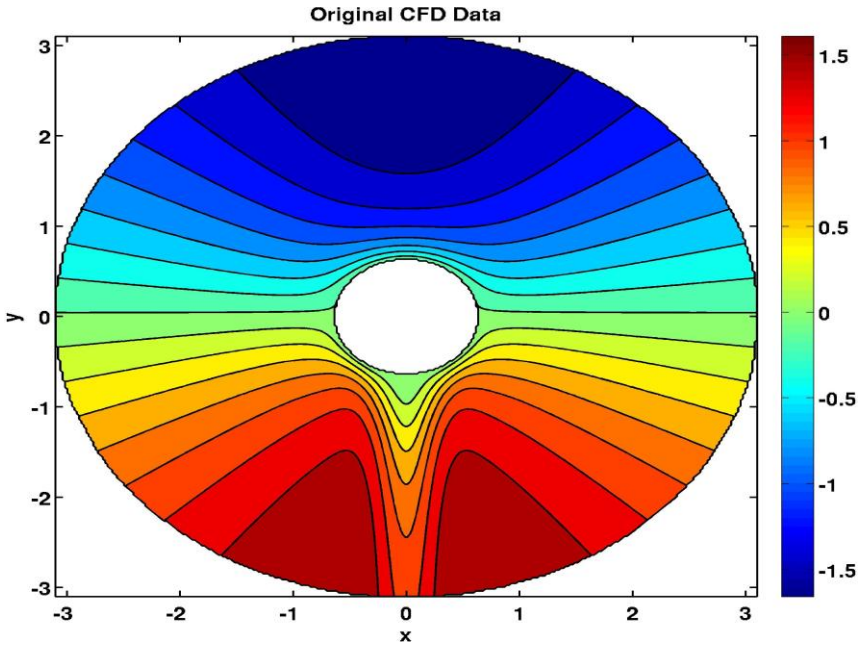

(d) Original CFD Data for Radial Co-ordinates

Figure 21: Comparison of Semi-analytical, Statistical, Semi-analytical and Statistical models with Original CFD Data for Radial Co-ordinates (Coetzee et al., 2012b)

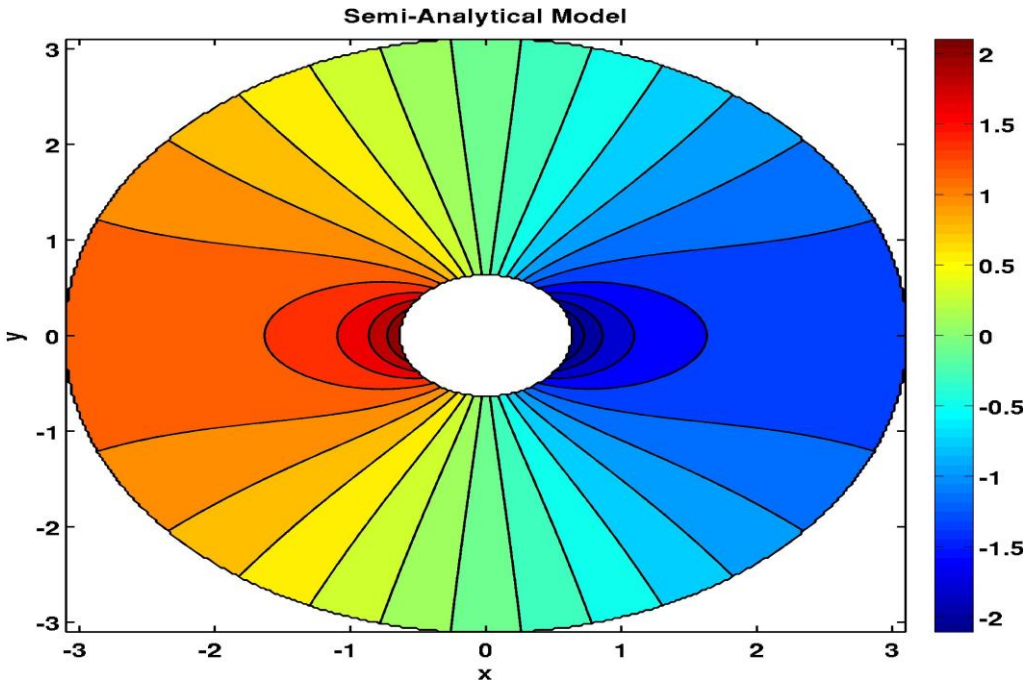

(a) Semi-Analytical Model for Angular Co-ordinates

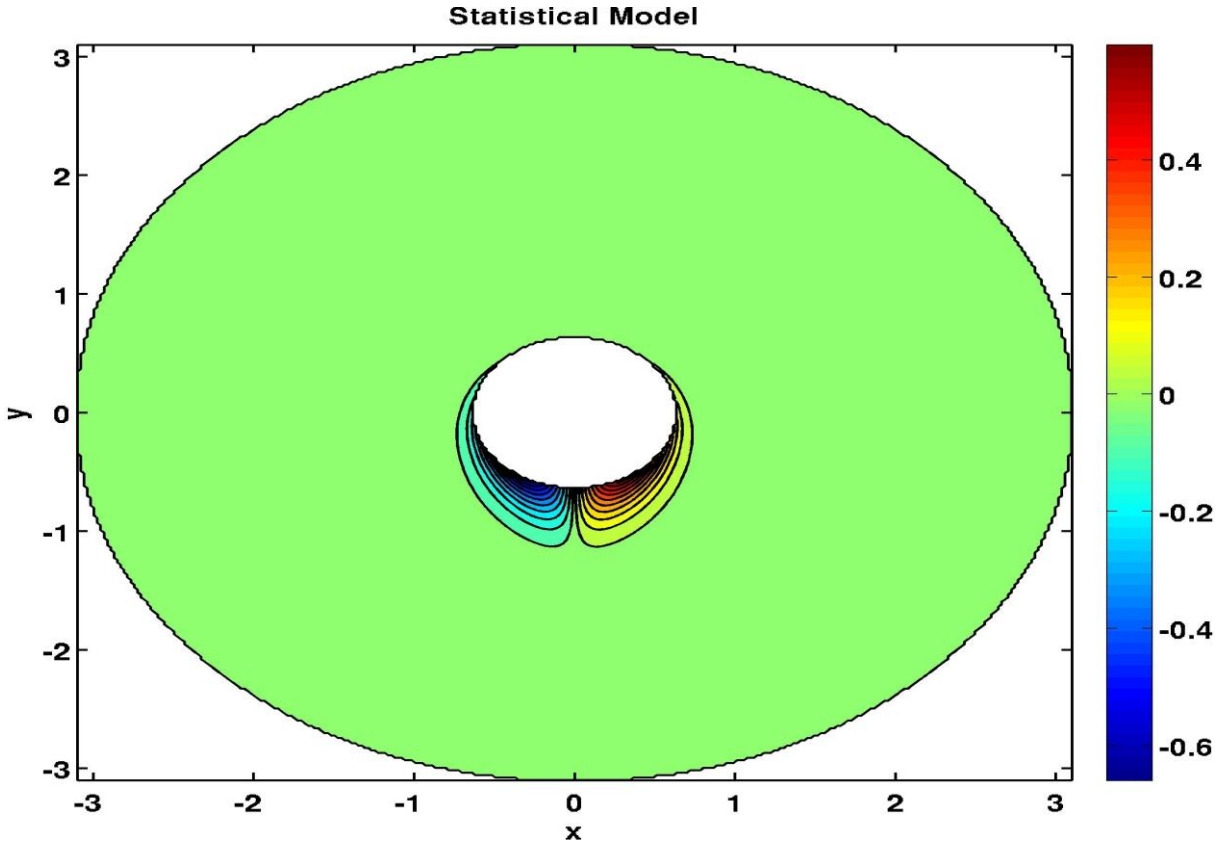

(b) Statistical Model for Angular Co-ordinates

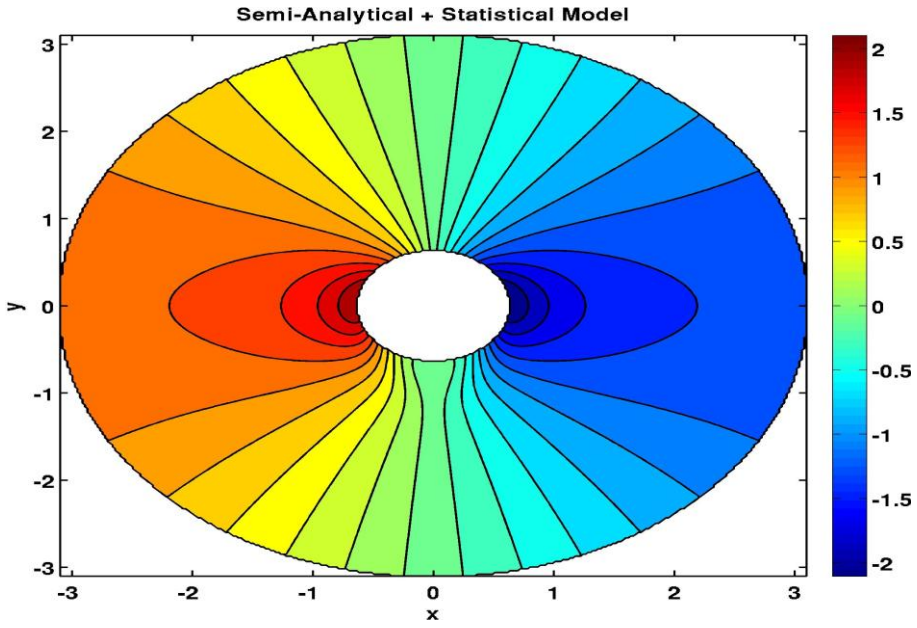

(c) Semi-Analytical and Statistical Model for Angular Co-ordinates

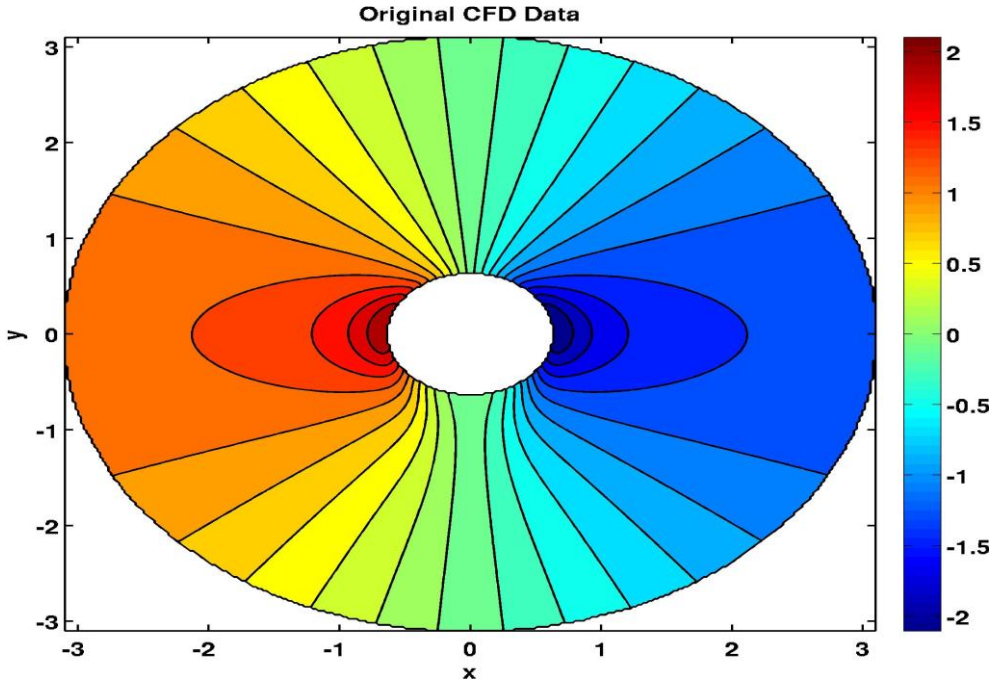

(d) Original CFD Data for Angular Co-ordinates

Figure 22: Comparison of Semi-analytical, Statistical, Semi-analytical and Statistical models with Original CFD Data for Angular Co-ordinates (Coetzee et al., 2012b)

Chapter 5 Mass Transfer Extension to the BCM

5. Mass Transfer Extension to the BCM

The flow around the bubble surface is analyzed by using the BCM developed by Coetzee *et al.* (2009, 2012a, b, c) which predicts the velocity vector fields around single bubbles in bubble column reactors. This model lacks the ability to predict average mass transfer coefficients; therefore a material/species balance capable of predicting the concentration field in the vicinity of the bubble is integrated into the model. The ANYSY CFX computer package (Fluent 13.0) is used to develop the simulation. The computer package uses the finite volume technique which generates the flux in its numerical solutions. The overall outcome is achieved by running several CFD simulations. The CFD results are then used to identify the average boundary layer which can then be used to determine the mass transfer coefficient.

5.1. Mass Transfer from Sphere

Mass transfer from a sphere to a flowing fluid applies the steady state transport equation (Navier-stokes and diffusion equations) shown below in Equation 34. This transport equation is derived by assuming constant diffusivity with no chemical reaction and is dependent on velocity.

The concentration in the sphere, C_o, remains constant and is assumed to be negligible compared to the overall concentration in the system. The concentration diffused to the external flowing stream is C_1. Equation 34 in its dimensionless form is Equation 35 and rearranging yields Equation 36 in terms of the cylindrical co-ordinates (Finlayson, 1972).

$$\boldsymbol{u}.\boldsymbol{\nabla c} = \boldsymbol{D_{AB}}\,\boldsymbol{\nabla^2 c} \quad (\mathbf{34})$$

$$\boldsymbol{c} = \frac{\boldsymbol{C} - \boldsymbol{C_1}}{\boldsymbol{C_0} - \boldsymbol{C_1}} \quad (\mathbf{35})$$

$$\boldsymbol{u_r}\frac{\boldsymbol{\partial c}}{\boldsymbol{\partial r}} + \frac{\boldsymbol{u_\theta}}{\boldsymbol{r}}\frac{\boldsymbol{\partial c}}{\boldsymbol{\partial \theta}} = \frac{\boldsymbol{D_{AB}}}{\boldsymbol{r^2}}\left[\frac{\boldsymbol{\partial}}{\boldsymbol{\partial r}}\left(\boldsymbol{r^2}\frac{\boldsymbol{\partial c}}{\boldsymbol{\partial r}}\right) + \frac{\mathbf{1}}{\mathbf{sin}\,\boldsymbol{\theta}}\frac{\boldsymbol{\partial}}{\boldsymbol{\partial \theta}}\left(\mathbf{sin}\,\boldsymbol{\theta}\frac{\boldsymbol{\partial c}}{\boldsymbol{\partial \theta}}\right)\right] \quad (\mathbf{36})$$

For negligible internal resistance and constant concentration in the sphere, the boundary conditions are Equations 37-40 (Clift *et al.,* 1978)

$$c_{|\,r\to R} = c_s \ (37)$$

$$c_{|\,r\to\infty} = c_\infty \ (38)$$

$$\frac{\partial c}{\partial \theta}_{|\,\theta\to 0} = 0 \ (39)$$

$$\frac{\partial c}{\partial \theta}_{|\,\theta\to \Pi} = 0 \ (40)$$

The Sherwood number is of primary interest when mass transfer is concerned and occurs when rearranging Equation 36 yields Equation 41(Finlayson, 1972).

$$Sh = \int_0^{\pi} \left(-\frac{\partial c}{\partial r}\right) \sin\theta \, d\theta \ (41)$$

For fluid sphere in creeping flow, Hadamard (1911) solved the Equation 36 numerically and approximated the following equation below.

$$Sh = 1 + \left(1 + 0.564 Pe^{2/3}\right)^{3/4} (42)$$

For Pe → 0, the solution emulates a situation where diffusion occurs into a stagnant fluid and Equation 42 becomes Equation 43 and applies to fluid and spheres (Dani *et al.,* 2006; Clift *et al.*, 1978).

$$Sh = 2 \ (43)$$

For Pe → ∞ the asymptotic solution Equation 43 becomes Equation 44 (Clift *et al.*, 1978).

$$Sh = 0.691 Pe^{1/2} \ (44)$$

At higher Reynolds numbers, Lochiel and Calderbank (1964) have proposed Equation 45. When the Reynolds number is very high, potential flow is observed and Equation 45 becomes Equation 46 (Dani *et al.,* 2006; Clift *et al.*, 1978).

$$Sh = 1.13 \left[1 - \frac{2.96}{Re^{1/2}}\right]^{1/2} Pe^{1/2} \ (45)$$

$$\boldsymbol{Sh = 1.13 Pe^{1/2}} \ \boldsymbol{(46)}$$

It should be pointed out that these Equations shown above are attempts derived from first principles and not from actual simulations. Dani *et al.,* (2006) developed equations from actual simulations on a spherical bubble with results agreeing to the film theory. However, their accuracies are to be put under scrutiny since the equations are empirical.

Chapter 6 Model Simulation

6. Model Simulation

6.1. Input and Output Parameters

The most important aspect of the simulation is the incorporation of the material balance into the fluent solver. For a basic fluid flow, only the species transport is used with no inlet diffusion and energy source. The materials required for the mass balance are selected and specific parameters such as; viscosity, density and mass diffusivity for the mixture are defined.

A non-reactive steady state nitrogen-water system is chosen to predict the mass transfer coefficient as a function of Re and Sc numbers. The velocity and mass diffusivity of nitrogen gas into liquid water are the only changing variables in the definition of Re and Sc numbers respectively. It should be noted that the mass diffusivity of water into nitrogen is assumed to be negligible in the present study.

The inlet velocity and species mass fraction, species mass diffusivity are imported into the CFX computer package (Fluent 13.0) and solved mathematically to get simulated results. Upon validation, the applications can later be extended to reactive systems. The physical properties of nitrogen-water system are shown in the Table 5 below. An incompressible laminar isothermal steady state process in two-dimensional flow is used for the research study.

Table 5: Physical Properties of Nitrogen and Water at 293.15K and 1atm

Properties	Nitrogen (gas)	Water (liquid)	References
Density, ρ (kg/m^3)		998.2	Weast,1988
Diffusivity, D_{AB} $10^9(m^2/s)$	2.36		Sada *et al*,1975
	1.88		Cussler, 2003
	2.01		Ferrel and Himmelblau,1967
Viscosity, μ (Pas)		1000	Weast,1988

A nitrogen mass fraction of $1.75e^{-5}$ at 25°C and 1 atm was derived from the product of N_2 Saturated concentration solubility in water (Henry's Law) at 0.625 mol/m^3 and

the molar mass of nitrogen is $2.8e^{-2}$ kg/mol. This product yields a mass per volume of $1.75e^{-2}$ and density of water, 998.2 kg/m^3.

Fluent 13.0 can simulate various operating conditions such as, laminar and turbulent flows, steady or unsteady states systems. The governing equations from the particular system are converted into algebraic equations. The discretization scheme is selected and formulates the equations on every location on the domain grid. The equations are then iterated over the domain until a converged solution is attained.

6.2. Species Transport Simulation

1. Mesh

Firstly, the axisymmetric mesh grid as shown in Figure 12 is imported into Fluent 13.0. The mesh scale is then verified to ensure that there is no difference in dimensions between Gambit and Fluent 13.0. The mesh grid is checked for co-ordinates, volume and face statistics such as the number of nodes per cell, face cells and so on. Even though, the mesh quality has been guaranteed in Gambit, Fluent 13.0 still gives a breakdown of the mesh skewness, smoothness and aspect ratio.

After all these procedures, the grid is ready to be displayed with the grid conditions. The pressure based solver is used with an absolute velocity formulation for the two dimensional planar and steady state system. In this nitrogen-water system, a double precision model was chosen because it resolves any pressure difference that drives flow (driving force) in the geometry. The pressure based model is typically chosen for incompressible flows (Tu *et al*., 2008).

2. Model Definition

This is the definition of the type of model and the mixture properties that is used in the simulation. For a basic fluid flow, only the species transport model is used with no inlet diffusion and energy source. The volumetric species for the mixture are selected; in this case which are nitrogen and water in their pure states.

3. Materials

The nitrogen and water mixture and fluid composition have been defined with the

following properties;

- Density (kg/m^3)– Incompressible ideal gas
- Specific Heat Capacity (j/kg-k) – Mixing law
- Thermal conductivity (w/m-k) – Constant (0.0454)
- Viscosity (kg/m-s) – Constant ($9.0796e^{-5}$)
- Mass diffusivity (m^2/s) – Constant-dilute-approximate ($2.93e^{-5}$)

4. Boundary Conditions

The momentum and species boundary conditions defined in section 4.1.1 are now integrated into the mesh grid. To summarise, the top and bottom walls are stationary with the no slip shear condition and zero nitrogen diffusive flux. The outlet has zero gauge pressure to induce a driving force. The inlet uses a magnitude, normal to boundary velocity specification method and absolute reference frame. The constant inlet velocity magnitude is inserted here. This is the point where the different velocities will be inserted as the Reynolds number is varied. The nitrogen species boundary condition is the specified mass fraction which is a constant defined in section 6.1 above.

5. Reference Values

The reference values are computed from the inlet boundary condition since the inlet velocity is being varied.

6. Solution Methods

Mass conservation within a flow domain is mainly accounted for by correct linkage of pressure and velocity. This is taken into consideration by the solution procedures or algorithms within the CFD codes (Tu *et al*., 2008). The discretization schemes for solving the governing equations was the Second-order Upwind whereas the pressure-velocity coupling scheme was Phase Coupled SIMPLE. This scheme was chosen because it minimizes the false diffusion presented in other interpolation techniques such as the first order upwind. The SIMPLE scheme is a standard pressure correction algorithm for finite volume calculations and is adequate for incompressible viscous flow.

7. **Solution Controls**

Under-relaxation factors assist in achieving a converged solution and moderate the iteration process of the system of algebraic equations that govern fluid flow (Tu *et al*., 2008). Default under-relaxation factors for pressure, density, body forces of 0.3, 1, 0.7 were used respectively and nitrogen mass fraction of $1.75e^{-2}$.

8. **Monitors**

An accurate CFD computational solution is characterised by convergence of the iterative process, the grid independence and the use of acceptable solution methods. The grid independence justifies the grid choice for simulation as demonstrated in Section 4.1.2. The convergence of the iterative process is obtained by calculating the imbalances called residuals in the algebraic equations.

Residuals, in other terms, can be viewed as estimates of computational errors and tell how accurate the results are. Accurate results also show that the system has reached quasi steady state and once in this state, average quantities are calculated in terms of the time, axial and radial coordinates.

9. **Solution Initialization and Run Calculation**

Finally, the solution procedure is initialized from the inlet conditions and the number of iterations required is given. The equations are calculated until steady-state converged concentration profiles are obtained as shown in Figure 24.

10. **Simulation Results**

A unique solution is reached when the residuals fall below certain convergence criteria. The absolute criteria for continuity, x-y velocity and nitrogen concentration are 1^{-12}, $1^{-6}, 1^{-6}$ respectively. Figure 23 shows the residuals converge after the required number of iterations. It should be noted that FLUENT 13.0 is deterministic model and therefore does not have any experimental errors coupled with it.

To simulate the different Reynolds numbers, only the corresponding inlet velocity is changed in the model with the solution initialized. The nitrogen species molar concentration contours around the bubble are generated and imported into Matlab.

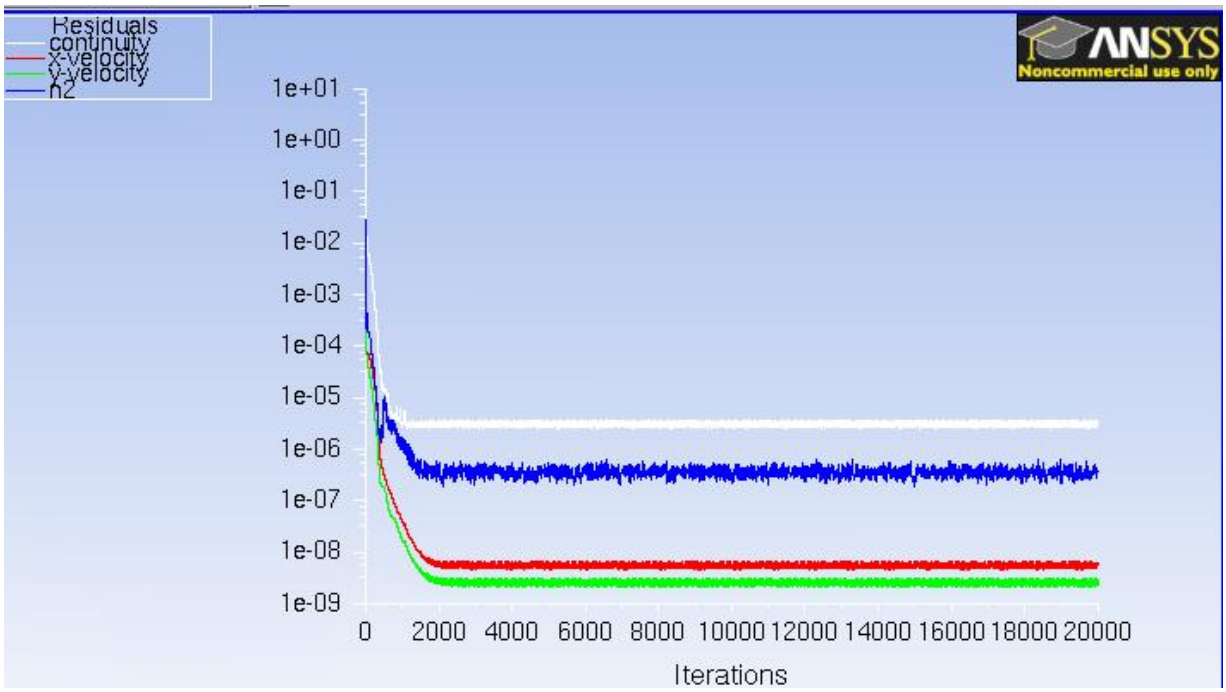

Figure 23: Converged Results from simulation

11. Mass Transfer Results

Mass transfer occurs due to concentration gradients; for this reason concentration profiles are generated. Once the CFD result is obtained, concentration profiles around the bubble are analyzed in the form of concentration iso-surface or boundary layer as in Figure 24. The identification of the species mass boundary layer thickness is defined by the film theory, which as mentioned previously, is the point from the bubble interface to 99% of the concentration of the diffusing component in the bulk liquid.

6.3. Average Boundary Layer Calculations

The iso-concentration contours from the simulation converge to a long tail as seen in Figure 24 and are clearly not uniform around the bubble; it is thinner at the front of the bubble and wider at the rear of the bubble. The mass boundary layer thickness around the bubble therefore, needs to be averaged to obtain a single representative film thickness so as to estimate the average mass transfer coefficient.

To achieve this, the long tail as shown in Figure 25 is cut off and the mass boundary

layer thickness at each angle around the hemisphere of the bubble of the axisymmetric axis are added and averaged as described in Equation 47.

$$\boldsymbol{\delta_m = \frac{1}{\pi}\int_0^{\pi} \delta_m(\theta) d\theta} \quad \boldsymbol{(47)}$$

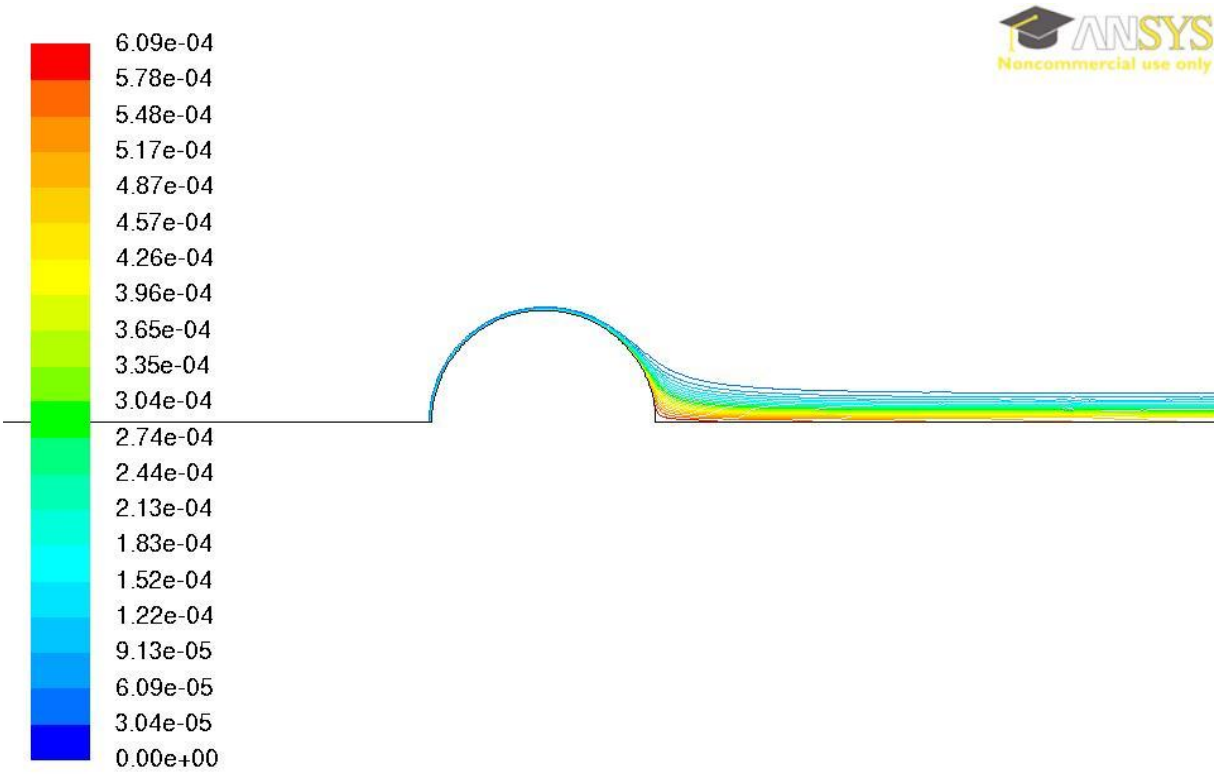

Figure 24: Long Tail of Concentration Iso-surfaces around the bubble

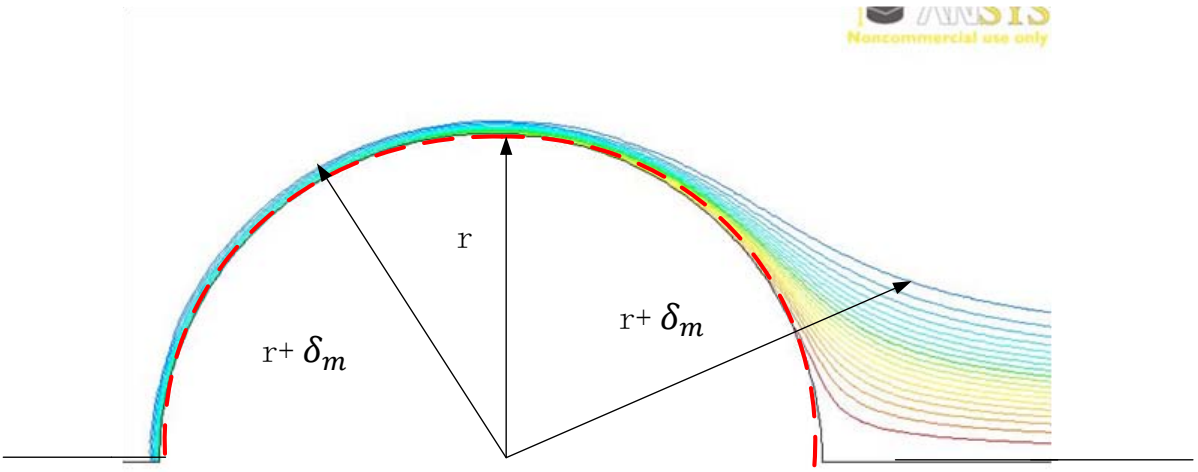

Figure 25: Derivation of the Average Concentration boundary layer with r, radius of bubble and δ_m

To perform the cut-off so that the mass boundary layer thickness is averaged around a bubble; a critical angle that exists where there is a point of flow separation is identified. Beyond this critical angle, there is a high circulation zone where the concentrations normalise such that there is no mass transfer driving force. Clift *et al*. (1978) applied Equation 48 to describe this angle which applies to fluid flow over rigid spheres and θ is in radians (20 ≤ Re ≤ 400).

$$\boldsymbol{\theta_c = 180 - 42.5 \ln\left(\frac{Re}{20}\right)^{0.483}} \quad \textbf{(48)}$$

Yan *et al*., (2002) actually explained this flow of separation with the layer around the rigid sphere thicker than that of a fluid sphere. By analysis, it was showed that the flow of separation near the rear encourages the development of a thicker boundary layer in front of the actual separation point.

On the other hand, Dani *et al*., (2006) shows that the spherical symmetry obtained around bubble at low Re occurs because the mass transfer is controlled by diffusion.

At higher Re numbers this symmetry breaks and the layer at the front of the bubble reduces. In this case, advection becomes the predominant factors controlling mass transfer

6.4. Mass Transfer Coefficient Calculations

The average mass transfer coefficient is calculated using the mass diffusivity and mass boundary layer thickness. The mass diffusivity of nitrogen into liquid water is obtained from experimental results (Sada *et al*., 1975; Cussler, 2003; Ferrel and Himmelblau, 1967). After the CFD simulation has compiled results, the concentration boundary layer around the bubble is located and hence, the mass boundary layer thickness is calculated.

However, the mass boundary layer thickness is not uniform around the bubble as seen in Figure 24. The mass boundary layer thickness is then averaged using Equation 49a. The average mass transfer coefficient is then calculated using the film theory (Equation 49b).

$$\overline{\delta_m} = \frac{1}{\pi}\int_0^{\pi} \delta_m(\theta)d\theta \quad (49a)$$

$$k_l = \frac{D_{AB}}{\overline{\delta_m}} \qquad (49b)$$

This approach of estimating the average mass transfer coefficient stemming from an extension to the BCM is a better approach. The BCM successfully predicts the velocity vectors, so a mass transfer addendum is also going to successfully provide concentration field vectors which are used in the average mass transfer coefficient calculation. Of course, the approach needs to be checked by simulation and compared to methods derived from first principles.

Chapter 7 Results and Discussion

7. Results and Discussion

This section focuses on the simulation results obtained and analysing the effects of Re and Sc numbers on the mass boundary layer thickness and mass transfer coefficients. Thereafter, the method of developing the mass transfer extension to the BCM is explained.

7.1. Boundary Layer Condition and Mass boundary layer thickness

7.1.1. Effect of the Boundary layer condition on Velocity Boundary Layer

Figure 26 shows the velocity contours around bubble at Re = 120 for Sc = 8.58 for free slip and no-slip boundary layer conditions. In free slip, the velocity magnitude at the front and rear of the bubble are low while around the top of the bubble, the velocity magnitude is high. On the other hand, when a no-slip condition is applied, low velocity magnitude is observed around the entire bubble surface and the contours are elongated.

There is shear stress on the bubble surface and the no-slip condition assumes that the fluid velocity at the bubble surface is zero explaining the low velocity magnitude around the bubble. Ponoth and McLaughlin (2000) investigated the mass transfer around a single bubble analysing the concentration contours around bubble and the same observations were made. Therefore, the type of boundary layer condition on the bubble surface has an effect on the velocity boundary layer.

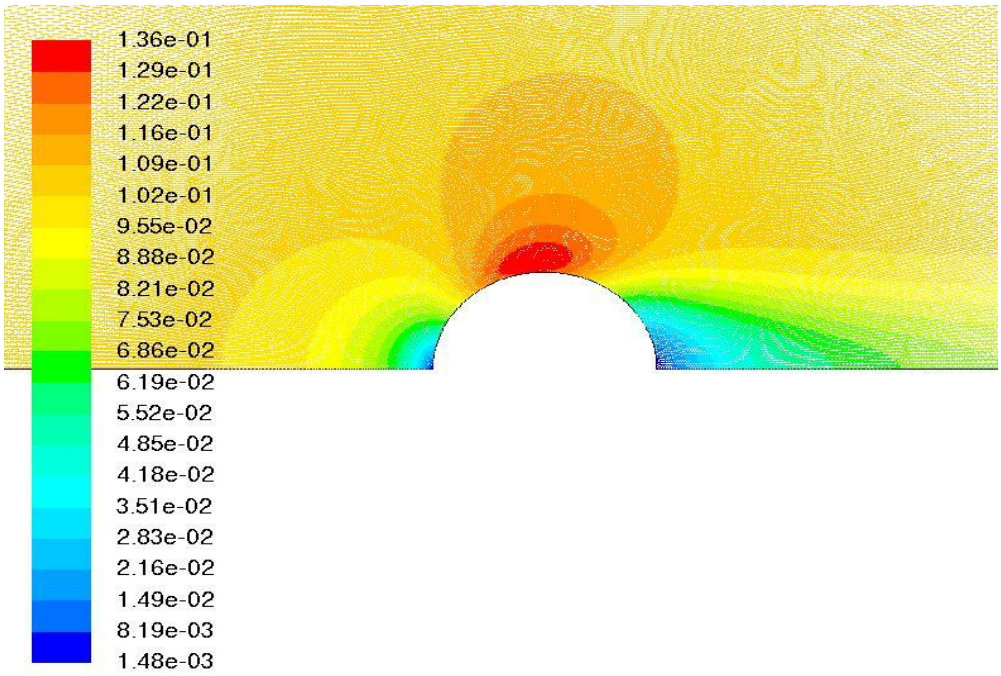

(a) Velocity vectors around bubble at Sc= 8.58 and Re=120 for free slip condition

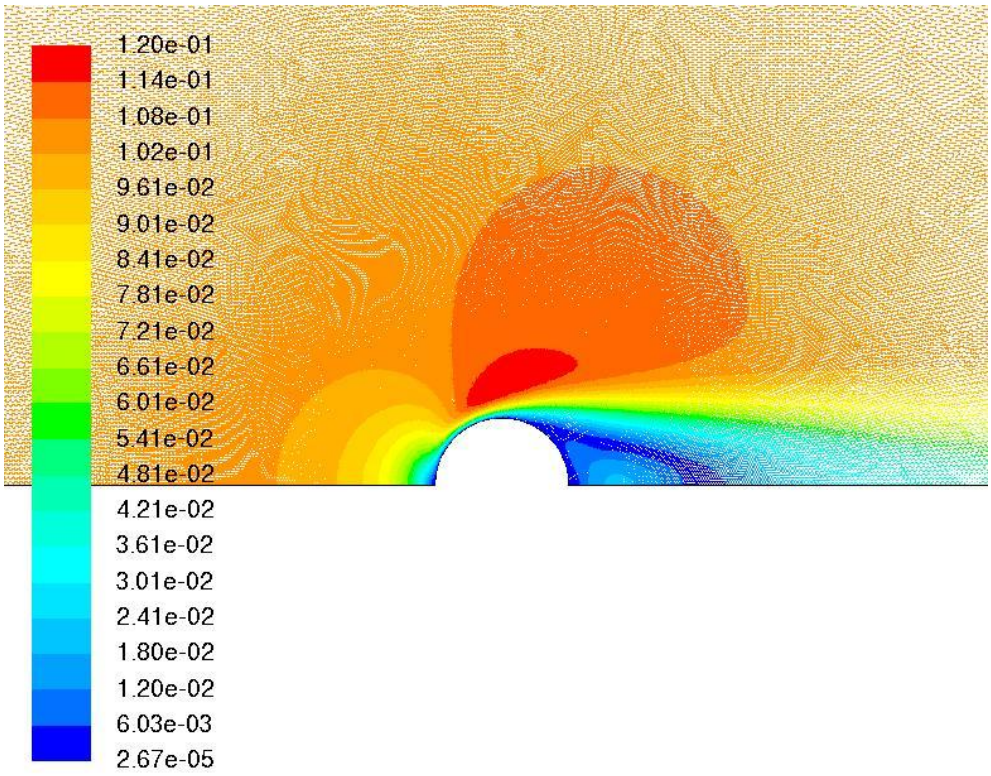

(b) Velocity vectors around bubble at Sc= 8.58 and Re=120 for No-slip condition

Figure 26: Velocity vectors coloured by Velocity Magnitude (m s^{-1}) around bubble for free slip condition and No-slip condition

7.1.2. Effect of the Boundary layer condition on Concentration Boundary Layer

The concentration contours around the bubbles in Figure 27 for the free slip and no-slip condition are not symmetrical where different regions of nitrogen concentration exist. The nitrogen concentration is high at the rear of the bubble and this region is known as the “concentration wake”. This concentration wake is seen to become narrower as the Reynolds number increases as observed when comparing Figure 27a and 27c. Dani *et al.,* (2006) similarly observed this axisymmetric zone at the wake of the bubble where high species concentrations were detected.

To be more precise, during a no-slip condition, a recirculating wake develops and the concentration contours are distorted as seen in Figure 27b. This is a clear difference between rigid solid and spheres as the concentration layer is thicker around a rigid sphere mainly due to flow separation.

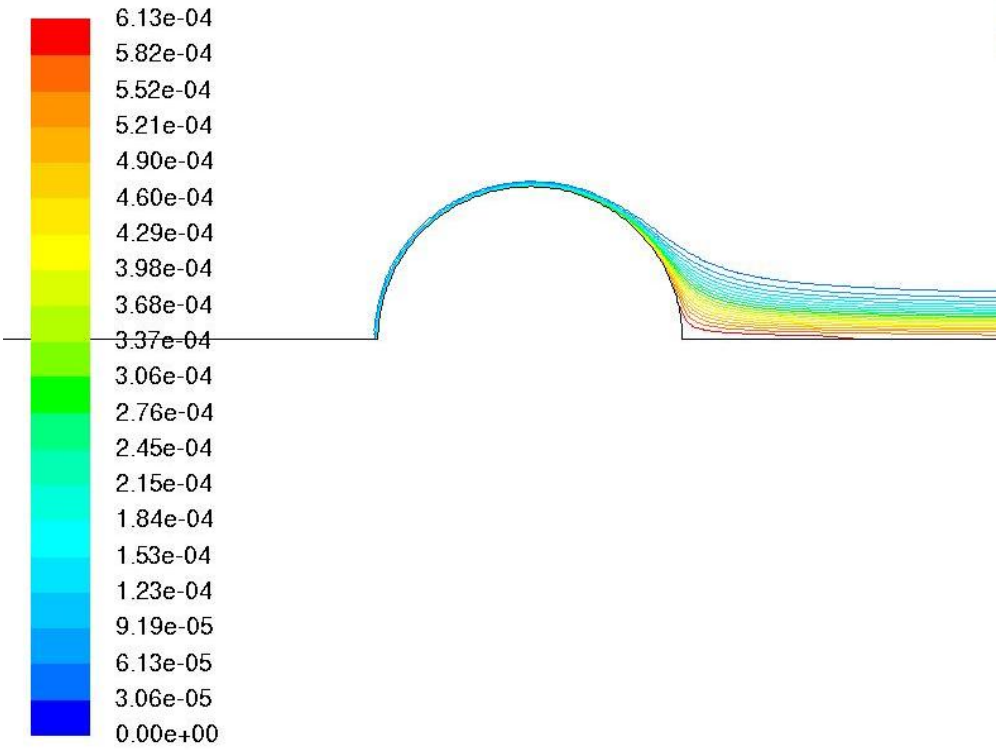

(a) *Nitrogen Concentration Contours around bubble at Sc= 8.58 and Re=75 for free slip condition*

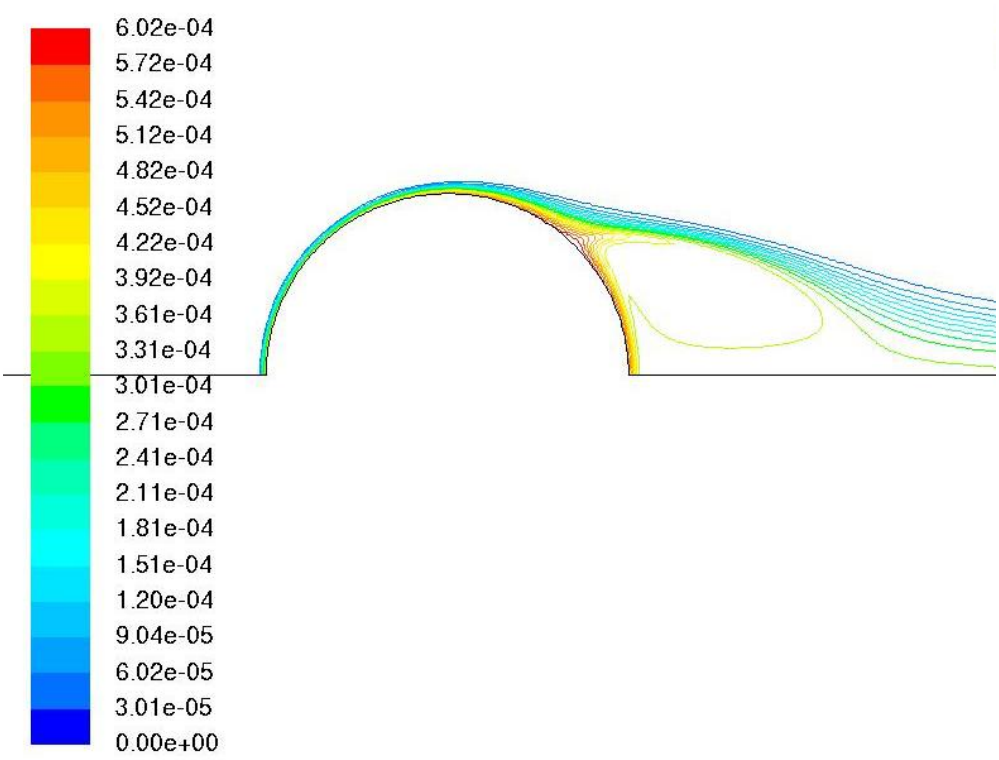

(b) *Nitrogen Concentration Contours around bubble at Sc= 8.58 and Re=75 for no-slip condition*

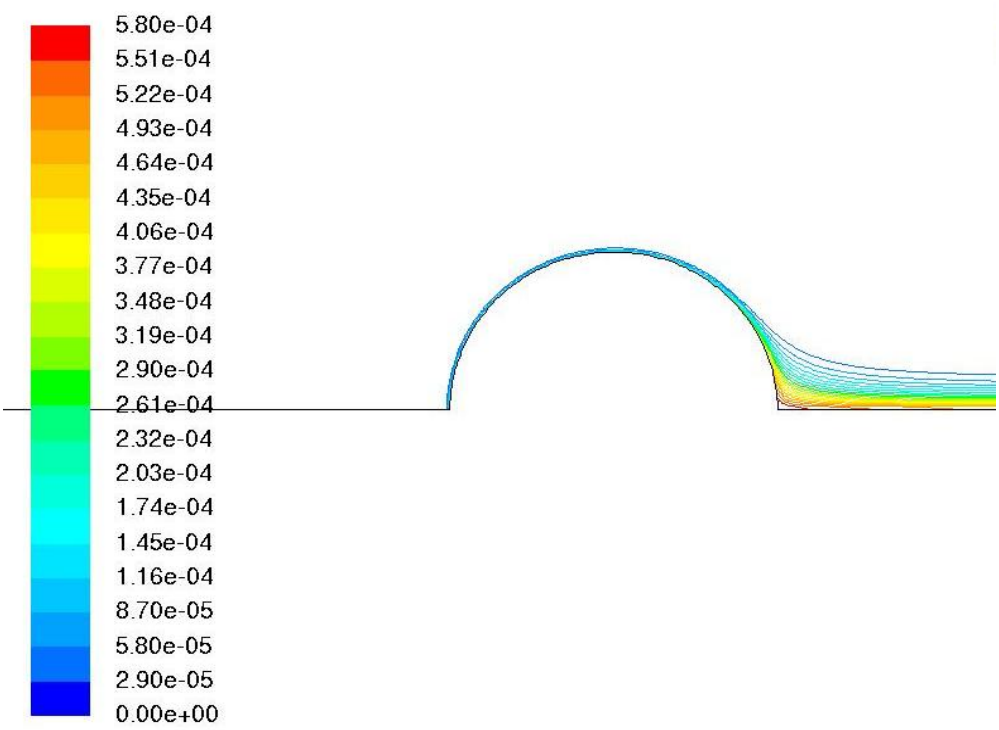

(c) *Nitrogen Concentration Contours around bubble at Sc= 8.58 and Re=270 for free slip condition*

Figure 27: Nitrogen Concentration Contours around bubble for Re =75 and 270

In conclusion, the boundary layer condition, be it free slip or no-slip affects the velocity and concentration boundary layer. The free-slip condition is more relevant to this project because it involves bubbles or spheres while the no-slip condition applies to rigid solids and particles. However, the no-slip allows the range of applicability to extend to particles as well.

7.1.3. The Effect of Reynolds number on the Mass Boundary Layer thickness

The Reynolds number is varied to determine its influence on the mass boundary layer thickness by changing the inlet fluid velocity of the system. In Figure 28, the bulk liquid velocity was varied while keeping mass diffusivity constant for the free slip boundary condition. The mass boundary layer thickness decreases with increasing Reynolds number. This outcome is expected, since there is no flow separation or recirculation wake at the rear of the bubble. It is concluded that, the velocity magnitudes influence the velocity boundary layer which in turn influences the concentration boundary layer.

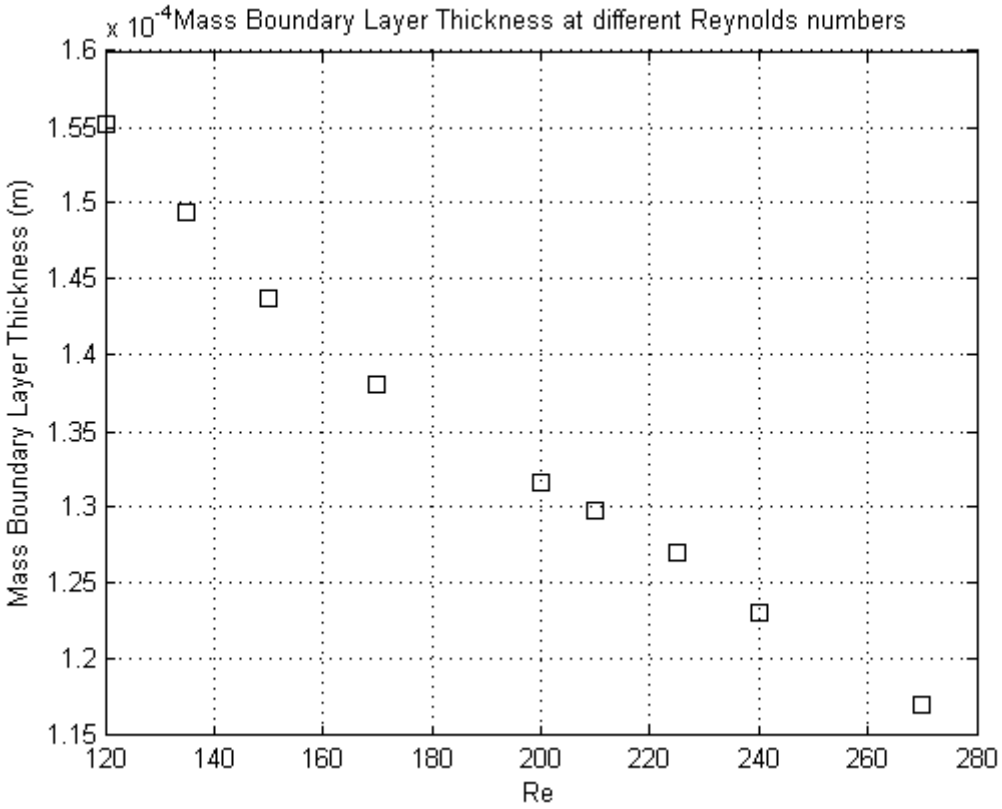

Figure 28:The effect of Reynolds number on Mass Boundary Layer Thickness

It should be noted, however, due to the nature of the applied assumptions, there is a constraint to low Re values; at this stage the interest is in whether this approach yields good enough results to justify investigations in a more general sense that is at higher Re values

7.1.4. The Influence of Schmidt number on the Mass Boundary layer thickness

The Schmidt number is varied by changing the mass diffusivity applied as in the simulation of some hypothetical fluid. The film theory as defined in Equation 6 shows that at high diffusivities the mass boundary layer thickness will be smaller and *vice versa*. In Figure 29, as the Sc increases, the mass boundary layer thickness also decreases.

The different mass diffusivities used in the simulation were taken from different authors in Table 4. Koeltzsch (2000) showed a strong dependence of Schmidt number on the mass boundary layer thickness in turbulent regime. Hasegawa and Kasagi (2001) showed that the connection between velocity and concentration fields remain unchanged in a free surface even at high Sc. The main goal was to show that Sc has an influence on the mass boundary layer thickness.

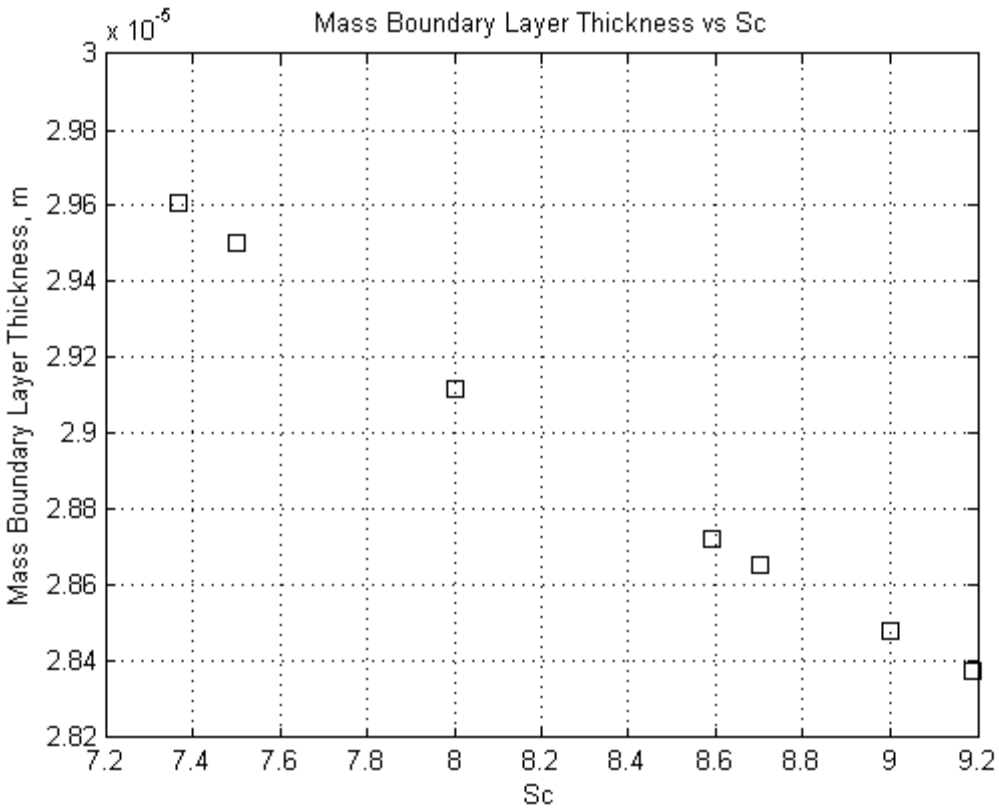

Figure 29: The effect of Schmidt number on mass boundary layer thickness

7.2. Mass Transfer Coefficient

7.2.1. The Effect of Reynolds number on $k_l a$

The mass transfer coefficient increases with increasing Reynolds number (bulk liquid velocity) as illustrated in Figure 30. As the Reynolds number is increased, the mass boundary layer thickness decreases while the mass transfer coefficient increases. These parameters are inversely proportional given by the film theory in Equation 6. As seen in the section 7.1.1 and 7.1.2, when the no-slip condition is applied, the complete opposite is observed in Figure 31 below. The effect of convection around the bubble explains the mass transfer phenomenon when increasing Re.

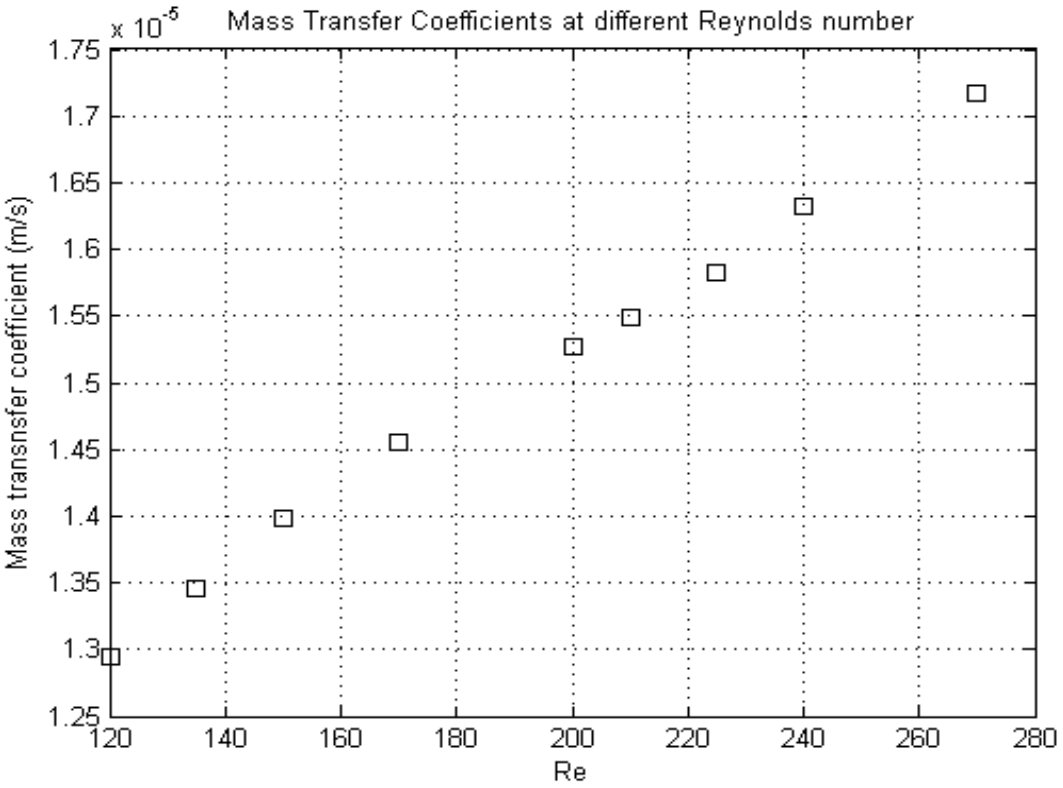

Figure 30: The effect of Reynolds number on mass transfer coefficient at free slip condition at Sc=8.58

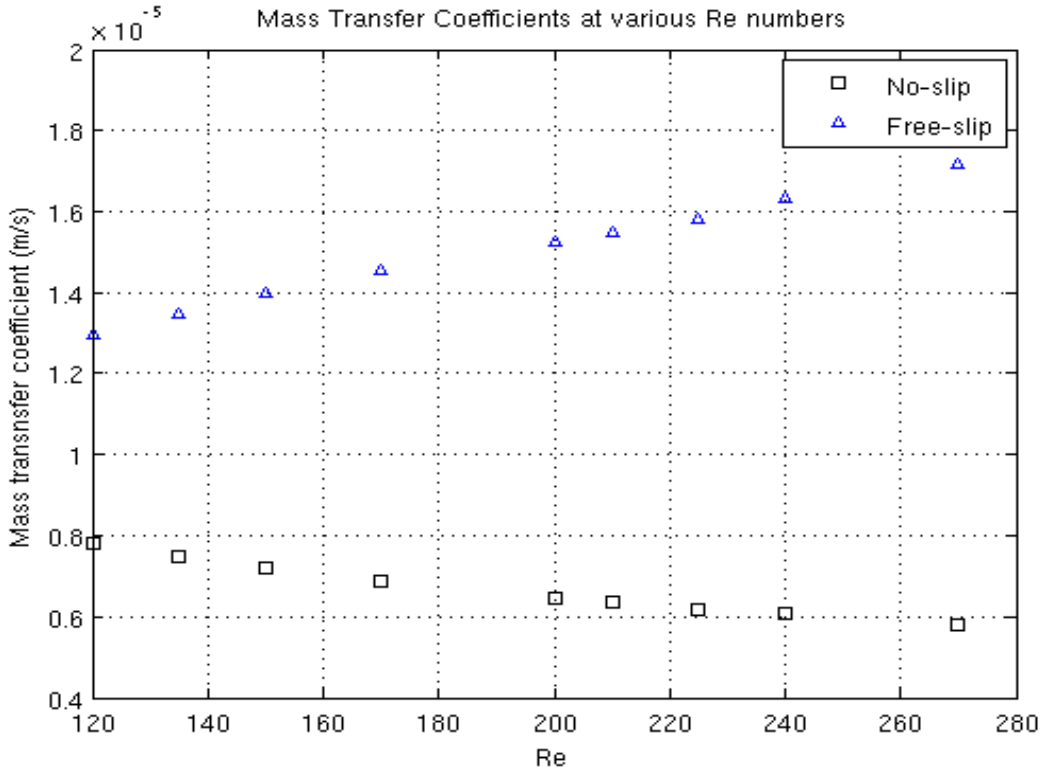

Figure 31: Mass transfer coefficient for free slip and no-slip condition

Figure 32 illustrates the spherical symmetry concentration contours at Re = 30, where the concentration of diffusing species decreases from the bubble surface to bulk fluid. At this stage, the mass transfer is principally controlled by diffusion.

When the Re is increased, the concentration contours in front of the bubble decrease in thickness and no symmetry is observed (Figure 33). The mass transfer mechanism changes from diffusion to advection (bulk fluid diffusion) especially around the rear of the bubble. In the case of no slip condition where there is separation of flow, mass transfer occurs. Due to the recirculation (concentration wake), the fluid approaching this region from the inlet has a certain concentration. Generally, the mass transfer elements in the bulk fluid flow move around the rear of the bubble. This movement causes the concentration in this region to increase and with continuous bulk liquid movement, the fluid elements are transported away with fluid flow.

This advection movement explains the long concentration tail as seen in Figure 33. It is important to note that in real turbulent reactors; the rate of mixing increases causing no formation of tails.

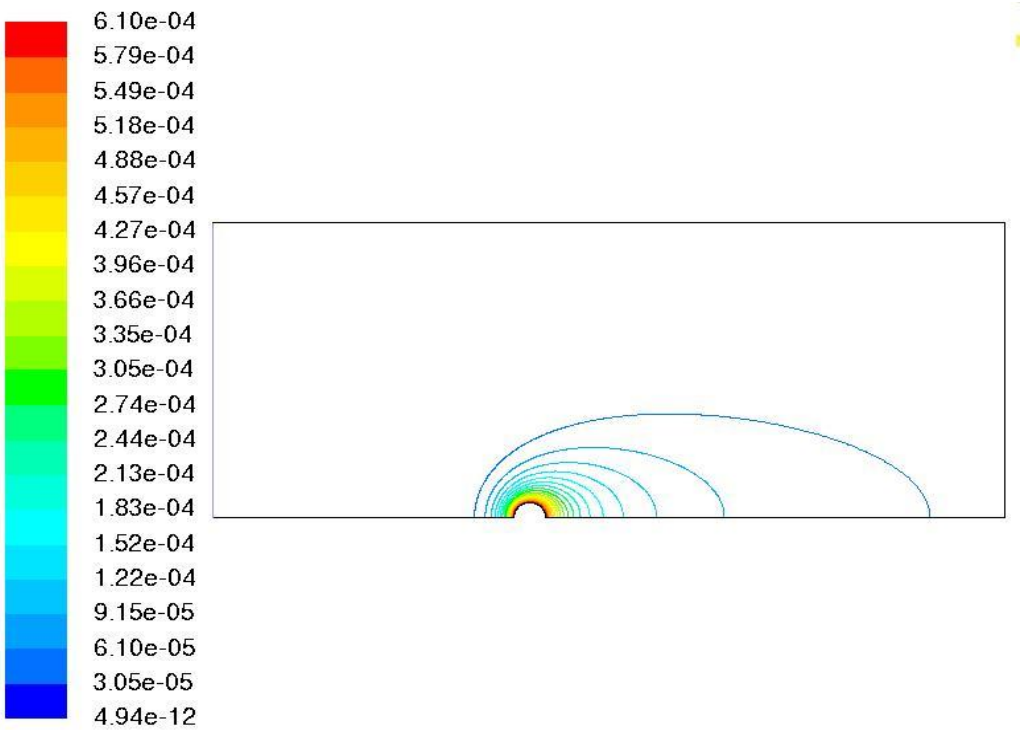

Figure 32 : Nitrogen Concentration fields around bubble at Re=30 and Sc=8.58

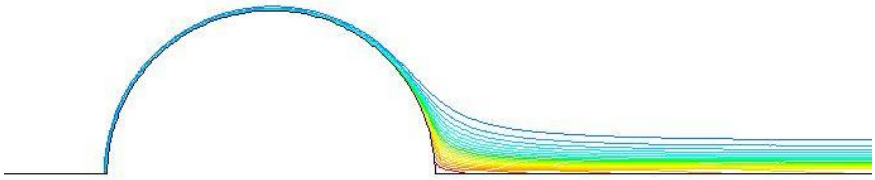

Figure 33: Concentration contours around bubble at Re=270 and Sc=8.58

7.2.2. The Influence of Schmidt number on $k_l a$

The mass transfer coefficient is directly proportional to the mass diffusivity (Schmidt number) as in Equation 6. As the diffusivity increases, the average mass transfer coefficient also increases; this expected trend is seen in Figure 34. Li *et al*., (2003) and Paschedag *et al*., (2005) also showed Sc has an effect on $k_l a$.

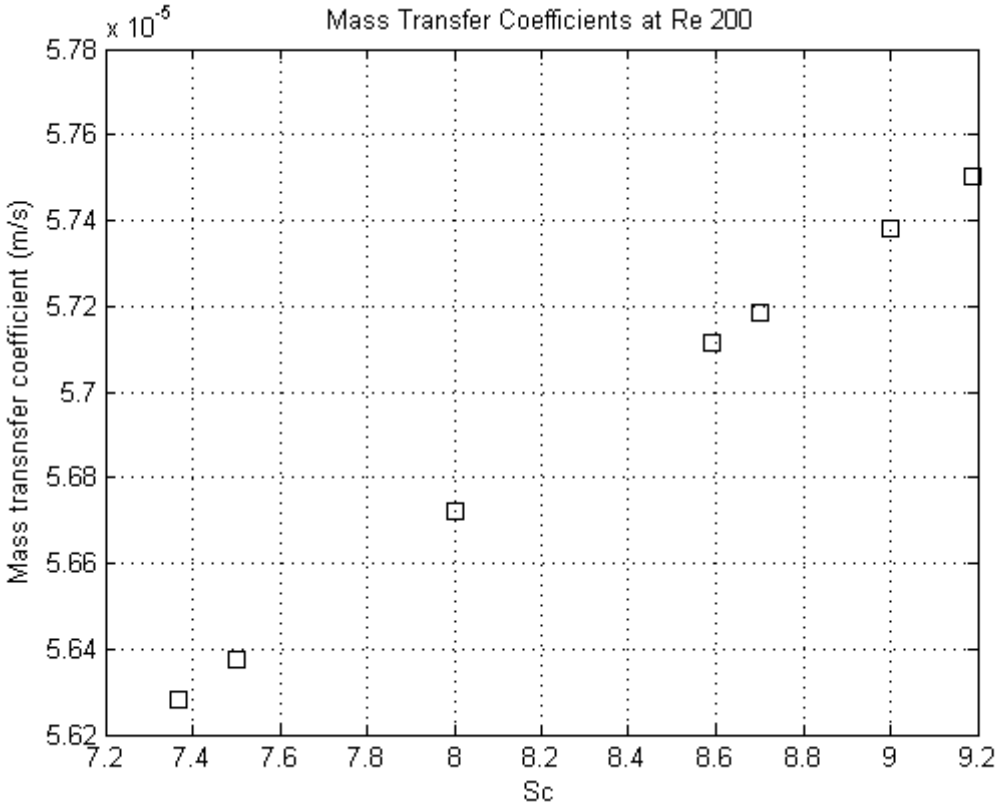

Figure 34: The effect of Schmidt number on mass transfer coefficient

7.3. Summary of Investigations

The boundary layer condition specified on the bubble surface is very important because it affects the velocity and concentration boundary layer. The velocity and concentration boundary layer in turn affects the mass boundary layer thickness. The mass boundary layer thickness and the mass diffusivity are used to calculate the average mass transfer coefficient.

The average mass transfer coefficient increases with increasing Reynolds number as the mass boundary layer thickness decreases for the free slip boundary condition. This is expected, since there is no recirculation wake at the rear of the bubble and these parameters are inversely proportional according to the film theory.

The same expected outcome is observed as the Schmidt number increases, the mass boundary layer thickness also decreases and average mass transfer coefficient increases. Therefore, as investigated, the Re and Sc numbers have an effect on the mass boundary layer thickness and average mass transfer coefficients.

7.4. Mass Transfer Coefficients and BCM

Section 7.2 shows that the estimated mass transfer coefficients are influenced by the velocity field vectors and mass boundary layers thickness around the bubble. In Figure 31, the simulated CFD results for free slip condition show the mass transfer coefficient increasing as the Reynolds number increases. This is the expected trend for the film theory; where mass transfer coefficients increase as Reynolds number increases.

The simulated CFD results obtained are coherent with literature predictions and can therefore be used to extend the BCM application to integrate mass transfer. The mass transfer application to the BCM can be achieved by developing a general algebraic function which directly estimates the mass transfer coefficient as a function of Re and Sc numbers. Three different methods are investigated to determine if the mass transfer coefficients can be estimated as a function of Re and Sc numbers.

7.4.1. Method 1 - Sherwood Number

The Reynolds number and Sherwood number have an integral part to play when estimating mass transfer coefficients. Several correlations as seen in Table 2 estimate mass transfer coefficient in the form of the Sherwood number. The mass transfer coefficients values from the simulated CFD results are used to calculate Sherwood number using Equation 9 and are illustrated in Figure 35. The observed result is expected: since the mass transfer coefficient increase with Reynolds number so does the Sherwood number.

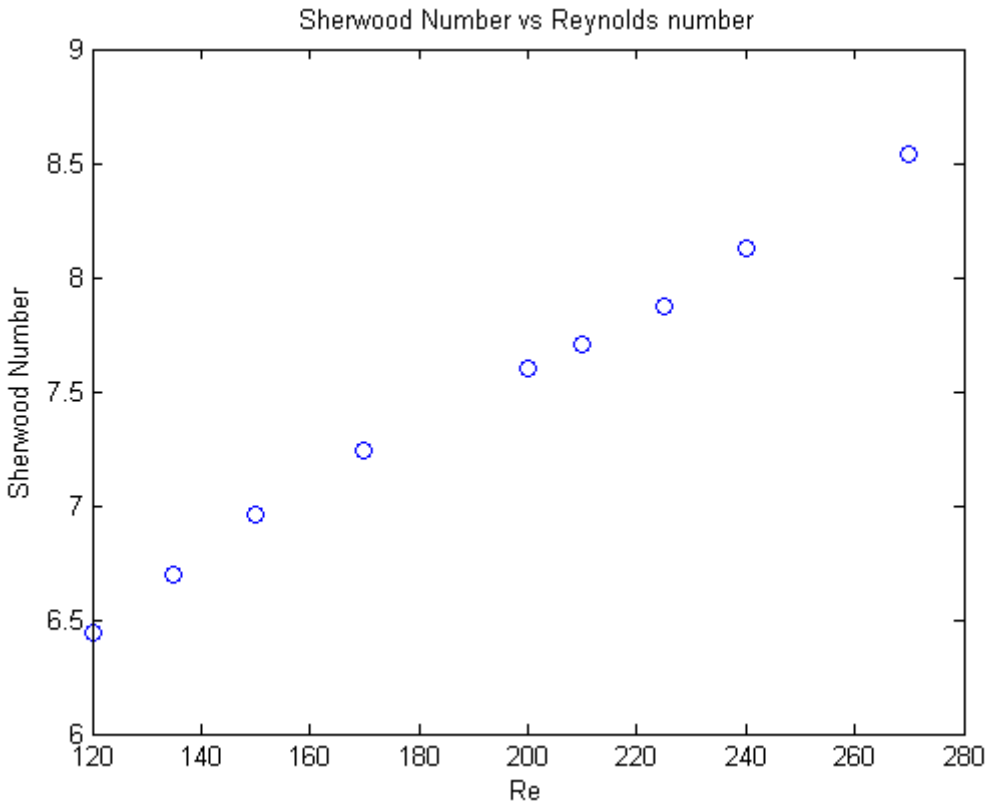

Figure 35: Sherwood Number versus Reynolds number from simulated CFD Results

A curve fitting approach not found in literature is used to determine which algebraic function suits the Sherwood in terms of Reynolds number. The results show that the best fitting types were the Linear Polynomial and Power models with R^2 of 0.9959 and 0.9939 respectively. Equations 50 and 51 below describe the models with the Sherwood as a function of Reynolds number.

$$\boldsymbol{Sh\,(Re) = 0.01355Re + 4.875} \qquad \boldsymbol{(50)}$$

$$\boldsymbol{Sh\,(Re) = 1.276 Re^{0.3377}} \qquad \boldsymbol{(51)}$$

The simulated CFD results are used as a point of reference to determine which model is most adapted to estimate mass transfer coefficients. The simulated CFD results are then compared to linear polynomial and power functions models and demonstrated in Figure 36. The polynomial function gives closer estimates to the simulated CFD results, thereby being the best option out of the two models. Therefore using Equation 50, the mass transfer coefficient can be estimated for a system by simply inserting the Reynolds number.

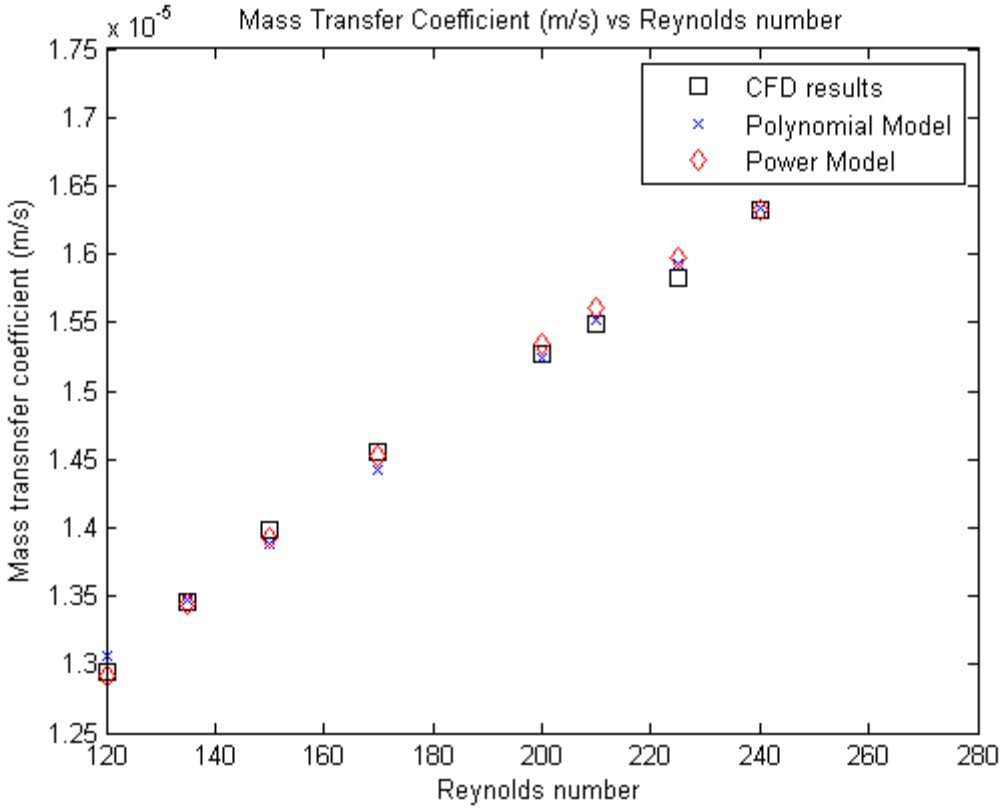

Figure 36: Comparison of Mass transfer coefficients between CFD, Linear Polynomial and Power models

7.4.2. Method 2 – Concentration Boundary Layer (Film Theory)

The mass boundary layer thickness is greatly influenced by the Reynolds number as described in Section 7.1.3. The outcome being that the mass boundary layer thickness decreases with increasing Reynolds number as expected from film theory.

A curve fitting approach was used to determine the mass boundary layer thickness and the mass transfer coefficient. The algebraic function was determined by using the film theory to estimate mass boundary layer thickness as a function of Reynolds number. The two best fitting models are the Second order polynomial and power models with R^2 of 0.9941 and 0.9956 respectively. Equations 52 and 53 shows the respective developed models and using the simulated CFD results as a point of reference are compared in Figure 37.

$$\delta_m\,(Re) = 5.865e^{-10}Re^2 - 4.719e^{-7}Re + 0.0002024 \qquad (52)$$

$$\delta_m\,(Re) = 0.0007617Re^{-0.3322} \qquad (53)$$

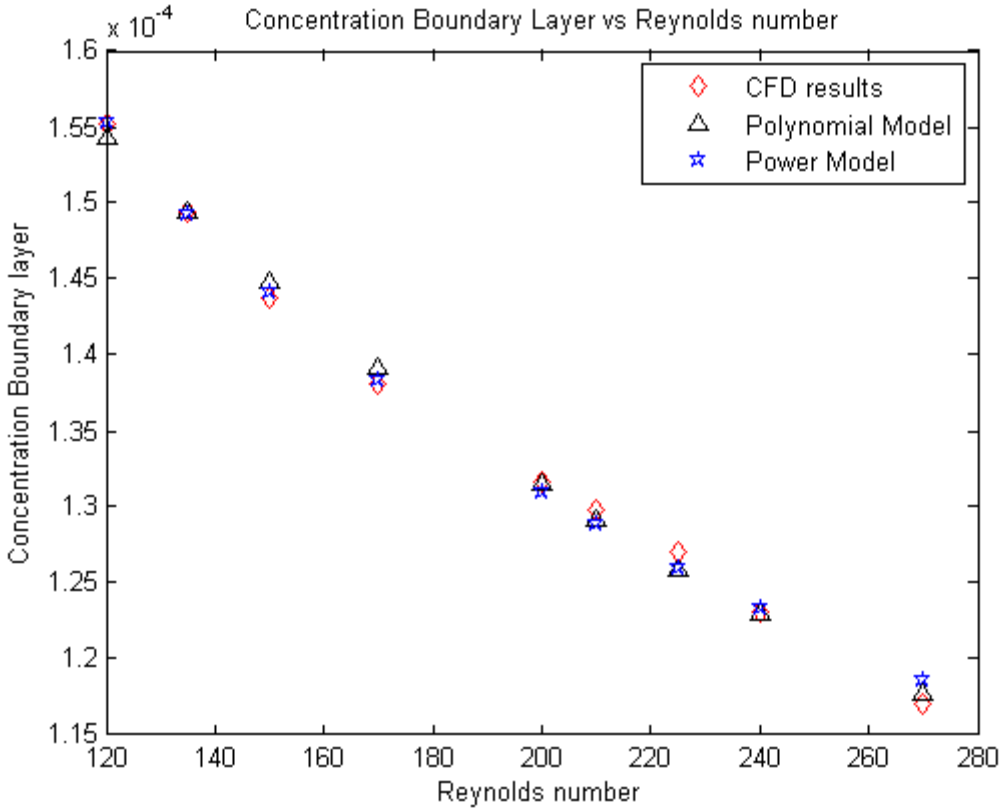

Figure 37: Comparison of Concentration between CFD results, Linear and power model

Mass transfer coefficients are estimated by using the mass diffusivity and the concentration boundary layers according to the film theory. Using the mass boundary layer thickness from the simulated CFD results and those from the polynomial and power model, the mass transfer coefficient is calculated at Sc 8.58. The comparison of the models in Figure 36 and 38 illustrate a close agreement between results which

shows that different methods of correlating data yield approximately the same results. These algebraic forms of estimating the mass transfer coefficient from the concentration boundary layers as function of Reynolds number are good enough. This method has an advantage because it not only gives the mass transfer coefficient but also the mass boundary layer thickness around the bubble.

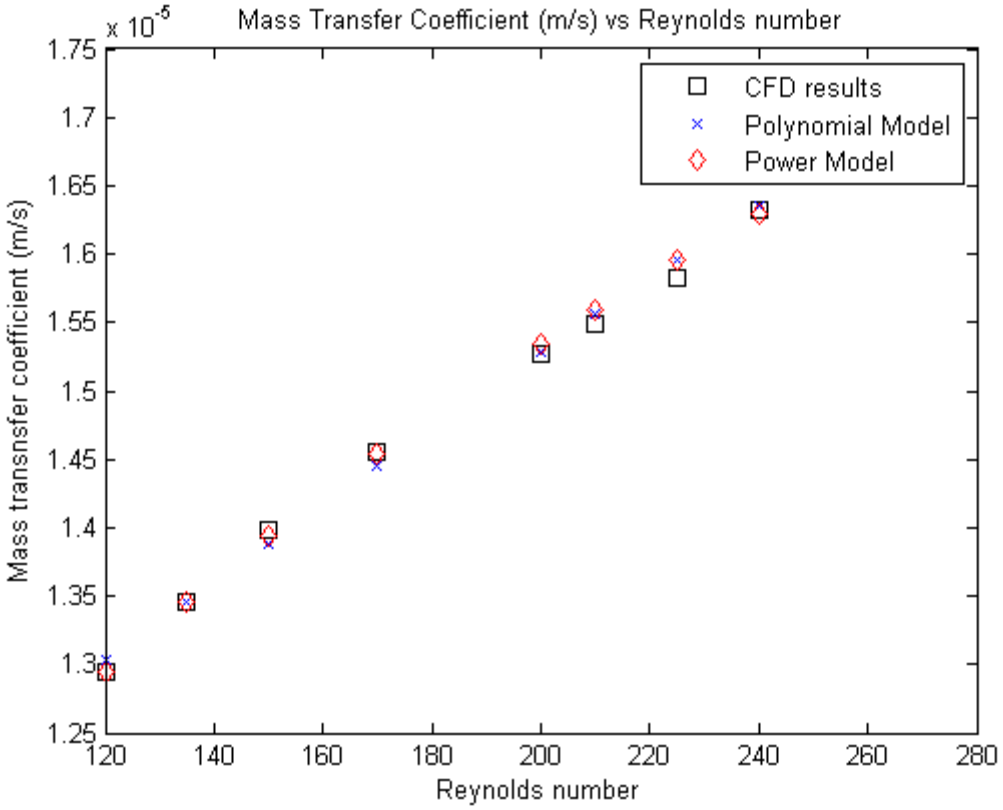

Figure 38: Comparison of Mass transfer coefficients between CFD, Linear Polynomial and Power models

7.4.3. Method 3 – Velocity and Concentration Boundary Layer

The film theory has been discussed in Section 2.1.1 and the simulated CFD results showed the expected trend. However, the boundary layer theory described in Section 2.1.2 predicts the mass transfer coefficient with dependence on diffusivity. This dependence is shown in Equation 14 which calculates the mass boundary layer thickness but requires the momentum boundary layer thickness as developed in Equation 13 (Dutta, 2007; Benitez, 2009). Figure 39 shows the estimated mass transfer coefficients from the boundary layer theory and the expected outcome is observed.

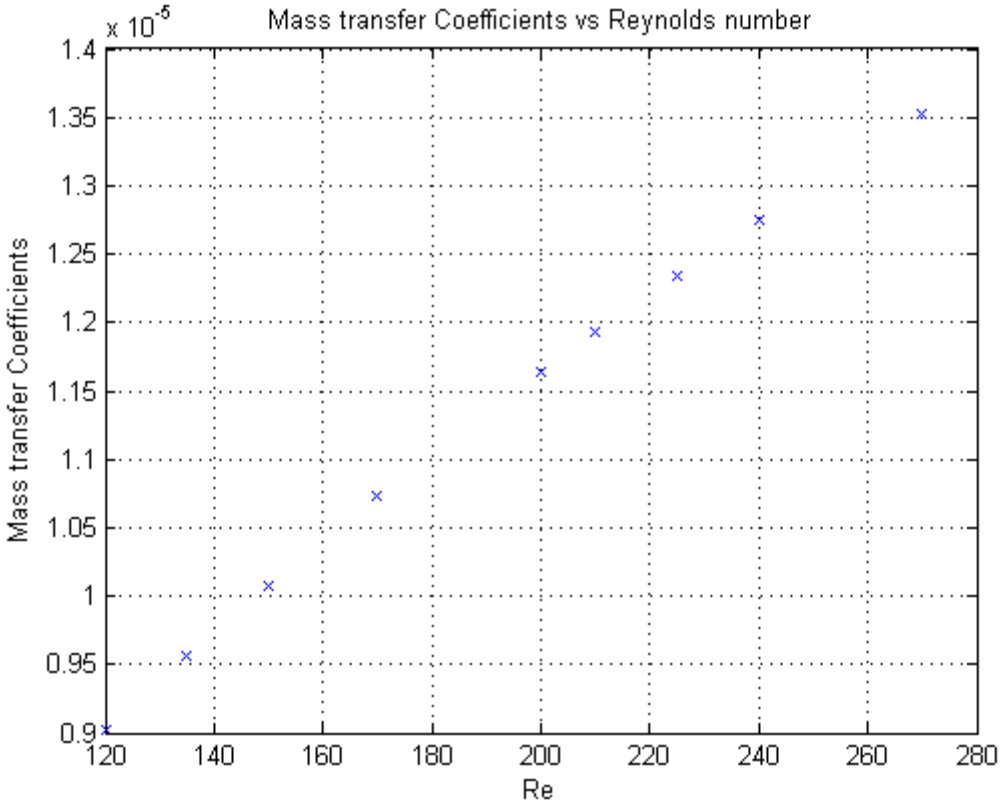

Figure 39: Estimated mass transfer coefficients from the boundary layer theory

A curve fitting approach was used to determine an algebraic function for estimating mass transfer coefficient as a function of Re. The second order polynomial and power model were the best fits for the velocity boundary layer with R^2 of 0.9987 and 1 respectively. The developed Equations 54 and 55 were used to calculate mass boundary thickness with Sc 8.58 as Equation 13 requires. There are no simulated results to compare models; therefore a correlation developed by Benitez (2009) was used as a point of reference. The comparison is shown in Figure 40 where the power model and results from Benitez (2009) are in very good agreement for the momentum boundary layer thickness and mass transfer coefficients.

$$\boldsymbol{\delta\,(Re) = 3.892e^{-9}Re^{2} - 2.505e^{-6}Re\; + 0.0006985} \qquad \boldsymbol{(54)}$$

$$\boldsymbol{\delta\,(Re) = 0.005Re^{-0.5}} \qquad \boldsymbol{(55)}$$

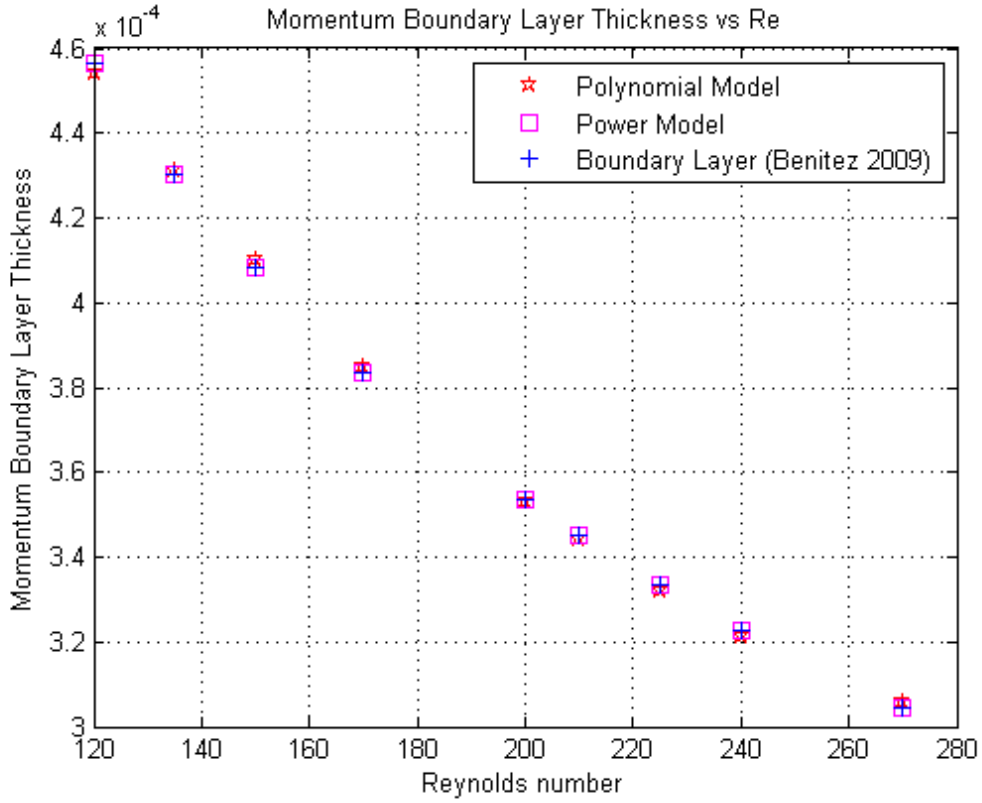

(a)

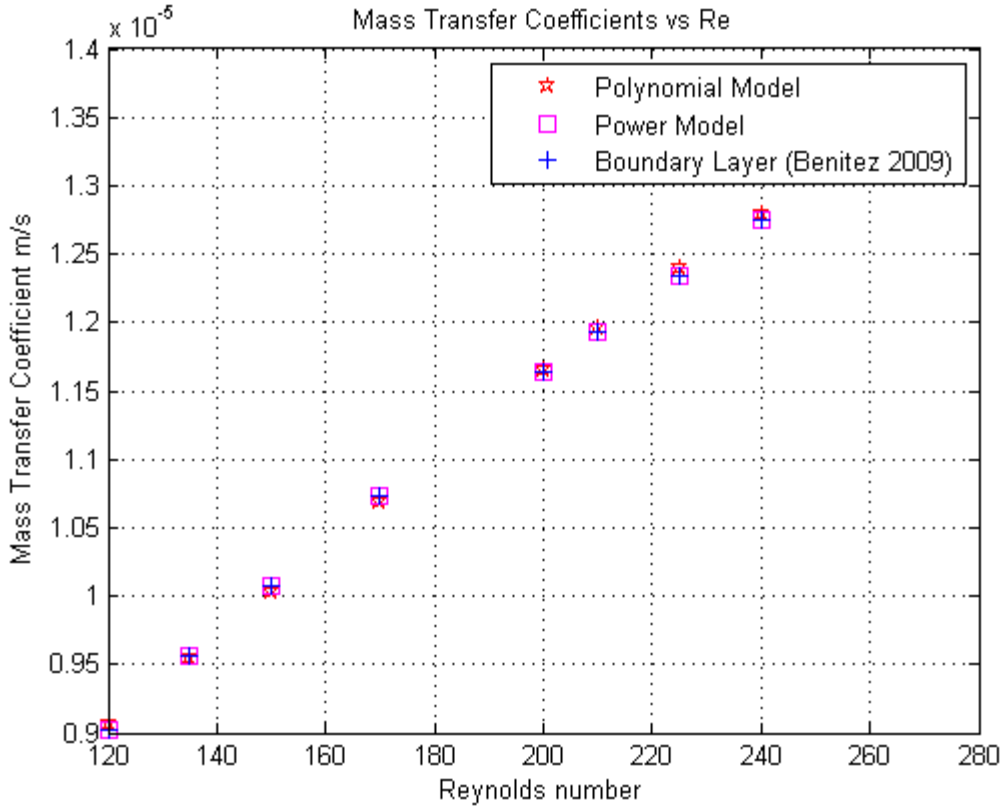

(b)

Figure 40: Comparison of (a) Momentum boundary layer thickness and (b) mass transfer coefficient between Benitez (2009), Polynomial and Power models

The same second order polynomial and power models gave good fits for the mass boundary layer thickness with R^2 of 0.9987 and 1 respectively. Equations 56 and 57 were directly used to calculate mass transfer coefficients using the film theory.

$$\delta_m\,(Re) = 1.901e^{-9}Re^2 - 1.223e^{-6}Re + 0.0003412 \qquad (56)$$

$$\delta_m\,(Re) = 0.002442\,Re^{-0.5} \qquad (57)$$

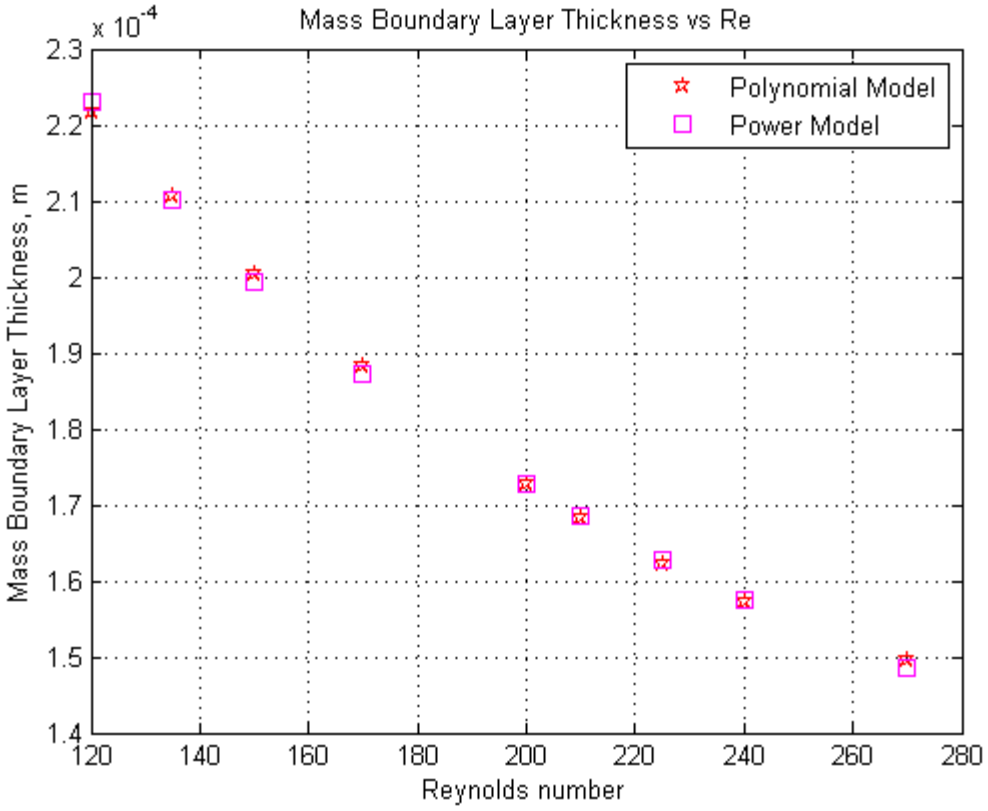

(a)

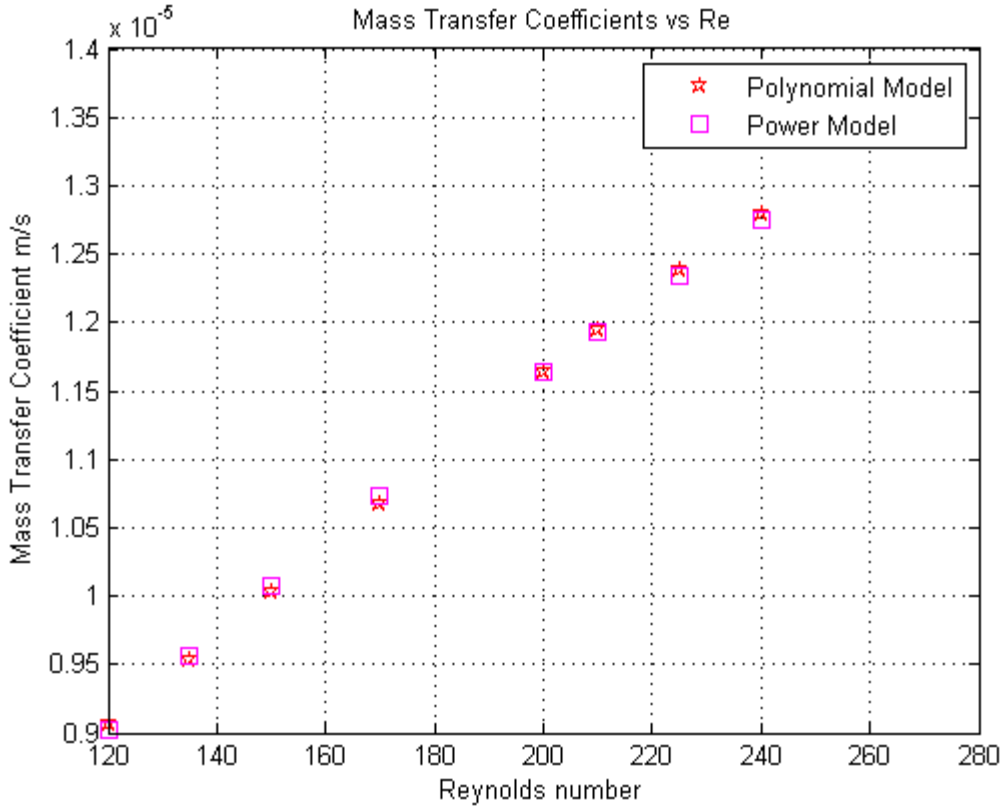

(b)

Figure 41: Comparison of (a) Momentum boundary layer thickness and (b) mass transfer coefficient between Polynomial and Power models

Figure 41 shows the good agreement between the estimated mass boundary layer thickness and mass transfer coefficients from the velocity and concentration models.

7.4.4. Method Comparison

A model is most reliable if the R^2 is at or closer to one and describes how accurate the model fits the data. Looking at Table 6 below, the Polynomial velocity and concentration boundary layer theory are the best models to use. However, it is important to note that there are other factors considered when choosing the best model. These factors include the validity and the effectiveness of the model.

Table 6: R^2 Model Comparison

Model	R^2
Polynomial Sherwood	0.9959
Power Sherwood	0.9939
Polynomial Concentration BL	0.9941

Power Concentration BL	0.9956
Polynomial Velocity BL Theory	1
Power Velocity BL Theory	0.9987
Polynomial Concentration BL Theory	1
Power Concentration BL Theory	0.9987

Firstly, the validity of the model deals with the type of model, in this case polynomials and power functions models. A power function also called a monomial function models data that represents a proportional relationship increasing at a specific rate. As shown above, all the power functions correspond to a direct or indirect variation as the Reynolds number increasing.

A polynomial function is a sum of several monomial functions and is used when data fluctuates but does not give details about the model, it only finding points that go near data points. Therefore, preference is given to the power function models instead of the polynomial models to estimate mass transfer coefficients.

Secondly, the effectiveness of the different models is compared to the simulated CFD results and correlations. The estimates of the mass transfer coefficients from the Sherwood number and Concentration boundary layer methods are very similar to the CFD simulated results.

In conclusion, the estimates from the polynomial velocity and concentration boundary layer theory give the best fit with R^2 values of 1. However, polynomials are not the desired models for this case study because it just fits the data points with no additional details. This means all the polynomial functions used are scrapped and not reliable for this project.

Looking now at only how the power functions models; the Sherwood and concentration boundary layer gave the closest estimates to the CFD simulated results with R^2 of 0.9939 and 0.9956 respectively. Therefore, the chosen model to predict mass transfer coefficients using the Reynolds and Schmidt number with an elapsed time of 0.0409s is the concentration boundary layer power function developed from the film theory in Equation 53 and rearranged in Equation 58 below.

$$k_l\,(Re, Sc) = 1313\mu\,(Sc\rho)^{-1} Re^{\,0.3322} \qquad (58)$$

7.4.5. Summary

Firstly, the estimated mass transfer coefficients from the simulation and the concentration boundary layer power function model show the expected trend with increasing Reynolds number. As the Reynolds number increases, the mass transfer coefficient also increases as in the film theory. The good agreement of the simulated CFD and developed model shows that indeed, the mass transfer model can be added to the BCM applications. Therefore, the mass transfer extension to the BCM generates a general approach to determining the mass transfer coefficients than using the various correlations in literature.

Secondly, inputs of Reynolds number and Schmidt number are required to estimate the mass transfer coefficient. Unlike other models or correlations where gas hold-up and superficial gas velocity calculations and so on are required before estimating the mass transfer coefficient. An example of gas hold-up and mass transfer correlations are shown in Dudley, 1995. Therefore, mass transfer extension to the BCM simply requires only two input parameters and eliminates the time consuming calculations.

More so, from the developed model, the mass boundary layer thickness and mass transfer coefficients for a nitrogen-water system are calculated. This indicates that, with the BCM, an in-depth understanding and research can be achieved by analysing the velocity pattern, concentration boundary layer formation, mass boundary layer thickness and the mass transfer coefficients.

Finally, the BCM extension which is the concentration power function so far demonstrates to be better and faster modelling approach. However, there is a need to compare the estimated mass transfer coefficients against experimental data in literature.

Chapter 8 Model Validation

8. Model Validation

Model validation is essential because it gives credibility to the developed mass transfer application to the BCM. The present study investigated the prediction of average mass transfer coefficients in Bubble Column reactors by integrating the mass balance into the BCM.

The simulated CFD results, BCM extension model and experimental data as indicated in Table 2 are compared in Figure 42 below. The correlations in Table 2 have different geometries and experimental conditions such as solid spheres, bubbles in liquid, drops, creeping regime just to name a few whereas the BCM approach being a fundamental study simulates a single bubble in flowing liquid.

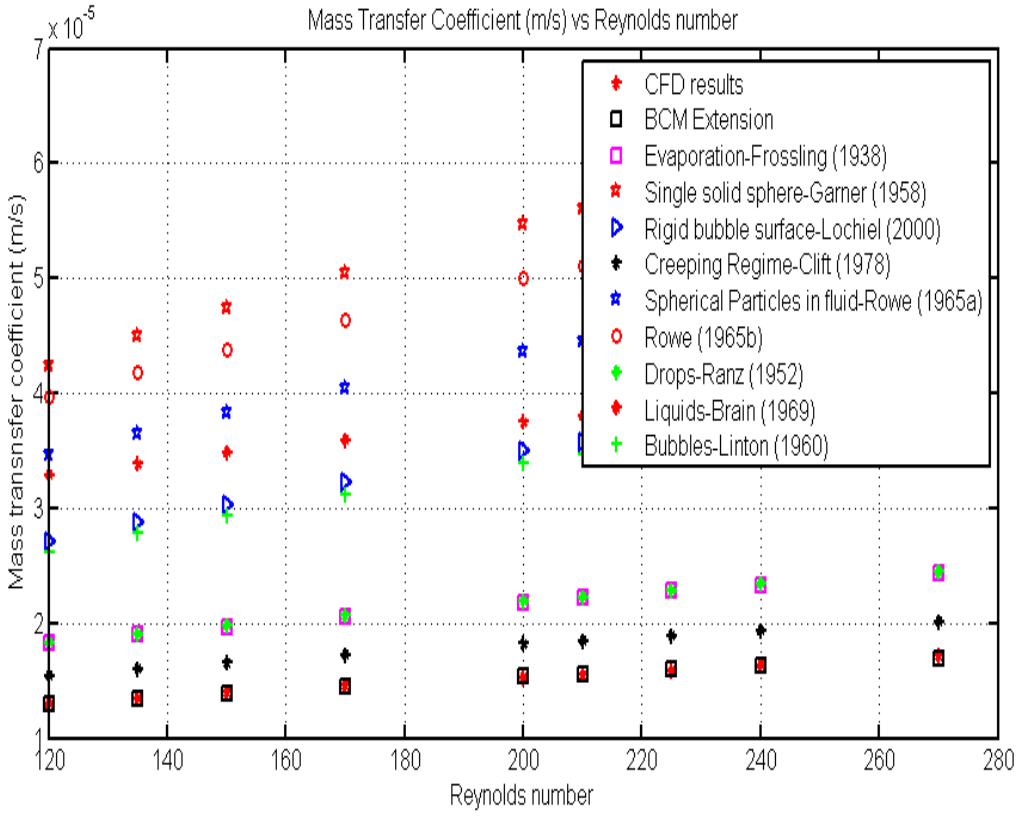

Figure 42: Model validation against experimental data

The following comments can be made when comparing the model with experimentally determined correlations obtained from literature;

- The literature correlations, CFD simulated results and the BCM extension show the expected trend; as the Reynolds number increases, the mass transfer coefficient also increases.

- The mass transfer coefficients obtained from the BCM extension in Equation 58 are in good agreement to those obtained by Clift *et al*. (1978). This illustrates how accurate the mass transfer extension to the BCM approach is and can suitably be used to estimate the mass transfer coefficient for any geometry or system.

- The mass transfer coefficients values deduced from the Frössling (1938) and Ranz and Marshal (1952) are also quite close to the BCM extension because of the similar conditions used.

- The correlations not in agreement with the BCM extension can be justified by how mass transfer is sensitive to the choice of system, material properties, operating conditions and equipment type. These parameters or factors have an impact on the mass transfer coefficient. In addition, the different conditions and geometry used in Table 2 like for example, single solid spheres, spherical particles in fluid, rigid bubble surface just to name a few also affect the mass transfer rate. Therefore, reproducing predictions or estimates of the mass transfer coefficients as in the correlations is quite challenging.

- Important to remember that the BCM Extension assumed the bubble size did not change as fluid flows over the surface.

However, the BCM extension relies on the Reynolds number and is therefore only valid for a limited range of applications. More so, chemical reactions were not considered in the BCM development; thereby also limiting its applicability. On the other hand, one way of improving its accuracy is to use the critical angle in Equation 48 for averaging of the mass boundary layer thickness.

Chapter 9 Conclusions

9. Conclusions

Numerous CFD models apart from the commonly used Euler-Euler, Euler-Lagrange models have been developed to predict mass transfer coefficients. These computationally expensive models are quite unique and depend on the operating system.

In this case study, the CFD simulation results show varying mass boundary layer thickness around a single spherical bubble in homogeneous nitrogen-water flow regime. These mass boundary layer thicknesses were averaged using an integral method to get a uniform mass boundary layer thickness around bubble. The mass diffusivity and uniform mass boundary layer thickness are used to obtain the average mass transfer coefficient.

The influence of the Reynolds and Schmidt numbers on mass boundary layer thickness and average mass transfer coefficients from the CFD results was investigated. It was shown that with increasing Re and Sc numbers, the mass boundary layer thickness decreases and while the mass transfer coefficients increase. As expected, simulation results indicate that to obtain high rates of mass transfer, bubble column reactors should be operated at high Reynolds and Schmidt numbers.

The BCM in its current approach only gives the velocity field vectors around a single bubble. A general approach for estimating the average mass transfer coefficient is required which is fundamentally based and not specific to equipment or operating condition as compared to the numerous correlations.

The data from the simulated results were integrated to the BCM to develop an algebraic function for estimating the mass transfer coefficient in bubble columns. Three different methods were investigated to estimate the mass transfer coefficient namely the Sherwood, Concentration boundary layer and the boundary layer theory. The concentration boundary layer power function model was the best model which gives the mass boundary layer thickness and the mass transfer coefficients.

The simulated results showed a close agreement when compared to literature published correlations within a range of 120<Re<280. More so, a speed test of 0.0409s, confirms that the BCM mass transfer extension approach is a faster method developed for generating the mass transfer coefficients. However, the range of applicability is limited in terms of the Reynolds number and which needs to be fully extended for major progress.

Therefore, a two dimensional semi-analytical fundamental model, the Bubble Cell Model, requires the Reynolds and Schmidt numbers to generate the steady-state velocity vector fields and estimate the gas-liquid mass transfer rate from spherical bubbles in bubble columns in a homogeneous regime.

The BCM mass transfer extension calculates the mass transfer coefficient which gives information on mass transfer rates in a non-reactive system. With the aid of the population balance model, the bubble size effect can be established and an entire Bubble Column simulated. Many systems in industry are reactive in one way or the other. BCM applications are set to increase upon validation with chemical balance in industry

Chapter 10 Recommendations

10. Recommendations

The mass transfer addition to the BCM approach needs the Reynolds number to estimate the average mass transfer coefficient. In this study, a limited range of Reynolds number was used and therefore makes the approach only valid for limited applications in homogeneous regimes. Furthermore, chemical reactions were not considered in the BCM development; thus limiting its applicability. The BCM approach will make strong progress in its development if applied in turbulent regime with chemical reactions.

Chapter 11 References and Appendices

11. References

[Online]. Available: http://www.fluent.com.

[Online]. Available: http://www.flowlab.fluent.com.

[Online]. Available: http://www.cfdrc.com.

[Online]. Available: http://www.cd-adapco.com.

[Online]. Available: http://www.software.aeat.com/cfx.

[Online]. Available: http://www.macs.hw.ac.uk/~ms713/lecture_1.pdf .

Akhtar, A. 2006. Two-fluid Eulerian simulation of bubble column reactors with distributors. *Journal of chemical engineering of japan.* 39(8):831-841.

Akita, K. 1973. Gas Hold-up and Volumetric Mass Transfer coefficient in Bubble

Akita, K. 1974. Bubble size, interfacial area, and liquid-phase mass transfer coefficient in bubble columns. *Industrial engineering chemistry process design and development.* 13(1):84.

Alvarez, E. and others. 2000. Model based in neural networks for the prediction of the mass transfer coefficients in bubble columns. Study in Newtonian and non-Newtonian fluids. *International communications in heat and mass transfer.* 27(1):93-98.

Alvarez - Cuenca, M. & Nerenberg, M. 1981. Oxygen mass transfer in bubble columns working at large gas and liquid flow rates. *AIChE journal.* 27(1):66-73.

Anil, M. 2007. CFD modeling of three-phase bubble column: 1. study of flow pattern. *Chemical and biochemical engineering quarterly.* 21(3):197.

Apte, S. and others. 2004. Large-eddy simulation of reacting turbulent flows in complex geometries. *Comput.phys.* 197:215-240.

Aroonwilas, A. and others. 2003. Mathematical modelling of mass-transfer and hydrodynamics in CO2 absorbers packed with structured packings. *Chemical engineering science.* 58(17):4037-4053.

Asgharpour, M. 2010. Effect of surface contaminants on oxygen transfer in bubble column reactors. *Biochemical engineering journal.* 49(3):351.

Baehr, H.D. & Karl, S. 2006. *Heat and Mass Transfer.* 2nd ed. Springer.

Baehr, H. & Stephan, K. 1998. *Heat and mass transfer .* Berlin and New York: Springer-Verlag.

Baker, T.J. 2005. Mesh generation: Art or science. *Progress in aerospace sciences.* 41(1):29-63.

Basmadjian, D. 2004. *Mass Transfer: Principles And Applications.* London: CRC Press.

Bauer, M. & Eigenberger, G. 2001. Multiscale modeling of hydrodynamics, mass transfer and reaction in bubble column reactors. *Chemical engineering science.* 56(3):1067-1074.

Bech, K. 2005. Dynamic simulation of a 2D bubble column. *Chemical engineering science.* 60(19):5294.

Becker, S., Sokolichin, A. & Eigenberger, G. 1994. Gas—liquid flow in bubble columns and loop reactors: Part II. Comparison of detailed experiments and flow simulations. *Chemical engineering science.* 49(24):5747-5762.

Becker, S. 1999. Dynamic flow behaviour in bubble columns. *Chemical engineering science.* 54(21):4929.

Benitez, J. 2009. *Principles and modern applications of mass transfer operations.*

Bergman, T.L. and others. 2011. *Fundamentals of heat and mass transfer.* Wiley.

Bhaga, D., Weber, M. E., 1981. Bubbles in viscous liquids: shapes, wakes and velocities. Journal of Fluid Mechanics 105, 301{318. ix, 21, 23

Bi, H. 2004. Multiscale analysis and modeling of multiphase chemical reactors. *Advanced powder technology.* 15(6):607.

Bin, A.K., Duczmal, B. & Machniewski, P. 2001. Hydrodynamics and ozone mass transfer in a tall bubble column. *Chemical engineering science.* 56(21-22):6233-6240.

Bird, R.B., Stewart, W.E. & Lightfoot , E.N. 1960. *Transport Phenomena.* New york: Wiley.

Botton, R., Cosserat, D. & Charpentier, J.C. 1980. Mass transfer in bubble columns operating at high gas throughputs. *The chemical engineering journal.* 20(2):87-94.

Bouaifi, M. and others. 2001. A comparative study of gas hold-up, bubble size, interfacial area and mass transfer coefficients in stirred gas–liquid reactors and bubble columns. *Chemical engineering and processing: Process intensification.* 40(2):97-111.

Bowman, C. and others. 1961. Mass transfer from fluid and solid spheres at low Reynolds numbers. *The Canadian journal of chemical engineering.* 39(1):9-13.

Brain, P.L.T. & Hales, H.B. 1969. Effects of transpiration and changing diameter on heat and mass transfer to spheres. *A.I.ch.E. J.* 15:419.

Brennen, C.E. 2005. *Fundamentals of multiphase flow.* Cambridge University Press. New York

Bukur, D.B. & Daly, J.G. 1987. Gas hold-up in bubble columns for Fischer-Tropsch synthesis. *Chemical engineering science.* 42(12):2967-2969.

Burnett, D.S. 1987. *Finite Element Analysis - From Concepts to Application..* Reading: Addison-Wesley Publishing Company.

Buwa, V.V., Deo, D.S. & Ranade, V.V. 2006. Eulerian–Lagrangrian simulations of unsteady gas–liquid flows in bubble columns. *International journal of multiphase flow.* 32(7):864-885.

Buwa, V.V. & Ranade, V.V. 2004. Characterization of dynamics of gas–liquid flows in rectangular bubble columns. *AIChE journal.* 50(10):2394-2407.

Cachaza, E. 2009. Simultaneous Computational Fluid Dynamics (CFD) simulation of the hydrodynamics and mass transfer in a partially aerated bubble column. *Industrial engineering chemistry research.* 48(18):8685.

Carra, S. & Morbidelli, M. 1987. Gas–liquid reactors. *Chemical reaction and reactor engineering, marcel dekker, New York.* :545-666.

Chang, H. 1989. Measurement of $K_l a$ by a gassing-in method with oxygen-enriched air. *Biotechnology and bioengineering.* 34(9):1147.

Chrysikopoulos, C.V. and others. 2003. Mass transfer coefficient and concentration boundary layer thickness for a dissolving NAPL pool in porous media. *Journal of hazardous materials.* 97(1-3):245-255.

Clarke, K.G. & Correia, L.D.C. 2008. Oxygen transfer in hydrocarbon–aqueous dispersions and its applicability to alkane bioprocesses: A review. *Biochemical engineering journal.* 39(3):405-429.

Clarke, K.G. and others. 2006. Enhancement and repression of the volumetric oxygen transfer coefficient through hydrocarbon addition and its influence on oxygen transfer rate in stirred tank bioreactors. *Biochemical engineering journal.* 28(3):237-242.

Clift, R., Grace J.R & Weber M.E 1978. *Bubbles, drops and particles.* New York: Academic Press.

Coetzee, W., Coetzee, R. & Rawatlal, R. 2009. A statistical approach to computational fluid dynamics in predicting bubble columns. International Symposium on Business and Industrial Statistics.

Coetzee, W., Coetzer, R. J. L., and Rawatlal, R. (2010). An analysis of response surface strategies in developing statistical models for application in bubble column modelling. submitted to: Computers & Chemical Engineering.

Coetzee, W., Coetzer, R.L.J. & Rawatlal, R. 2012a. Response surface strategies in constructing statistical bubble flow models for the development of a novel bubble column simulation approach. *Computers & chemical engineering.* 36:22-34.

Coetzee, W., Coetzer, R. & Rawatlal, R. 2012b. Development of a computationally efficient bubble column simulation approach by way of statistical bubble micro-flow modelling. *Advances in fluid mechanics IX.* 9:275.

Coetzee, W., Coetzer, R.L. & Rawatlal, R. 2012c. Semi analytical Bubble-Flow Models for the Development of a Novel Bubble-Column Simulator. *Industrial & engineering chemistry research.* 51(21):7398-7409.

Correia, L.D.C., Aldrich, C. & Clarke, K.G. 2010. Interfacial gas–liquid transfer area in alkane–aqueous dispersions and its impact on the overall volumetric oxygen transfer coefficient. *Biochemical engineering journal.* 49(1):133-137.

Crumpton, P.I., Moinier, P. & Giles, M.B. 1997. An unstructured algorithm for high Reynolds number flows on highly stretched meshes. *Numerical methods in laminar and turbulent flow.* :561–572.

Cussler, E.L. 2003. *Diffusion: Mass Transfer in Fluid Systems.* 2nd ed. Cambridge University Press.

Dani, A., Cockx, A. & Guiraud, P. 2006. Direct numerical simulation of mass transfer from spherical bubbles: the effect of interface contamination at low Reynolds numbers. *International journal of chemical reactor engineering.* 4(1).

Darmana, D. 2007. Detailed modelling of hydrodynamics, mass transfer and chemical reactions in a bubble column using a discrete bubble model: Chemisorption of CO2 into NaOH solution, numerical and experimental study. *Chemical engineering science.* 62(9):2556.

Darmana, D., Deen, N.G. & Kuipers, J.A.M. 2005. Detailed modeling of hydrodynamics, mass transfer and chemical reactions in a bubble column using a discrete bubble model. *Chemical engineering science.* 60(12):3383-3404.

Deckwer, W.D., Burckhart, R. & Zoll, G. 1974. Mixing and mass transfer in tall bubble columns. *Chemical engineering science.* 29(11):2177-2188.

Deckwer, W.D. 1992. *Bubble column reactors.* Chichester: .

Deckwer, W.-. 1983. APPLICABILITY OF AXIAL DISPERSION MODEL TO ANALYZE MASS TRANSFER MEASUREMENTS IN BUBBLE COLUMNS. *AICHE journal.* 29(6):915.

Deen, N.G., Solberg, T. & Hjertager, B.H. 2001. Large eddy simulation of the gas–liquid flow in a square cross-sectioned bubble column. *Chemical engineering science.* 56(21):6341-6349.

Degaleesan, S. 2001. Experimental study of gas - induced liquid - flow structures in bubble columns. *AIChE journal.* 47(9):1913.

Deindoerfer, F. & Humphrey, A. 1961. Mass transfer from individual gas bubbles. *Industrial & engineering chemistry.* 53(9):755-759.

Delnoij, E., Kuipers, J. & Van Swaaij, W. 1999. A three-dimensional CFD model for gas–liquid bubble columns. *Chemical engineering science.* 54(13):2217-2226.

Delnoij, E. and others. 1997. Dynamic simulation of dispersed gas-liquid two-phase flow using a discrete bubble model. *Chemical engineering science.* 52(9):1429-1458.

Delnoij, E. 1997. Dynamic simulation of gas-liquid two-phase flow: Effect of column aspect ratio on the flow structure. *Chemical engineering science.* 52(21):3759.

Delnoij, E. 1999. A three-dimensional CFD model for gas-liquid bubble columns. *Chemical engineering science.* 54(13):2217.

Dhaouadi, H. and others. 2008. Gas–liquid mass transfer in bubble column reactor: Analytical solution and experimental confirmation. *Chemical engineering and processing: Process intensification.* 47(4):548-556.

Dudley, J. 1995. Mass transfer in bubble columns: a comparison of correlations. *Water research.* 29(4):1129-1138. .

Dutta, B.K. 2007. *Principles of mass transfer and separation processes.* Prentice-Hall of India.

Ekambara, K. 2003. CFD simulation of mixing and dispersion in bubble columns. *Chemical engineering research and design.* 81(8):987.

Ekambara, K. 2005. CFD simulations of bubble column reactors: 1D, 2D and 3D approach. *Chemical engineering science.* 60(23):6733.

Ekambara, K. 2010. CFD simulation of bubble column. *Nuclear engineering and design.* 240(5):963.

Ekambara, K. 2005. Computational fluid dynamics simulations in bubble-column reactors: Laminar and transition regimes. *Industrial engineering chemistry research.* 44(5):1413.

Ekambara, K. 2008. CFD simulation of bubble column reactor using population balance. *Industrial engineering chemistry research.* 47(21):8505.

Ellenberger, J. 2002. Improving mass transfer in gas-liquid dispersions by vibration excitement. *Chemical engineering science.* 57(22):4809.

Erkey, C. 1990. Correlation for predicting diffusion coefficients in alkanes. *The Canadian journal of chemical engineering.* 68(4):661.

Eymard, R., Gallouet, T. & Herbin, R. Eds. 2006. *Finite Volume Methods*. 7th ed. Marseille: Ciarlet, P.G. and Lions eds,.

Ferrel, R.T. & Himmelblau, D.M. 1967. Diffusion coefficients of nitrogen and oxygen in water. *Journal of chemical and engineering data.* 12(1):111-115.

Fleischer, C., Becker, S. & Eigenberger, G. 1996. Detailed modeling of the chemisorption of CO2 into NaOH in a bubble column. *Chemical engineering science.* 51(10):1715-1724.

Friedlander, S. 1957. Mass and heat transfer to single spheres and cylinders at low Reynolds numbers. *AIChE journal.* 3(1):43-48.

Frössling, N. 1938. Uber die Verdunstung fallender Tropfen. *Gerlands beitr. geophys.* 52:170.

Gandhi, A. 2009. Development of unified correlations for volumetric mass-transfer coefficient and effective interfacial area in bubble column reactors for various gas-liquid systems using support vector regression. *Industrial engineering chemistry research.* 48(9):4216.

Garcia, M.J., Boulanger, P. & Giraldo, S. 2008. CFD based wing shape optimization through gradient-based method. *EngOpt 2008-International Conference on Engineering Optimization.* 01.

Garcia-Ochoa, F. 2005. Prediction of gas - liquid mass transfer coefficient in sparged stirred tank bioreactors. *Biotechnology and bioengineering.* 92(6):761.

Garcia-Ochoa, F. & Gomez, E. 2004. Theoretical prediction of gas–liquid mass transfer coefficient, specific area and hold-up in sparged stirred tanks. *Chemical engineering science.* 59(12):2489-2501.

Garner, F.H. & Keey, R.B. 1958. Mass Transfer from Single Solid Spheres - I. Transfer at Low Reynolds numbers. *Chem. eng. sci.* 9:119.

Garner, F.H. & Keey, R.B. 1959. Mass Transfer from Single Solid Spheres - II. Transfer in free Convection. *Chem. eng.sci.* 9:218.

Gartling, D.K. 2002. Applied CFD Techniques: An Introduction based on Finite Element methods. by R. Löhner, John Wiley Sons, Chichester 2001, Number of

pages: 376. ISBN 0 - 471 - 49843 - 2. Price: $95.00. *International journal for numerical methods in fluids.* 39(1):97.

Gestrich, W., Esenwein, H. & Krauss, W. 1976. Der flüssigkeitsseitige Stoffübergangskoeffizient in Blasenschichten. *Chemie ingenieur technik.* 48(5):399. [Online]. Available: http://dx.doi.org/10.1002/cite.330480509.

Gogate, P.R. & Pandit, A.B. 1999. Survey of measurement techniques for gas–liquid mass transfer coefficient in bioreactors. *Biochemical engineering journal.* 4(1):7-15.

Gómez-Díaz, D. & Navaza, J.M. 2005. Gas/liquid mass transfer in carbon dioxide–alkanes mixtures. *Chemical engineering journal.* 114(1-3):131-137.

Gómez-Díaz, D. and others. 2009. Oxygen mass transfer to emulsions in a bubble column contactor. *Chemical engineering journal.* 152(2-3):354-360.

Gorji, M. 2006. *A three dimensional CFD modeling of hydrodynamics and mass transfer in a gas-liquid impeller stirred tank reactor.*

Gray, M. 1993. Liquid-side mass transfer coefficients for liquids and slurries in a rotating drum. *Chemical engineering science.* 48(19):3442.

Grund, G., Schumpe, A. & Deckwer, W.-. 1992. Gas-Liquid mass transfer in a bubble column with organic liquids. *Chemical engineering science.* 47(13-14):3509-3516.

Hadamard, J. S. (1911). "Mouvement permanent lent d'une sphère liquide et visqueuse dans un liquide visqueux". CR Acad. Sci. 152: 1735. Rybczynski, W.

Hamborg, E.S. & Versteeg, G.F. 2012. Absorption and desorption mass transfer rates in chemically enhanced reactive systems. Part I: Chemical enhancement factors. *Chemical engineering journal.* 198–199(0):555-560.

Hammer, H. and others. 1984. New Sub functions on Hydrodynamics, Heat and Mass Transfer for Gas/Liquid and Gas/Liquid/Solid Chemical and Biochemical Reactors. *Front.chem.reac.eng.* 464.

Han, L. 2007. Gas-liquid mass transfer in a high pressure bubble column reactor with different sparger designs. *Chemical engineering science.* 62(1):131.

Hasegawa, Y. & Kasagi, N. 2001. The effect of Schmidt number on air-water interface mass transfer. *Proceeding of the 4th international conference on multiphase flow, New Orleans.*

Hashemi, S. 2009. Gas-liquid mass transfer in a slurry bubble column operated at gas hydrate forming conditions. *Chemical engineering science.* 64(16):3709.

Haut, B. & Cartage, T. 2005. Mathematical modeling of gas–liquid mass transfer rate in bubble columns operated in the heterogeneous regime. *Chemical engineering science.* 60(22):5937-5944.

Hikita, H. and others. 1980. Gas hold-up in bubble columns. *The chemical engineering journal.* 20(1):59-67.

Hikita, H. and others. 1981. The volumetric liquid-phase mass transfer coefficient in bubble columns. *The chemical engineering journal.* 22(1):61-69.

Hua, J. and Lou, J. (2007). Numerical simulation of bubble rising in viscous liquid. Journal of Computational Physics, 222:769{795.

Hughmark, G.A. 1967. Holdup and mass transfer in bubble columns. 6(2):218-220.

Hung, T. and others. 2007. An innovative improvement of engineering learning system using computational fluid dynamics concept. *Computers & education.* 48(1):44-58.

Incropera, F.P. and others 2011. *Fundamentals of heat and mass transfer. Wiley*

Irani, M. & Khodagholi, M.A. 2011. INVESTIGATION OF BUBBLE COLUMN HYDRODYNAMICS USING CFD SIMULATION (2D AND 3D) AND EXPERIMENTAL VALIDATION. *Petroleum & coal.* 53(2):146-158.

Jajuee, B. 2006. Application of surface-renewal-stretch model for interface mass transfer. *Chemical engineering science.* 61(12):3917.

Jin, H. 2004. Experimental study of oxygen mass transfer coefficient in bubble column with high temperature and high pressure. *Chemical engineering technology.* 27(12):1267.

Jorge, M.T.V., Orvalho, S.P. & Sebastiao, S.A. 2002. *Alche journal.* 48(6):1145-1154.

Joshi, J.B. 2001. Computational flow modelling and design of bubble column reactors. *Chemical engineering science.* 56(21):5893.

Joshi, J. 2003. Computational fluid dynamics for designing process equipment: Expectations, current status, and path forward. *Industrial engineering chemistry research.* 42(6):1115.

Kang, Y. 1999. Diagnosis of bubble distribution and mass transfer in pressurized bubble columns with viscous liquid medium. *Chemical engineering science.* 54(21):4887.

Kantarci, N., Borak, F. & Ulgen, K.O. 2005. Bubble column reactors. *Process biochemistry.* 40(7):2263-2283.

Kawase, Y., Halard, B. & Moo-Young, M. 1987. Theoretical prediction of volumetric mass transfer coefficients in bubble columns for Newtonian and non-Newtonian fluids. *Chemical engineering science.* 42(7):1609-1617.

Kawase, Y. & Moo-Young, M. 1987. Theoretical prediction of gas hold-up in bubble columns with Newtonian and non-Newtonian fluids. *Industrial & engineering chemistry research.* 26(5):933-937.

Kawase, Y., Umeno, S. & Kumagai, T. 1992. The prediction of gas hold-up in bubble column reactors: Newtonian and non-Newtonian fluids. *The chemical engineering journal.* 50(1):1-7.

Kayode Coker, A. 2001. *Modelling of Chemical Kinetics and Reactor Design.* Boston: Gulf Publ.,.

Kelly, W. 2008. Using computational fluid dynamics to characterize and improve bioreactor performance. *Biotechnology and applied biochemistry.* 49(3):225.

Kenig, E.Y. 2007. Advanced modeling of reactive separation units with structured packings. *Chemical product and process modeling.* 2(1).

Koeltzsch, K. 2000. The height dependence of the turbulent Schmidt number within the boundary layer. *Atmospheric environment.* 34(7):1147-1151.

Kojima, H., Sawai, J. & Suzuki, H. 1997. Effect of pressure on volumetric mass transfer coefficient and gas holdup in bubble column. *Chemical engineering science.* 52(21-22):4111-4116.

Krishna, R. 1994. Strategies for multiphase reactor selection. *Chemical engineering science.* 49(24):4029.

Krishna, R. 2002. Improving gas-liquid mass transfer in bubble columns by applying low-frequency vibrations. *Chemical engineering technology.* 25(2):159.

Krishna, R. 2003. Mass transfer in bubble columns. *Catalysis today.* 79:67.

Krishna, R. & Ellenberger, J. 2002. Improving gas–liquid contacting in bubble columns by vibration excitement. *International journal of multiphase flow.* 28(7):1223-1234.

Krishna, R. & Sie, S.T. 2000. Design and scale-up of the Fischer–Tropsch bubble column slurry reactor. *Fuel processing technology.* 64(1–3):73-105.

Kulkarni, A.A. 2007. On the development of flow pattern in a bubble column reactor: Experiments and CFD. *Chemical engineering science.* 62(4):1049.

Kulkarni, A.A. & Joshi, J.B. 2004. Simultaneous measurement of flow pattern and mass transfer coefficient in bubble columns. *Chemical engineering science.* 59(2):271-281.

Kumar, A. 2009. CFD Modeling of Gas-Liquid-Solid Fluidized Bed. B.Tech. NIT,Rourkela,.

Kumar, S., Srinivasulu, N., & Khanna, A. CFD Simulations to Validate Two & Three Phase Up-flow in Bubble Columns.

Kundu, A. 2003. Mass transfer characteristics in gas-liquid-liquid system. *The canadian journal of chemical engineering.* 81(3):640.

Kuzmin, D. & Turek, S. 2000. *Efficient numerical techniques for flow simulation in bubble column reactors.* Univ. Dortmund, Fachbereich Mathematik.

Löhner, R. 2001. *Applied CFD Techniques: An Introduction based on Finite Element methods.* Chichester: John-Wiley and Sons Ltd.

Laari, A. 1997. Gas-liquid mass transfer in bubble columns with a T-junction nozzle for gas dispersion. *Chemical engineering technology.* 20(8):550.

Laın, S. 2002. Modelling hydrodynamics and turbulence in a bubble column using the Euler–Lagrange procedure. *International journal of multiphase flow.* 28(8):1381.

Lau, R. and others. 2004. Gas-liquid mass transfer in high-pressure bubble columns. *Industrial & engineering chemistry research.* 43(5):1302-1311.

Law, D. 2006. Numerical simulations of gas-liquid flow dynamics in bubble columns. *Fed.*

Lee, K. D. ,Loellbach, J. M and . Kim. M. S 1991. "Adaptive control of grid quality for computational fluid dynamics", Journal of Aircraft, Vol. 28, No. 10, pp. 664-669. doi: 10.2514/3.46080

Lemoine, R. and others. 2008. An algorithm for predicting the hydrodynamic and mass transfer parameters in bubble column and slurry bubble column reactors. *Fuel processing technology.* 89(4):322-343.

Levenspiel, O. 1988. Chemical engineering's grand adventure. *Chem. engng sci.* 43:1427-1435.

Levenspiel, O. 1999. *Chemical Reaction Engineering.* Chichester: Wiley J.

Li, W.Z., Yan, Y.Y. & Smith, J.M. 2003. A numerical study of the interfacial transport characteristics outside spheroidal bubbles and solids. *International journal of multiphase flow.* 29(3):435-460.

Linton, M. & Sutherland, K. 1960. Transfer from a sphere into a fluid in laminar flow. *Chemical engineering science.* 12(3):214-229.

Liu, S.X., Peng, M. & Vane, L. 2004. CFD modeling of pervaporative mass transfer in the boundary layer. *Chemical engineering science.* 59(24):5853-5857.

Lochiel, A. & Calderbank, P. 1964. Mass transfer in the continuous phase around axisymmetric bodies of revolution. *Chemical engineering science.* 19(7):471-484.

Lu, S. and others. 2003. Measurement of the Bubble Parameters in Bubble Column by Conductivity Probe. *Chemical reaction engineering and technology.* 19(4):344-351.

Maalej, S. 2001. Influence of pressure on the hydrodynamics and mass transfer parameters of an agitated bubble reactor. *Chemical engineering technology.* 24(1):77.

MacCormack, R.W. & Baldwin, B.S. 1975. A numerical method for solving the Navier-Stokes equations with application to shock-boundary layer interactions. *American institute of aeronautics and astronautics, aerospace sciences meeting, 13th, pasadena, calif., jan. 20-22, 1975, 9 p.*

Maceiras, R., Santana, R. & Alves, S.S. 2007. Rise velocities and gas–liquid mass transfer of bubbles in organic solutions. *Chemical engineering science.* 62(23):6747-6753.

Madhavi, T. 2007. Studies on bubble dynamics with mass transfer. *Chemical engineering journal.* 128(2):95.

Mahajan, V. 2010. *CFD analysis of hydrodynamics and mass transfer of a gas-liquid bubble column.*

Mahesh, K. 2006. Large-eddy simulation of reacting turbulent flows in complex geometries. *Journal of applied mechanics.* 73(3):374.

Mangartz, K.H. 1981. Interpretation of Mass Transfer Measurements in Bubble Columns considering dispersion of both. *Chemical engineering science.* 36(6):1069.

Mangartz, K. 1980. Studies of the Gas Phase Dispersion in Bubble Column Reactors. *Verfahrenstechnik.* 14(1):40.

Maretto, C. & Krishna, R. 1999. Modelling of a bubble column slurry reactor for Fischer–Tropsch synthesis. *Catalysis today.* 52(2-3):279-289.

Margavey, R.H. and Bishop, R.L., “Transition ranges for three-dimensional wakes”, Can. J. Phys., 39, 1418-1422, 1961.

Mark M.Clark Ed. 2009. *Transport Modelling for Environmental Engineers and Scientist*. 2nd ed. United Kingdom: John Wiley & Sons,Inc.,.

Martín, M., Montes, F.J. & Galán, M.A. 2009a. Mass transfer from oscillating bubbles in bubble column reactors. *Chemical engineering journal.* 151(1-3):79-88.

Martín, M., Montes, F.J. & Galán, M.A. 2009b. Theoretical modelling of the effect of surface active species on the mass transfer rates in bubble column reactors. *Chemical engineering journal.* 155(1-2):272-284.

Mashelkar, R. & Sharma, M. 1970. Mass transfer in bubble and packed bubble columns. *Transactions of the institution of chemical engineers.* 48:T162-T162.

McCready, M.J. 2003. Principles and modern applications of mass transfer operations. By Jaime Benitez, Wiley, New York 2002, 499 pp., $89.95. *AIChE journal.* 49(1):288.

Medic, L. and others. 1989. Volumetric gas-liquid mass transfer coefficients in a rectangular bubble column with a rubber aeration pad. *The chemical engineering journal.* 41(3):B51-B54.

Merchuk, J.C. & Ben-Zvi(Yona), S. 1992. A novel approach to the correlation of mass transfer rates in bubble columns with non- Newtonian liquids. *Chemical engineering science.* 47(13-14):3517-3523.

Michaelides, E.E. 2006. *Particles, Bubbles & Drops*
Thier Motion,Heat and Mass transfer. Singapore: World Scientific Publishing Co. Pte. Ltd.

Miyahara, T. 1997. Gas holdup, gas-liquid interfacial area and mass transfer coefficient in external-loop airlift bubble column containing low density particles. *Journal of chemical engineering of japan.* 30(5):958.

Mohapatra, D. & Rakh, K. 2007. CFD Modeling of Multi-phase Fluidized Bed. B. Tech. NIT.

Motarjemi, M. & Jameson, G. 1978. Mass transfer from very small bubbles—the optimum bubble size for aeration. *Chemical engineering science.* 33(11):1415-1423.

Mousavi, S.M. 2008. Experiments and CFD simulation of ferrous bio oxidation in a bubble column bioreactor. *Computers chemical engineering.* 32(8):1681.

Mudde, R. 1999. Two- and three-dimensional simulations of a bubble plume using a two-fluid model. *Chemical engineering science.* 54(21):5061.

Muller, F.L. & Davidson, J.F. 1992. On the contribution of small bubbles to mass transfer in bubble columns containing highly viscous liquids. *Chemical engineering science.* 47(13-14):3525-3532.

Nakamura, I., “Steady wake behind a sphere”, Phys. Fluids, 19(1), pp. 5-8, 1976.

Natarajan, R. and Acrivos, A., “The instability of the steady flow past spheres and disks”, J. Fluid Mech. 254, 323-344, 1993.

Ouyoung, P.K., Nam Chang, H. & Moo-Young, M. 1988. Determination of gas-liquid mass transfer coefficient in a bubble column by an eigenvalue method. *Chemical engineering science.* 43(4):821-827.

Oyevaar, M.H. and others. 1989. Interfacial areas and gas hold-ups in bubble columns and packed bubble columns at elevated pressures. *Chemical engineering and processing: Process intensification.* 26(1):1-14.

Öztürk, S. & Schumpe, A. 1987. The influence of suspended solids on oxygen transfer to organic liquids in a bubble column. *Chemical engineering science.* 42(7):1781-1785.

Pantankar, S. V. (1980). Numerical Heat Transfer and Fluid Flow. Taylor & Francis. Tomiyama, A., Celata, G. P., Hosokawa, S., and Yoshida, S. (2002). Terminal velocity of single bubbles in surface tension force dominant regime. International Journal of Multiphase Flow, 28:1497{1519.

Parasu Veera, U. & Joshi, J.B. 2000. Measurement of Gas Hold-up Profiles in Bubble Column by Gamma Ray Tomography: Effect of Liquid Phase Properties. *Chemical engineering research and design.* 78(3):425-434.

Paschedag, A., Piarah, W. & Kraume, M. 2005. Sensitivity study for the mass transfer at a single droplet. *International journal of heat and mass transfer.* 48(16):3402-3410.

Peraire, J., Morgan, K. & Peiro, J. 1989. Unstructured finite element mesh generation and adaptive procedures for CFD. *AGARD FDP: specialist's meeting, Loen, Norway.* DTIC Document.

Pfleger, D. & Becker, S. 2001. Modelling and simulation of the dynamic flow behaviour in a bubble column. *Chemical engineering science.* 56(4):1737-1747.

Pilhofer, T. 1978. Determination of Fluid Dynamic Parameters in bubble Column Design. *ACS symposium series.* (65):372.

Ponoth, S.S. & McLaughlin, J. 2000. Numerical simulation of mass transfer for bubbles in water. *Chemical engineering science.* 55(7):1237-1255.

Ranade, V.V. 2001. *Computational flow modeling for chemical reactor engineering.* Academic press.

Ranade, V.V. 2002. Computational Flow Modeling for Chemical Reactor Engineering.

Ranz, W.E. & Marshall, W.R. 1952. Evaporation from drops Part II. *Chem.eng.prog.* 48:173.

Rodemerck, U. & Seidel, A. 1991. Analysis of transient mass transfer measurements in bubble columns. *Chemical engineering science.* 46(3):908-912.

Rowe, P.N.C., K.T. & Lewis, J.B. 1965. Heat and Mass Transfer from a single sphere in an extensive flowing fluid. *Trans. inst. chem. eng.* 41:T14.

Sada, E. and others. 1975. Diffusivities of gases in binary mixtures of alcohols and water. *The chemical engineering journal.* 10(1):155-159.

Sada, E. 1986. Gas holdup and mass-transfer characteristics in a three-phase bubble column. *Industrial engineering chemistry process design and development.* 25(2):472.

Samareh, J.A. 2005. Geometry and grid/mesh generation issues for CFD and CSM shape optimization. *Optimization and engineering.* 6(1):21-32.

Sawant, S.B., Pangarkar, V.G. & Joshi, J.B. 1979. Gas hold-up and mass transfer characteristics of packed bubble columns. *The chemical engineering journal.* 18(1):143-149.

Schlichting, H. Boundary Layer Theory, McGraw-Hill, New York, 1968

Schlüter, S. 1995. Simulation of bubble column reactors with the BCR computer code. *Chemical engineering and processing.* 34(2):127.

Schumpe, A. & Deckwer, W.D. 2004. Organic liquids in a bubble column: holdups and mass transfer coefficients. *AIChE journal.* 33(9):1473-1480.

Seader, J.D., Henley, E.J. & Roper, D.K. Eds. 2010. *Separation Process Principles*. 3rd ed.: John Wiley and Sons.

Seader, J. & Henley, E. Separation Process Principles. 2006, Hoboken.

Seader, J. & Henley, E. 1998. Separation process principlesWiley. *New york.*

Seebauer, E.G. 1995. Estimating surface diffusion coefficients. *Progress in surface science.* 49(3):265.

Shah, Y.T. 1982. DESIGN PARAMETERS ESTIMATIONS FOR BUBBLE COLUMN REACTORS. *AICHE journal.* 28(3):353.

Shaikh, A. & Al-Dahhan, M. 2007. A Review on Flow Regime Transition in Bubble Columns. *International journal of chemical reactor engineering.* 5.

Sherwood, T.K., Pigford, R.L. & Wilke, C.R. 1975. *Mass Transfer.* New York: McGraw-Hill.

Shimizu, K. 2000. Phenomenological model for bubble column reactors: Prediction of gas hold-ups and volumetric mass transfer coefficients. *Chemical engineering journal.* 78(1):21.

Silva, E., Teixeira, S. & Lobarinhas, P. 2008. The influence of different grid approaches on a cardiovascular computational model, *Proceeding of the 17th*

IASTED I nternational Conference on Applied Simulation and Modelling 2008,9780889867482, Corfu, Greece, June 2008, ACTA Press,Calgary

Silva, E., Teixeira, S. & Lobarinhas, P. 2011. Computational Fluid Dynamics Simulations:an Approach to Evaluate Cardiovascular Dysfunction, Modelling Simulation and Optimization, Gregorio Romero Rey and Luisa Martinez Muneta (Ed.), ISBN: 978-953-307-048-3, InTech, Available from: http://www.intechopen.com/books/modelling-simulation-and optimization/computational-fluid-dynamicssimulations-an-approach-to-evaluate-cardiovascular-dysfunction.

Singh, M.K. & Majumder, S.K. 2011. Co-and counter-current mass transfer in bubble column. *International journal of heat and mass transfer.* 54(11):2283-2293.

Singh, M. & Majunder, S. 2010. Theoretical study on effect of operating parameters on mass transfer in bubbly flow 2(5):163-170.

Slattery, J. C. 1999. *Advanced transport phenomena*. Cambridge University Press.

Smolianski, A., Haario, H. & Luukka, P. 2008. Numerical study of dynamics of single bubbles and bubble swarms. *Applied mathematical modelling.* 32(5):641-659.

Snijder, E. 1993. Diffusion coefficients of several aqueous alkanolamine solutions. *Journal of chemical engineering data.* 38(3):475.

Sokolichin, A. & Eigenberger, G. 1994. Gas—liquid flow in bubble columns and loop reactors: Part I. Detailed modelling and numerical simulation. *Chemical engineering science.* 49(24, Part 2):5735-5746.

Suzzia, D., Radlb, S. & Khinasta, J. 2009. Validation of euler-euler and euler-lagrange approaches in the simulation of bubble columns. *Chemical engineering.* 17:535.

Taneda, S., “Experimental Investigation of the Wake behind a Sphere at Low Reynolds Numbers”, J. Phys. Soc. Japan, 11 (10), pp. 1104-1108, 1956.

Taneda, S., “Visual observations of the flow past a sphere at Reynolds numbers between 104 and 106”, J. Fluid Mech., 85, 187-192, 1978.

Terasaka, K., Hullmann, D. & Schumpe, A. 1998. Mass transfer in bubble columns studied with an oxygen optode. *Chemical engineering science.* 53(17):3181-3184.

Thakre, S.S. 1999. CFD simulation of bubble column reactors: Importance of drag force formulation. *Chemical engineering science.* 54(21):5055.

Thakre, S. 1999. CFD modeling of flow, macro-mixing and axial dispersion in a bubble column. *The Canadian journal of chemical engineering.* 77(5):826.

Thirumaleshwar, M. 2006. *Fundamentals of heat and mass transfer. Pearson*

Thompson, J.F., Soni, B.K. & Weatherill, N.P. 1998. *Handbook of grid generation.* CRC.

Trambouze, P., Van Landeghem, H. & Wauquier, J.P. 1988. *Chemical Reactors. Design, Engineering and Operation.* Paris: Technip.

Troshko, A. 2009. CFD modeling of slurry bubble column reactors for Fisher-Tropsch synthesis. *Chemical engineering science.* 64(5):892.

Tu, J., Yeoh, G.H. & LIU , C. 2008. ***Computational Fluid Dynamics : A Practical Approach.*** 1st ed. Oxford: Butterworth-Heinemann.

Valluri, P. 2002. Modelling hydrodynamics and mass transfer in structured packings - A review. *Multiphase science and technology.* 14(4):303.

Van Baten, J. & Krishna, R. 2004. CFD simulations of mass transfer from Taylor bubbles rising in circular capillaries. *Chemical engineering science.* 59(12):2535-2545.

Van Baten, J.M. 2002. Gas and liquid phase mass transfer within KATAPAK-S® structures studied using CFD simulations. *Chemical engineering science.* 57(9):1531.

Van der Hoef, M. and others. 2006. Multi-scale modeling of gas-fluidized beds. *Advances in chemical engineering.* 31:65-149.

Van Sint Annaland, M., Deen, N. & Kuipers, J. 2005. Numerical simulation of gas–liquid–solid flows using a combined front tracking and discrete particle method. *Chemical engineering science.* 60(22):6188-6198.

Van Sint Annaland, M., Dijkhuizen, W., Deen, N. G., and Kuipers, J. A. M. (2006). Numerical simulation of behavior of gas bubbles using a 3-d front-tracking method. American Institute of Chemical Engineers, 52:99{110.

Vandu, C.O. & Krishna, R. 2004. Influence of scale on the volumetric mass transfer coefficients in bubble columns. *Chemical engineering and processing.* 43(4):575-579.

Vandu, C. 2005. Gas-liquid mass transfer in a slurry bubble column at high slurry concentrations and high gas velocities. *Chemical engineering technology.* 28(9):998.

Vasconcelos, J.M.T., Orvalho, S.P. & Alves, S.S. 2004. Gas–liquid mass transfer to single bubbles: effect of surface contamination. *AIChE journal.* 48(6):1145-1154.

Vermeer, D.J. & Krishna, R. 1981. Hydrodynamics and mass transfer in bubble columns in operating in the churn-turbulent regime. *Industrial & engineering chemistry process design and development.* 20(3):475-482.

Vincent, G. 2011. CFD modelling of an annular reactor, application to the photo catalytic degradation of acetone. *Process safety and environmental protection.* 89(1):35.

Wang, T. & Wang, J. 2007. Numerical simulations of gas–liquid mass transfer in bubble columns with a CFD–PBM coupled model. *Chemical engineering science.* 62(24):7107-7118.

Weast, R.C. 1988. *CRC handbook of chemistry and physics.*

Welty, J.R. and others. 1984. Fundamentals of momentum. *Heat and mass transfer.* 3(1).

White, F.M. Fluid Mechanics, McGraw-Hill, New York, 2011.

Whitman, W.G. 1962. The two film theory of gas absorption. *International journal of heat and mass transfer.* 5(5):429.

Whitman, W.G. 1923. The two-film theory of gas absorption. *Chem. metal. eng.* 29:146–150.

Wilkinson, P.M., Haringa, H. & Van Dierendonck, L.L. 1994. Mass transfer and bubble size in a bubble column under pressure. *Chemical engineering science.* 49(9):1417-1427.

Wilkinson, P.M. & v. Dierendonck, L.L. 1990. Pressure and gas density effects on bubble break-up and gas hold-up in bubble columns. *Chemical engineering science.* 45(8):2309-2315.

Wu, J.S. and Faeth, G.M., “Sphere wakes in still surroundings at intermediate Reynolds numbers”, AIAA J., 31, 1448-1455, 1993.

Wylock, C. and others. 2011. Direct numerical simulation of bubble-liquid mass transfer coupled with chemical reactions: Influence of bubble shape and interface contamination. *Colloids and surfaces A: Physicochemical and engineering aspects.* 381(1):130-138.

Xu, T. 2004. Determination of effective diffusion coefficient and interfacial mass transfer coefficient of bovine serum albumin (BSA) adsorption into porous polyethylene membrane by microscope FTIR-mapping study. *Chemical engineering science.* 59(21):4569.

Yan, Y. Y., Li, W. Z., & Smith, J. M. 2002. Numerical modelling of fluid flow with heat and mass transfer at the surface of a gas bubble. *Chemical Engineering Research and Design*, *80*(6), 674-680.

Yoshida, F. 1965. Performance of gas bubble columns: Volumetric liquid - phase mass transfer coefficient and gas holdup. *AIChE journal.* 11(1):9.

Yoshimoto, M. 2007. Gas-liquid interfacial area, bubble size and liquid-phase mass transfer coefficient in a three-phase external loop airlift bubble column. *Chemical and biochemical engineering quarterly.* 21(4):365.

You,D., Mittal R., Wang M. & Moin P., 2006. Analysis of stability and accuracy of finite-difference schemes on a skewed mesh. *Journal of Computational Physics* 213: 184–204. doi:10.1016/j.jcp.2005.08.007

Zhang, D., Deen, N.G. & Kuipers, J.A.M. 2007. Numerical modeling of hdrodynamics, mass transfer and chemical reaction in bubble column. July. 6th International Conference on Multiphase flow.

Zhang, D., Deen, N.G. & Kuipers, J. 2008. Euler− Euler Modeling of Flow, Mass Transfer, and Chemical Reaction in a Bubble Column. *Industrial & engineering chemistry research.* 48(1):47-57.

12. Appendices

Appendix A: Derivation of Film Theory

Mass transfer rate between the surface and the fluid is written as follows;

$$N_A = k_l a(C_A - C_\infty) \quad \textbf{(A.1)}$$

At the surface, mass transfer is by diffusion and is expressed as follows:

$$\boldsymbol{N_A} = -\boldsymbol{D_{AB}}\left(\frac{\boldsymbol{dC_A}}{\boldsymbol{dx}}\right)\Big| y = 0 \quad \textbf{(A.2)}$$

Equations (A.1) and (A.2) are equal

$$k_l a(C_A - C_\infty) \quad = -\boldsymbol{D_{AB}}\left(\frac{\boldsymbol{dC_A}}{\boldsymbol{dx}}\right)\Big| y = 0 \quad \textbf{(A.3)}$$

Rearranging (A.3) results in

$$k_l = \frac{-\boldsymbol{D_{AB}}\left(\frac{\boldsymbol{dC_A}}{\boldsymbol{dx}}\right)\Big| y=0}{C_A - C_\infty} \quad \textbf{(A.4)}$$

Since the concentration boundary layer can be written as

$$\delta_C = \frac{\frac{\partial(C_A - C_\infty)}{\partial y}\Big| y=0}{C_A - C_\infty} \quad \textbf{(A.5)}$$

Equation (A.5) can be rearranged and written as

$$k_l = \frac{D_{ab}}{\delta_c} \quad \textbf{(A.6)}$$

Appendix B: Concentration Boundary Layer thickness according to the Film Theory

$$\frac{C_{AS} - C_A}{C_{AS} - C_{A\infty}} = 0.99 \quad (13)$$

$$C_{A\infty} = 0$$

$$1 - \frac{C_A}{C_{AS}} = 0.99$$

$$\frac{C_A}{C_{AS}} = 0.01$$

$$C_A = 0.01 \times C_{AS}$$